5-2014

# Petrology and Geochemistry of the Crawfish Inlet and Krestof Island Plutons, Baranof Island, Alaska

Adrian Allan Wackett
*Trinity University*, awackett@trinity.edu

**PETROLOGY AND GEOCHEMISTRY OF THE CRAWFISH INLET AND KRESTOF ISLAND PLUTONS, BARANOF ISLAND, ALASKA**

Adrian Wackett

A departmental senior thesis submitted to the Department of Geosciences at Trinity University in partial fulfillment of the requirements for graduation with departmental honors.

April 15, 2014

[redacted]

Thesis Advisor

Department Chair

# TABLE OF CONTENTS

# LIST OF FIGURES

# LIST OF TABLES

# ABSTRACT

The Sanak-Baranof plutonic belt (SBPB) includes a series of 61 – 48 Ma biotite tonalite, granodiorite, and granite near-trench plutons that intrude the Campanian to Eocene flysch of the Chugach-Prince William terrane for 2100 km along the southern Alaskan margin (Hudson et al., 1979; Hill et al., 1981; Bradley et al., 2003; Haeussler et al., 2003). The time-transgressive nature of these forearc plutons makes them central to tectonic reconstructions of the North American Cordillera through the Paleocene-Eocene (Hudson et al., 1979; Bradley et al., 2003; Haeussler et al., 2003; Cowan, 2003).

The coeval Crawfish Inlet (53 – 47 Ma) and Krestof Island (52 Ma) plutons on Baranof Island mark the eastern limit of the SBPB. The plutons are dominated by medium-grained granodiorites and tonalites, which are host to fine-grained magmatic enclaves. The enclaves exhibit a wide range in composition, from gabbrodiorite to granite. The least evolved enclaves (< 62 wt% $SiO_2$) in the Crawfish pluton are geochemically distinct from enclaves in Krestof pluton. With the exception of Pb, Y and the heavy rare earth elements, least evolved Crawfish enclaves are enriched in trace elements relative to the Krestof enclaves. In addition, initial Sr and Nd isotopic ratios are distinct between Crawfish and Krestof enclaves. All the isotopic analyses for both enclaves and their host granitoids lie within or near the mantle array.

Krestof enclaves plot in the field for typical mid-ocean ridge basalt (MORB) on a Sr/Y versus Y diagram, where as the least evolved Crawfish enclaves plot in fields for adakites and island arc basalts, along with Krestof and Crawfish granitoids. These adakitic characteristics ($Sr/Y > 25$ and $La/Yb_{CN} > 5$) are shared by ~50 Ma intrusive rocks occurring in the eastern SBPB and the Coast Plutonic Complex.

Assimilation-fractional crystallization (AFC) models assuming a variety of mafic parental magmas and accretionary wedge assimilants were generally unsuccessful in producing Crawfish and Krestof compositions. The most plausible model for the origin of Krestof enclaves and granitoids involves MORB parental magma assimilating isotopically evolved sediment. Isotopic compositions of all Crawfish and Krestof rocks may be explained by mixing between mantle and sedimentary endmembers.

Minor and trace element and isotopic compositions for the Krestof enclaves, which are MORB-like, and the least evolved Crawfish enclaves, which are similar to ocean island basalts, suggest distinct mantle sources and/or parental magmas. The spatial and temporal proximity of these two enclave types suggests mantle heterogeneity on a relatively local scale.

# INTRODUCTION

The southern Alaska and Canadian Cordillera margins have a long and complicated tectonic and magmatic history (Figure 1). Intrusive rocks of the Sanak-Baranof plutonic belt (SBPB; Figure 2) have been interpreted to be the result of subduction of either the Kula-Farallon or the Kula-Ressurection spreading ridge beneath the Chugach-Prince William (CPW) composite terrane at a trench-ridge-trench (T-R-T) triple junction (Hudson et al., 1979; Hill et al., 1981; Sisson et al., 2003b; Bradley et al., 2003; Haeussler et al., 2003; Cowan, 2003; Ayuso et al., 2009).

A slab window is thought to have opened where the obliquely subducting ridge encountered the continental margin at 61 Ma (Hudson et al., 1979; Hill et al., 1981; Sisson et al., 2003b; Bradley et al., 2003; Haeussler et al., 2003; Cowan, 2003; Ayuso, 2009). A slab window is thought to have opened where the obliquely subducting ridge encountered the continental margin at 61 Ma (Hudson et al., 1979; Thorkelson et al., 1998; Bradley et al., 2003; Haeussler et al., 2003). The oblique component was important in opening the slab window, because the subducting slab from the Kula and/or Resurrection plate was pulled northward relative to the Farallon plate (Figure 3). Contemporary examples of T-R-T encounters around the world include T-R-T interactions observed in Chile and British Columbia (Sisson et al., 2003a; Forsythe and Nelson, 1985). Another historic example of a trench-ridge-transform system is present in Central America, where forearc magmatism has been shown to display ocean-island geochemical characteristics and localized adakites (Drummond et al., 1995; Johnston and Thorkelson, 1997).

The time-transgressive nature of the SBPB intrusive rocks makes them critical to tectonic reconstructions of the North American Cordillera. Their importance in resolving the debate over mobile versus non-mobile terranes throughout the Cordillera was recognized in a Geological Society of America Special Paper (Bradley et al., 2003) focusing exclusively on the southern Alaskan margin and the SBPB. Two very different tectonic models have been born out of this debate. The Baranof-Leech River and Resurrection plate hypotheses, proposed by Cowan (2003) and Haeussler et al. (2003), respectively, constitute the two prevailing theories attempting to reconcile coeval near-trench magmatism in southern Alaska and Cascadia during the Early Tertiary.

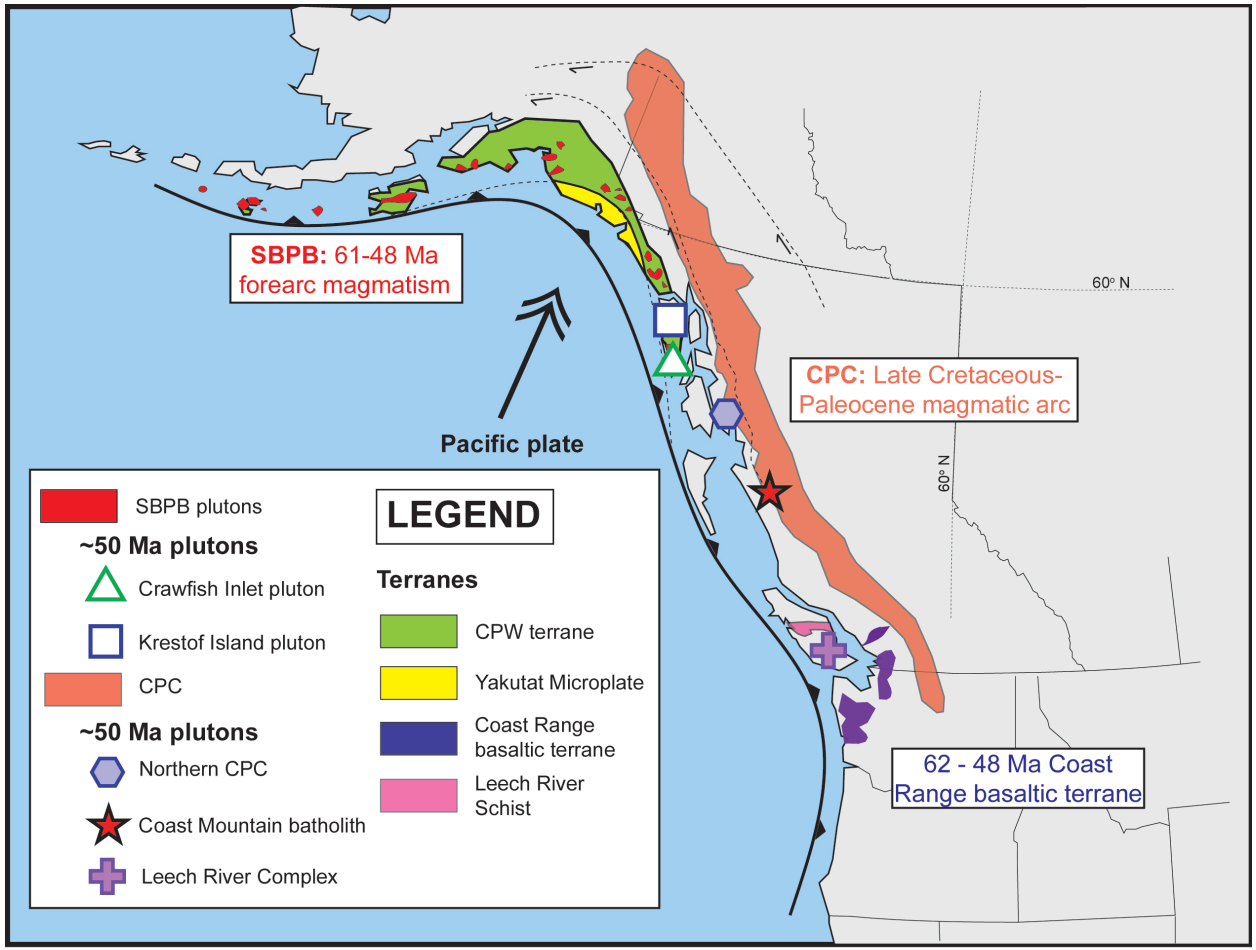


**Figure 1.** Map of southern Alaska and the Canadian Cordillera showing locations of terranes and 62-48 Ma forearc magmatism across the entire continental margin, from the northern Cascades to western Alaska. The figure also shows the location of the Coast Plutonic Complex (CPC), the magmatic arc that stretches the length of the Canadian Cordillera. Symbols defined in legend for: Crawfish and Krestof plutons (this study); Northern CPC (Arth and Barker, 1988); Coast Mountain batholith (Girardi et al., 2012); Leech River Complex (Groome et al., 2003) which mark the position of ~ 50 Ma CPC intrusive suites compared to the Crawfish and Krestof plutons in this study. Original figure modified from Madsen et al., 2006.

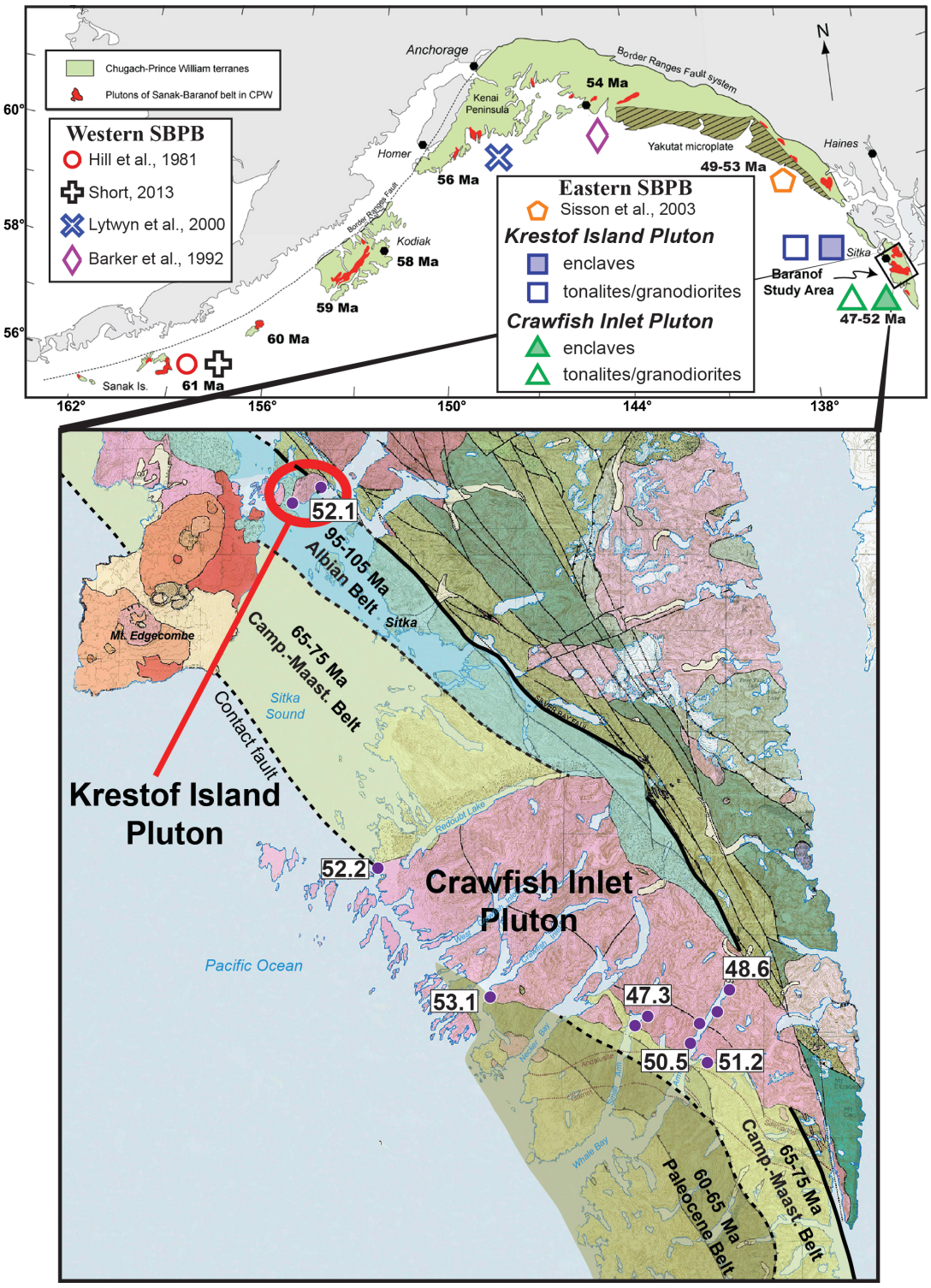


**Figure 2.** Simplified tectonic map (top) of the southern Alaska margin showing location of the study area on Baranof Island within the CPW terrane. Symbols correspond to other geochemical studies of SBPB intrusive rocks. Inset (bottom) shows locations of the Krestof Island and Crawfish Inlet plutons on southern Baranof Island. Sample locations for this study are indicated by purple dots. Base map for Baranof Island modified from Karl et al., 2014 (in press).

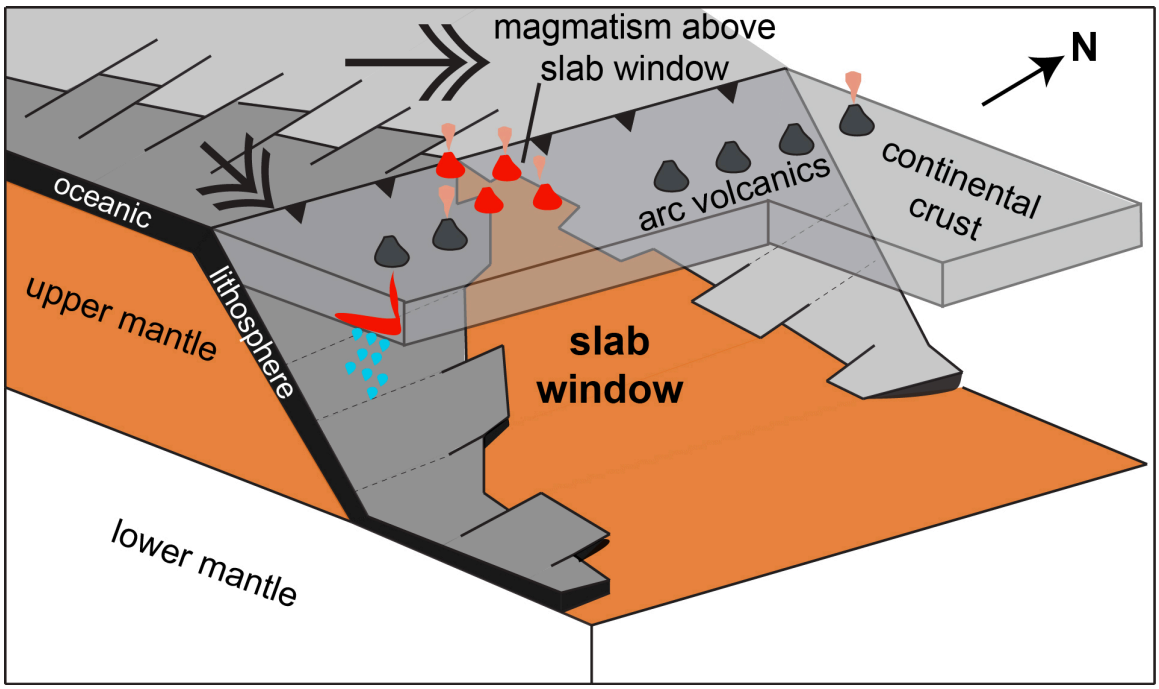


**Figure 3.** Schematic showing forearc magmatism occurring as a slab window opens up from oblique subduction at a T-R-T triple junction. The oblique component (arrows) induces differential motions for the two subducting plates at the T-R-T junction, which aids in opening the window and allowing mantle upwelling in the forearc. Base figure modified slightly from Hauessler et al. (2003).

In Cowan's Baranof–Leech River model, a single TRT junction fixed at 48°N (present-day) is proposed to be responsible for coeval forearc magmatism in southern Alaska and the Cascade. In this reconstruction, the CPW terrane passed over the fixed slab window between 61-50 Ma as it was displaced northward along a series of margin parallel, dextral strike-slip faults (Cowan, 2003; Figure 4). The model gets its name from two rock units (the Baranof schist on Baranof Island and the Leech River schist on Southern Vancouver Island) that Cowan suggests are contiguous based on the paleo-location of the CPW terrane at 48°N. Because the Baranof–Leech River model advocates subduction of a single spreading ridge at 48°N, the theory must subsequently accommodate 1100 km of coastwise displacement for the CPW terrane (Figure 4). This

large coastwise transport distance is often where advocates of the opposing theory focus their criticism (Haeussler et al., 2003; Sisson et al., 2003b; Bradley et al., 2003; Farris and Paterson, 2009; Ayuso et al., 2009). Cowan attributes the majority of this northward coast-parallel displacement to early Tertiary (post-50 Ma) transport along the Border Ranges fault system (800 km) and, to a lesser extent, the Chatham Strait–Denali system (200 km).

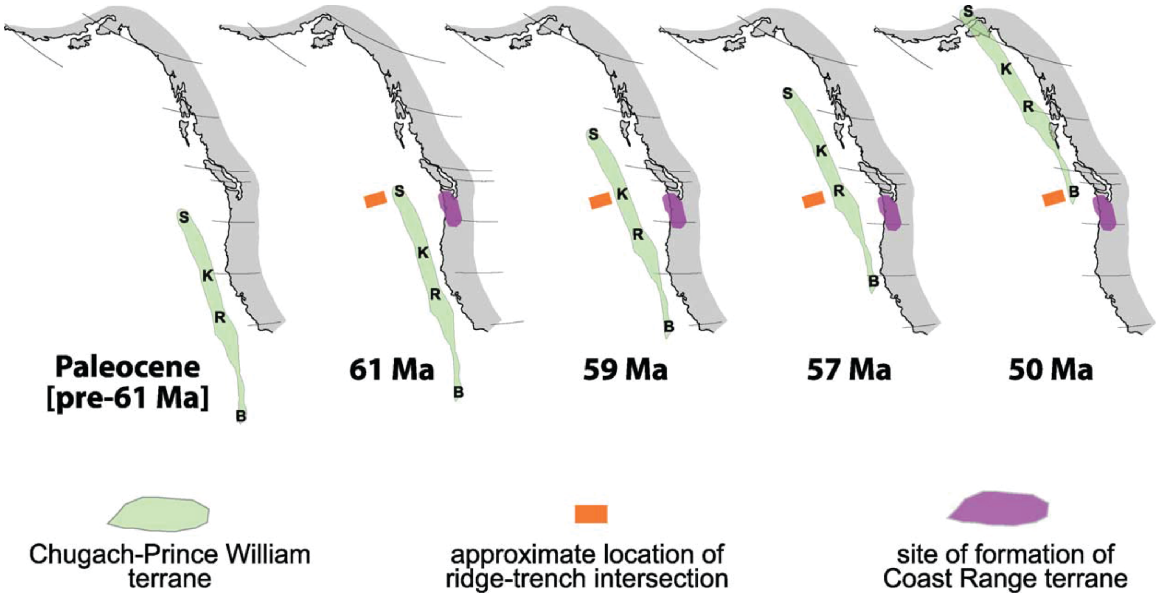


**Figure 4.** Simplified tectonic reconstruction for the Baranof-Leech River hypothesis proposed by Cowan (2003). This model involves a single, fixed-location T-R-T encounter at ~48 °N and the Chugach terrane passing sequentially over the slab window established in the forearc. Letters marked within the CPW terrane refer to the following locations of SBPB intrusions: S = Sanak Island; K = Kodiak Island; R = Resurrection ophiolite; B = Baranof Island. Figure taken from Cowan (2003).

The Resurrection plate hypothesis of Haeussler et al. (2003) refutes the single, fixed-location TRT intersection from Cowan's model and alternatively asserts that a plate is missing from tectonic reconstructions of the Paleocene-Eocene northeastern Pacific (Figure 5). They propose the existence of the Resurrection plate and its two resultant TRT triple junctions – an eastward migrating TRT intersection in southern Alaska and a

fixed-location TRT encounter in Cascadia – is a superior explanation for the onshore geologic record. This model assumes that the CPW terrane has always been located more or less where it is today, but it still allows for some motion along dextral transform faults. This model has generally been the preferred model in subsequent investigations of the SBPB (Bradley et al., 2003; Sisson et al., 2003b; Ayuso, 2009; Farris and Paterson, 2009). Other studies have expanded on Haeussler's original reconstruction and inserted additional microplates to the Cenozoic southern Alaska margin (Madsen et al., 2006).

Understanding and interpreting geochemical variations among the SBPB intrusions are critical to evaluations of the tectonic evolution of southern Alaska margin (Farris and Paterson, 2009). The goals of this study are two-fold. First, petrographic and geochemical data are used to inform the relationship between the Crawfish Inlet and Krestof Island plutons on Baranof Island to other igneous rocks of the SBPB and coeval plutons of the Coast Plutonic Complex (Figure 1). Trace element and isotopic data are then utilized in petrogenetic models to evaluate the relative contributions of mantle and crustal material to magmas emplaced as enclaves and their host granodiorites/tonalites.

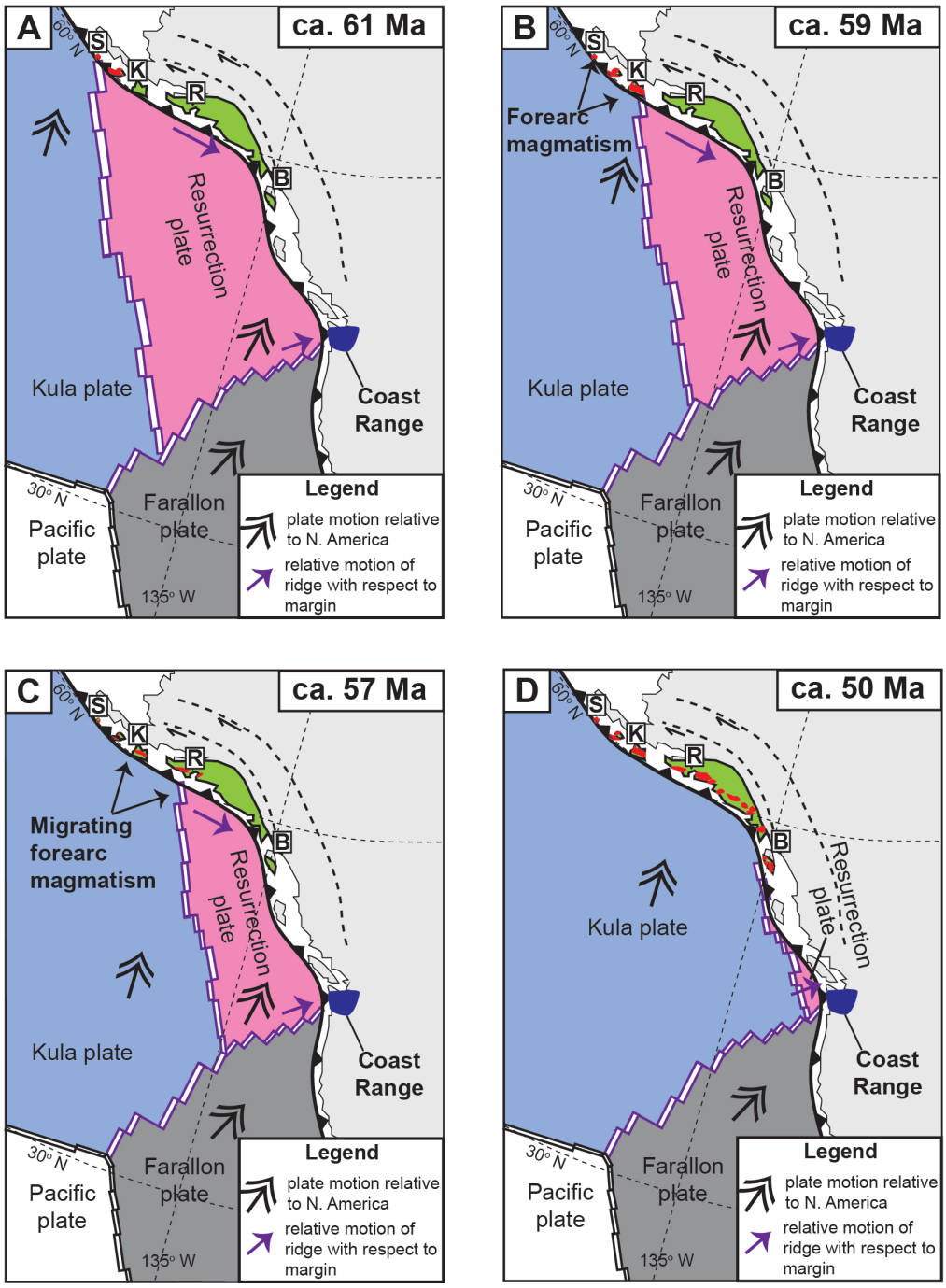


**Figure 5.** Schematic illustrating the evolution of the southern Alaska margin and Canadian Cordillera via the Resurrection plate hypothesis proposed by Hauessler et al. (2003). A. This panel shows the margin at 61 Ma with coeval magmatism at Sanak Island in the West and the Coast Range in Cascadia. B-D. These panels illustrate migrating magmatism in the Alaskan forearc at 59 Ma (Kodiak Island - K) and 57 Ma (Resurrection ophiolite - R). The 53-47 Ma plutons on Baranof Island were emplaced around the same time as the plate's hypothesized demise at 50 Ma. Marks for the SBPB intrusive suite are as in Figure 3. Figure modified from Hauessler et al., 2003.

# GEOLOGIC SETTING

*Regional Geologic Setting: Chugach-Prince William terrane*

The Crawfish Inlet and Krestof Island plutons intrude the Chugach-Prince William (CPW) terrane over 2100 km along the curvilinear Alaska margin from Sanak Island in the west to Baranof Island in the east (Figure 2). The CPW terrane, along with the Saint Elias and Ghost Rocks micro-terranes, make up the extensive Mesozoic to early Cenozoic accretionary complex called the Southern Margin composite terrane (Plafker et al., 1991). These accretionary terranes were emplaced sequentially against a series of 'backstop' terranes (i.e., Wrangellian composite terrane) at a time when the Kula and Farallon plates were moving N/NE relative to North America during the Late Cretaceous to Paleocene (Plafker et al., 1989; Plafker et al., 1991; Farmer et al., 1993).

The CPW terrane is composed largely (~ 90%) of Campanian to Maastrichtian volcaniclastic flysch and oceanic metabasalts. The flyschoid rocks of the Chugach terrane have been assigned multiple names depending on their location in the belt. For example, the Maastrichtian turbidites are called the Valdez group in Prince William Sound and the Sitka greywacke on Baranof Island. Despite their different names, these units are known to be contiguous and exhibit remarkably similar geochemical compositions (Plafker et al. 1989, 1987; Farmer et al., 1993). The extremely thick turbidites are thought to have formed over an extensive area on the floor of the Kula plate. Petrographic and geochemical evidence suggests the source of detritus for the turbidity deposits was a progressively eroded magmatic arc (Plafker et al., 1989; Lull and Plafker, 1985). The deposition of Late Cretaceous flysche in the Chugach terrane is thought to be a product of rapid uplift and weathering in the northern Coast Plutonic

Complex (CPC), which resulted in massive amounts of sediment accumulation along the continental shelf. The Chugach terrane is bounded by the Border Ranges fault system to the north and Contact fault system to the south (Figure 2; Plafker et al., 1989; Plafker et al., 1991).

The Late Paleocene to Early Eocene Orca Group underlies an area approximately 150 km wide from eastern Prince William Sound to Kodiak Island (Plafker et al., 1989; Plafker et al., 1991). The Orca Group makes up the entirety of the Prince William terrane, which bounds the Chugach terrane along the Contact fault system. New U-Pb zircon ages from Rick et al. (2014) extend the Prince William terrane all the way to southern Baranof Island (Figure 1), which has major implications for re-working depositional links across the southern Alaska margin as well as informing crustal contributions to magmas of the Crawfish and Krestof plutons. Petrographic and geochemical evidence also suggest a Coast Mountains provenance (i.e., Northern CPC) for the Orca Group (Farmer et al., 1993).

Previous studies considering the tectonic environment of the SBPB have attributed the anomalous forearc magmatism to subduction of a spreading ridge beneath the CPW terrane. This has been supported by petrogenetic studies suggesting that SBPB compositions are a combination of anatectic melts from the accretionary wedge and a mantle-derived component (Hudson et al., 1979; Hill et al., 1981; Sisson et al., 2003b; Bradley et al., 2003; Haeussler et al., 2003; Cowan, 2003; Ayuso et al., 2009). These studies consistently assume the mantle component to be N-MORB. Until this study, previous workers did not investigate the petrology and geochemistry of mafic magmatic enclaves emplaced within the SBPB intrusions.

Volcanic rocks occurring in the Coast Range basaltic terrane of northern Washington and Southern British Columbia are 62 – 48 Ma (Figure 1). The lavas have characteristics of both mid-ocean ridge basalt (MORB) and ocean island basalt (OIB). Thus, it's possible that other mantle sources, in addition to MORB sources, could have been present in the forearc during the Paleocene. Some studies that consider the composition, field relationships, and stratigraphy of the Crescent, Siletz River, and Metchosin volcanic rocks (that comprise the Coast Range basaltic terrane; Figures 1, 4 and 5) attributed their emplacement to the ancestral Yellowstone hot spot (Murphy et al., 2003). Other igneous island arc rocks with OIB compositions exist as accreted exotic terranes throughout the Cordillera (Murphy et al., 2003, and references therein). The presence of distinct mantle reservoirs throughout the Cordillera suggests that careful characterization of mafic magmas emplaced as enclaves within SBPB plutons may be useful in constraining the mantle source(s) of the SBPB intrusive suite.

*Paleocene Intrusive Rocks on Baranof Island*

The Crawfish Inlet pluton intrudes the Maastrichtian Sitka Graywacke and Paleocene Baranof Schist (thought to be correlative to the Orca Group in Prince William Sound; Rick et al., 2014) and is exposed over ~560 $km^2$ on southern Baranof Island in southeast Alaska (Loney et al., 1975; Figure 2). The Krestof Island pluton intruded older Albian-age accretionary wedge material slightly north of the Crawfish pluton and is exposed over ~ 80 $km^2$ (Figure 2). These plutons have been considered to mark the eastern boundary of the SBPB based on their anomalous forearc location and field relationships (Hudson et al., 1979; Haeussler et al., 2003; Bradley et al., 2003). Magmatic zircons from the Crawfish Inlet pluton yield U-Pb crystallization ages ranging from 53 to

47 Ma (Roig et al., 2014). Magmatic zircons from the Krestof pluton yield U-Pb crystallization ages of 52 Ma (Roig et al., 2014). The spatial (<75 km) and temporal proximity of the coeval Crawfish Inlet and Krestof Island plutons offers an opportunity to assess the geochemical composition of multiple SBPB intrusive bodies within a small area.

# FIELD RELATIONS

All samples were collected from the Crawfish Inlet and Krestof Island plutons exposed on Baranof Island, Alaska (see Appendix I). Study sites were restricted to outcrops exposed at sea level; the rugged terrain made sampling of the pluton interior extremely difficult. Because one of the goals of this study was to examine the geochemical nature of the parental magma(s) emplaced in the Crawfish and Krestof plutons, sampling of mafic magmatic enclaves was conducted. The abundance of enclaves was quite variable across the plutons. Two enclave swarms were identified (one in the Crawfish and one in the Krestof) and are shown in Figure 6.

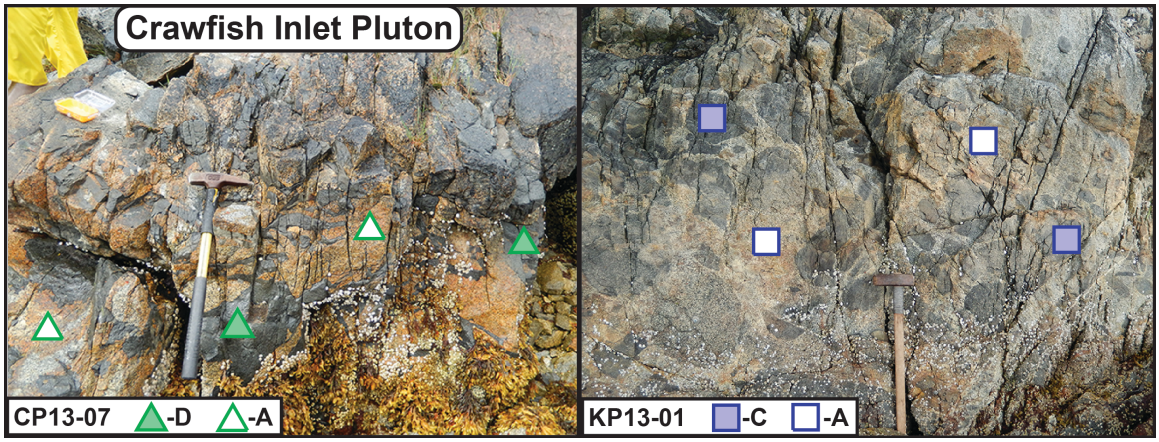


**Figure 6.** Field photos of enclave swarms emplaced in the Crawfish Inlet and Krestof Island plutons on Baranof Island, Alaska. The symbols overlaid on the photo establish a legend for the remainder of variation diagrams here. Filled green triangles represent Crawfish enclaves while open triangles indicate host tonalites/granodiorites. Filled purple squares indicate Krestof Island enclaves and open squares their host tonalites.

# ANALTYICAL METHODS

Thirty-one samples (16 enclaves, 15 host granitoids) were collected from the Crawfish Inlet and Krestof Island plutons. Of these 31, five were sampled from the Krestof pluton (three enclaves, two host granitoids). All samples were billeted for thin sections using an oil-based saw. Thin sections were prepared from the billets at both Carelton and Union Colleges.

*X-ray fluorescence and inductively coupled plasma-mass spectrometry analysis*

Twenty-three samples (14 enclaves, nine host granitoids) were selected for major and trace element analysis by XRF and ICP-MS at the Washington State University GeoAnalytical Laboratory in Pullman, WA. The least-altered chips from each of the samples were selected for powdering. In the case of enclaves containing some of the host granitoid in the sample, the granitoid portions were removed using a water-based trim saw. Selected chips were then sonicated for 45 minutes (three 15 minute sonication cycles with removal of the finest grains between each cycle) to remove unwanted dirt and dust. Sonicated samples were rinsed thoroughly with soapy water and pure isopropanol, then placed in an oven to dry at 105 °C overnight.

At the WSU GeoAnalytical Lab, fresh chips were made by a steel jaw crusher to less than 2-mm and then run through a rotary splitter to isolate 20 g fractions from each sample. Each 20 g fraction was ground to a fine powder in an agate ball mill for 2 minutes. Following powdering, 3.5 g of sample powder was transferred into a mixing jar with 7.0 g of pure dilithium tetraborate ($Li_2B_4O_7$) to create a 2:1 ratio sample:$Li_2B_4O_7$ powder that was mixed for 10 minutes. This mixed powder was transferred to a graphite

crucible and placed on a silica tray for fusion. Sample beads were fused in a furnace at 1000 °C for 5 minutes, removed and allowed to cool, then re-ground in the agate ball mill and fused at 1000 °C for another 5 minutes. Following the second fusion, sample beads were engraved and ground on 600 silicon carbide grit. The lower surface of the bead was ground flat before the beads were sonicated, rinsed with alcohol, and wiped dry. Once dry, beads were analyzed via X-ray fluorescence spectrometry using the ThermoARL Advant XP sequential X-ray fluorescence spectrometer.

Powdered samples were mixed with approximately 2 g of dilithium tetraborate flux and fused at 1000 °C in a furnace for 30 minutes. After allowing the bead to cool, the fusion bead was ground in a carbon-steel ring mill and 250 mg was weighed into a 30 mL Teflon vial for dissolution. The first dissolution step involved evaporation in 2 mL nitric acid ($HNO_3$), 6 mL hydrofluoric acid (HF), and 2 mL perchloric acid ($HClO_4$) at 110 °C. This mixture was evaporated to dryness before the vial was rinsed with a small amount of water and a second evaporation was executed with 2 mL $HClO_4$ at 160 °C. The sample was then brought into solution by adding approximately 10 mL nanopure $H_2O$, 3 mL $HNO_3$, 5 drops of hydrogen peroxide ($H_2O_2$), and 2 drops of HF while heating gently on a hot plate. The final solubilized sample was quantitatively transferred to a clean vial and diluted to a final weight of 60 g with nanopure $H_2O$.

Solutions were analyzed on an Agilent 4500 inductively coupled plasma-mass spectrometer. All samples were diluted an additional 10x during analysis using Agilent's integrated sampling system, yielding a final dilution factor of 1:4800 relative to the amount of original sample pre-fusion. Instrumental drift was corrected using Ru, In, and Re for internal standards. Long-term precision for the method is better than 5% relative

standard deviation for the rare earth elements (REEs) and about 10% for additional trace elements.

*Sr and Nd isotopic analysis*

Fourteen samples (eight enclaves, six host granitoids) were selected for Sr and Nd isotopic analysis at the Jackson School of Geosciences, University of Texas-Austin. Initial preparation of each sample required dissolving 20-40 mg aliquots of sample powders in Teflon high-pressure dissolution vessels with HF and $HNO_3$ for four days, followed by HCl for one day. Eichrom strontium specific residue was utilized to isolate Sr from each sample. For every one $\mu$L of sample that was taken, 2 N $HNO_3$ was added. Aliquots were then loaded and analyzed by Thermal Ionization Mass Spectrometry (TIMS).

All analyzed sample aliquots contained 10-30 $\mu$g of Sr. The full procedural blank analyzed during collection of the sample data yielded 100 pg Sr, so it can be assumed that only 100 pg of Sr was added to the samples during processing and analysis. Therefore, lab contamination is insignificant. Sr isotopic ratios were corrected for fractionation according to $^{88}Sr/^{86}Sr = 8.375209$ and an exponential fractionation law. The $^{88}Sr/^{84}Sr$, $^{84}Sr/^{86}Sr$, and $^{87}Sr/^{86}Sr$ isotopic ratios were also corrected for fractionation. In addition to fractionation, $^{87}Sr/^{86}Sr$ was corrected for $^{87}Rb$ based on simultaneous measurement of $^{85}Rb$ and $^{87}Rb/^{85}Rb = 0.38600$. The mean $^{87}Sr/^{86}Sr$ value for the NBS987 standard through 28 analyses over the previous six-months is $0.710228 \pm 0.000020$. All $^{87}Sr/^{86}Sr$ sample ratios were adjusted for the accepted isotopic composition for NBS987 of $^{87}Sr/^{86}Sr = 0.710248$. Finally, $^{87}Sr/^{86}Sr$ compositions were adjusted using the Rb and Sr

concentrations (ppm) and an age of 50.8 Ma ($t_{average} \approx 50.8$ Ma for Crawfish and Krestof plutonic rocks) to obtain the $^{87}Sr/^{86}Sr_{initial}$ ratio. Equations and constants utilized in the derivation of $^{87}Sr/^{86}Sr_{measured}$ and $^{87}Sr/^{86}Sr_{initial}$ are listed in Table 1.

**Table 1.** Correction factors, constants, and equations for Rb-Sr isotopic system

| | | |
|---|---|---|
| **Correction Factors** | $^{87}Rb/^{85}Rb$ | 0.3860* |
| | $^{88}Sr/^{86}Sr$ | 8.375209* |
| | $t_{sample}$ | 50.8 Ma |
| **Constants** | $t_{1/2}$ | $4.88 \times 10^{9}$ years |
| | $\lambda$ (Rb-Sr) | $1.42 \times 10^{-11}$ /yr |
| **Equations** | $^{87}Sr/^{86}Sr_{measured} = {}^{87}Sr/^{86}Sr_{initial} + {}^{87}Rb/^{86}Sr(e^{\lambda t} - 1)$ | |
| | $^{87}Sr/^{86}Sr_{initial} = {}^{87}Sr/^{86}Sr_{measured} - {}^{87}Rb/^{86}Sr(e^{\lambda t} - 1)$ | |

*From Rollinson (1993) and reference therein

Sample powders from Sr isotopic analysis were also used for Nd measurements. After dissolution in HF, $HNO_3$, and HCl, aliquots were loaded and analyzed by TIMS. All analyzed sample aliquots contained 200-700 ng of Nd, including the Nd spike for quantification. The full procedural blank analyzed during collection of the sample data yielded 15 pg Nd; thus, lab contamination is again insignificant. Nd isotopic ratios were corrected for fractionation according to $^{146}Nd/^{144}Nd = 0.7219$ and an exponential fractionation law. The $^{147}Sm/^{144}Nd$ isotopic ratio was measured using TIMS and $^{142}Nd/^{144}Nd$, $^{145}Nd/^{144}Nd$, $^{146}Nd/^{144}Nd$, $^{150}Nd/^{144}Nd$ and $^{143}Nd/^{144}Nd$ were recorded and corrected for fractionation in addition to $^{147}Sm$. All Nd data was also corrected for $^{144}Sm$ based on simultaneous measurement of $^{147}Sm$ and $^{144}Sm/^{147}Sm = 0.206700$. The mean $^{143}Nd/^{144}Nd$ value for five analyses of the Ames Nd standard over the previous six-months is $0.512083 \pm 0.000010$. All $^{143}Nd/^{144}Nd$ sample ratios were adjusted for the accepted isotopic composition of the Ames Nd standard. Finally, $^{143}Nd/^{144}Nd$ compositions were adjusted using the Sm and Nd concentrations (ppm) and an age of

50.8 Ma to obtain the $^{143}Nd/^{144}Nd_{initial}$ and $\varepsilon_{Nd}$ values. Equations and constants utilized in the determination of $^{143}Nd/^{144}Nd_{measured}$, $^{143}Nd/^{144}Nd_{initial}$, and $\varepsilon_{Nd}$ (normalized to the chondritic uniform reservoir – i.e., CHUR) are listed in Table 2.

**Table 2.** Correction factors, constants, equations, and normalization values for Sm-Nd isotopic system

| | | |
|---|---|---|
| **Correction Factors** | $^{144}Sm/^{147}Sm$ | 0.206700 |
| | $^{146}Nd/^{144}Nd$ | 0.7219* |
| | $^{146}Nd/^{142}Nd$ | 0.63223* |
| | $t_{sample}$ | 50.8 Ma |
| **Constants** | $t_{1/2}$ | $1.06 \times 10^{11}$ years |
| | $\lambda$ (Sm-Nd) | $6.54 \times 10^{-12}$ /yr |
| **Equations** | $^{143}Nd/^{144}Nd_{measured} = {}^{143}Nd/^{144}Nd_{initial} + {}^{147}Sm/^{144}Nd(e^{\lambda t} - 1)$ | |
| | $^{143}Nd/^{144}Nd_{initial} = {}^{143}Nd/^{144}Nd_{measured} - {}^{147}Sm/^{144}Nd(e^{\lambda t} - 1)$ | |
| | $\varepsilon_{Nd} = [[(^{143}Nd/^{144}Nd_{initial})/(^{143}Nd/^{144}Nd)_{CHUR,t=50.8}] - 1] \times 10^4$ | |
| **Normalizing values** | $^{144}Sm/^{147}Sm_{CHUR,today}$ | 0.1967* |
| | $^{143}Nd/^{144}Nd_{CHUR,today}$ | 0.512638* |
| | $^{143}Nd/^{144}Nd_{DM,today}$ | 0.513114* |

*From Rollinson (1993) and references therein

# RESULTS

*Petrography*

Igneous rocks of the Crawfish and Krestof Island plutons consist predominantly of biotite tonalite and biotite-hornblende granodiorites based on petrographic observations and Ab-An-Or normative mineralogy (Barker, 1979; Appendix II). Most samples are hypidiomorphic, with euhedral plagioclase and anhedral ferromagnesian phases. Most rocks of the granodiorite/tonalite suite exhibit seriate grain-size distributions, with some euhedral plagioclase grains displaying evidence for secondary alteration. Krestof Island samples are notably finer-grained and contain higher fractions of ferromagnesian phases and accessory opaque minerals than their Crawfish Inlet counterparts. Hornblende is relatively abundant in Krestof samples, which differs markedly from most Crawfish assemblages. None of the samples display the appropriate mineral assemblage for Al-in-hornblende geobarometry (Hammarstrom and Zen, 1986). Zircon and apatite are common accessory phases, with chlorite commonly present as a secondary mineral after biotite.

The granodiorites/tonalites contain inclusions that show strong evidence for magmatic quenching processes, including acicular apatite and poikilitic and myrmekitic textures (Flood and Vernon, 1988; Vernon, 1990). Thus, these inclusions are interpreted as being magmatic enclaves. Examples of acicular apatite and poikilitc textures are shown in Figures 7 and 8. These textural features are ubiquitous in the least evolved enclaves ($SiO_2 < 62$ wt%), and are rarely present in enclaves with $SiO_2 > 66$ wt% (Appendix III). These microstructural features are more abundant in the low $SiO_2$

Crawfish inclusions (CP13-07B and -07D) than their Krestof counterparts (KP13-01C, -02B, and -2C).

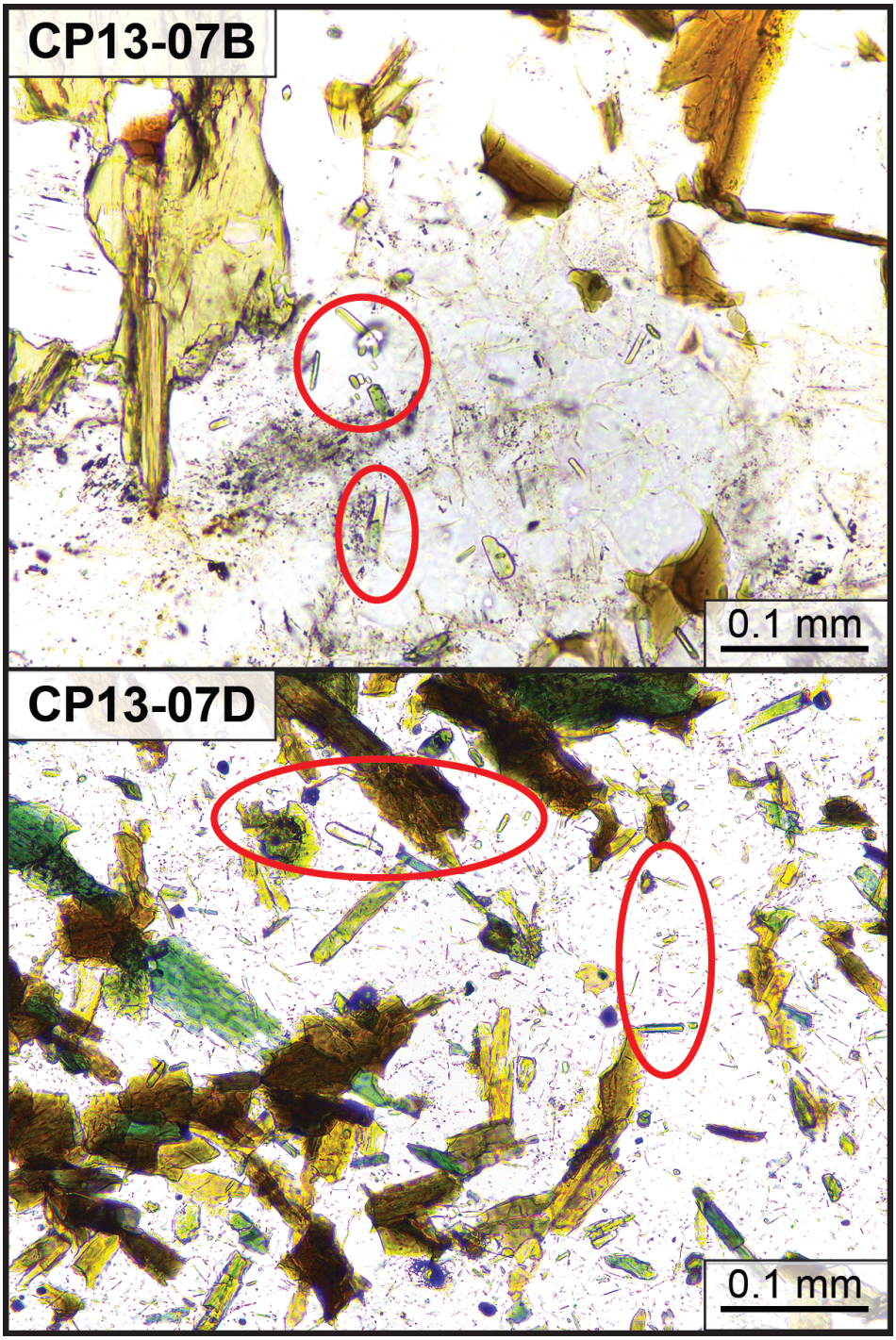


**Figure 7.** Photomicrographs showing microstructures indicative of quenching in least evolved Crawfish enclaves CP13-07B (top) and CP13-07D (bottom). The high relief, rod-like inclusions within the colorless plagioclase grains are acicular apatite (red circles).

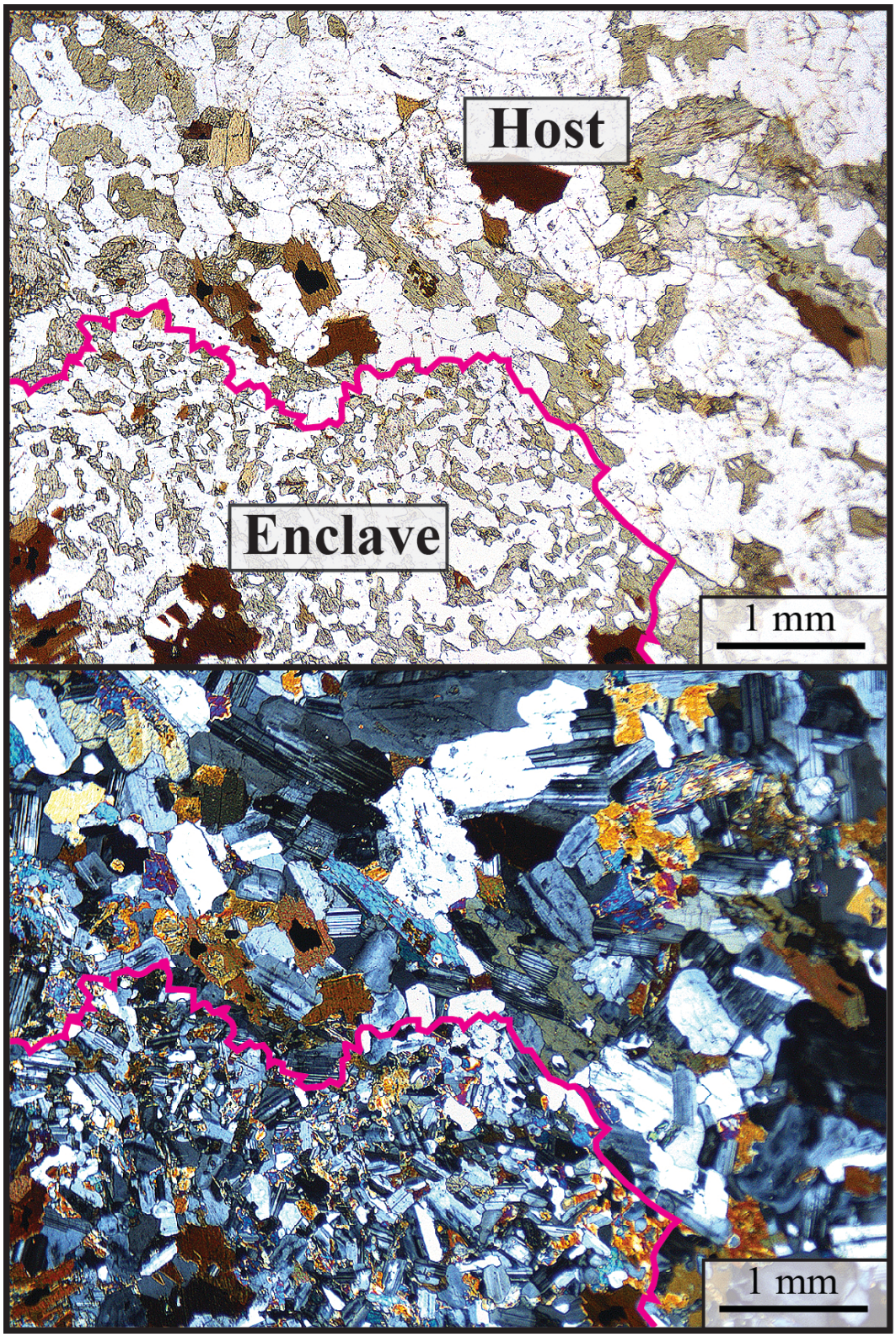


**Figure 8.** Photomicrographs (upper - uncrossed polars; lower - crossed polars) illustrating a crenulated contact (pink line) between enclave KP13-02B and its host.

*Whole-rock major element geochemistry*

All whole-rock major element data for Crawfish and Krestof samples are given in Table 3. All Crawfish and Krestof samples plot within the subalkaline field on a total alkalis versus $SiO_2$ (TAS) diagram (Figure 9). The two host granitoid samples from the Krestof pluton are classified as diorite and granodiorite. The Crawfish host granitoids are classified as granodiorites and granites. The enclaves show a wide range in composition, including gabbrodiorite, diorite, granodiorites, and granites. Enclaves with < 62 wt% $SiO_2$ are referred to as the least evolved enclaves. Evolved enclaves have > 66 wt% $SiO_2$.

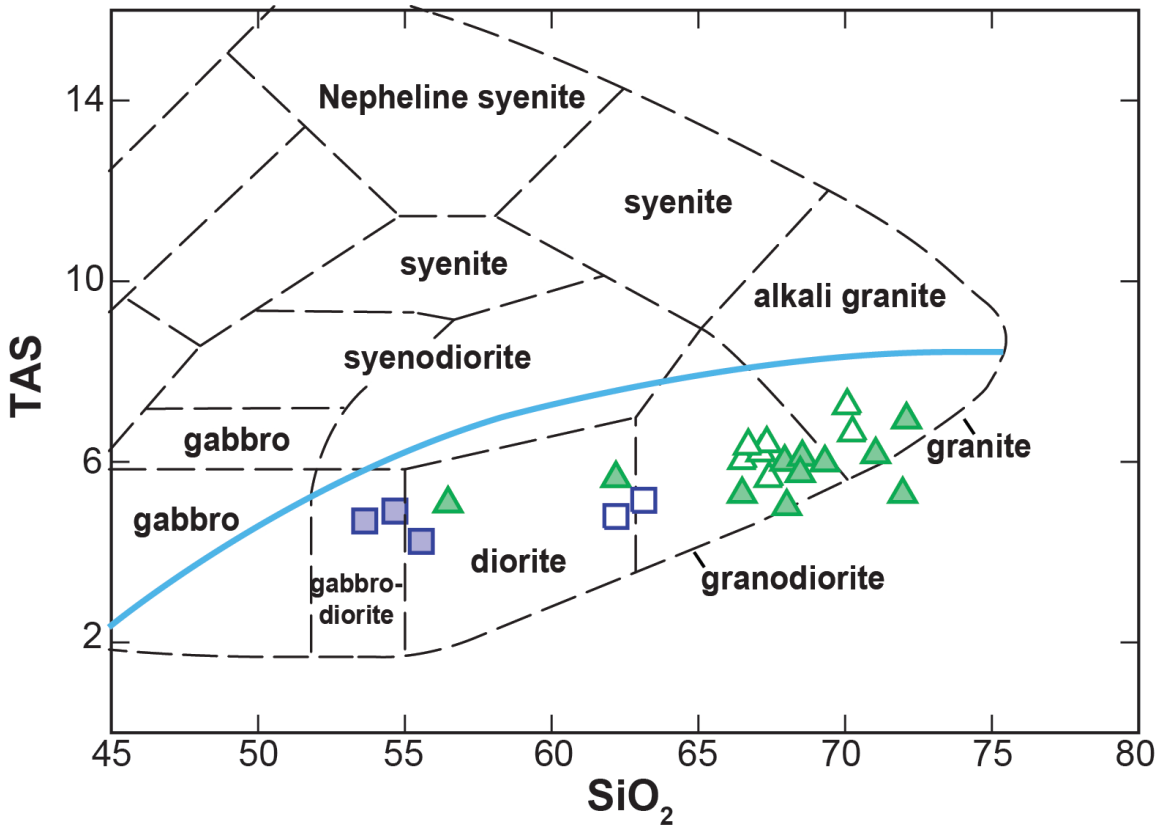


**Figure 9.** Crawfish and Krestof enclaves and host pluton samples plotted on the total alkalis ($Na_2O + K_2O$) versus wt% $SiO_2$ classification scheme for plutonic systems (Cox et al., 1979; Wilson, 1989). The blue curve separates alkalic from subalkalic rocks. Symbols as in Figure 6.

**Table 3.** Whole-rock major and trace element data

| Pluton Name | Crawfish | Crawfish | Crawfish | Crawfish | Crawfish |
|---|---|---|---|---|---|
| Sample | CP13-01 | CP13-03A | CP13-03B | CP13-03C | CP13-03D |
| Rock Type | host granodiorite | host granodiorite | enclave granite | enclave granite | enclave granodiorite |
| $SiO_2$ | 66.51 | 67.13 | 72.09 | 71.04 | 67.94 |
| $TiO_2$ | 0.45 | 0.42 | 0.21 | 0.29 | 0.37 |
| $Al_2O_3$ | 16.9 | 16.8 | 15.2 | 15.9 | 16.7 |
| FeO* | 3.31 | 3.14 | 2.09 | 2.47 | 3.04 |
| MnO | 0.06 | 0.06 | 0.04 | 0.06 | 0.06 |
| MgO | 1.32 | 1.40 | 0.62 | 1.01 | 1.35 |
| CaO | 4.34 | 4.17 | 2.52 | 3.36 | 3.95 |
| $Na_2O$ | 3.85 | 4.17 | 4.45 | 4.53 | 4.54 |
| $K_2O$ | 2.18 | 2.03 | 2.48 | 1.63 | 1.45 |
| $P_2O_5$ | 0.11 | 0.13 | 0.10 | 0.11 | 0.22 |
| Cs | 3.20 | 2.67 | 5.71 | 2.47 | 3.36 |
| Ba | 901 | 744 | 1218 | 580 | 513 |
| Rb | 67 | 61 | 75 | 59 | 67 |
| Sr | 267 | 434 | 356 | 326 | 392 |
| Y | 19.5 | 11.4 | 6.41 | 11.8 | 13.8 |
| Zr | 165 | 99 | 120 | 117 | 122 |
| Nb | 5.14 | 3.93 | 17.6 | 12.0 | 12.1 |
| V | 41 | 52 | 17 | 33 | 48 |
| Ni | 9 | 5 | 4 | 5 | 7 |
| Cu | 9 | 4 | 3 | 5 | 4 |
| Cr | 20 | 13 | 9 | 11 | 17 |
| Sc | 11 | 7 | 4 | 6 | 7 |
| Ga | 18 | 19 | 18 | 18 | 19 |
| Zn | 59 | 62 | 56 | 52 | 63 |
| La | 16.3 | 22.3 | 26.9 | 19.1 | 17.4 |
| Ce | 32.1 | 43.9 | 47.8 | 35.7 | 33.0 |
| Pr | 4.01 | 5.32 | 5.29 | 4.15 | 3.94 |
| Nd | 15.8 | 20.0 | 18.5 | 15.3 | 14.8 |
| Sm | 3.62 | 3.71 | 3.29 | 3.19 | 3.14 |
| Eu | 0.99 | 0.85 | 0.92 | 0.71 | 0.80 |
| Gd | 3.49 | 2.80 | 2.33 | 2.66 | 2.80 |
| Tb | 0.58 | 0.41 | 0.30 | 0.41 | 0.45 |
| Dy | 3.59 | 2.28 | 1.41 | 2.34 | 2.63 |
| Ho | 0.75 | 0.42 | 0.24 | 0.42 | 0.50 |
| Er | 2.10 | 1.14 | 0.57 | 1.09 | 1.36 |
| Tm | 0.32 | 0.17 | 0.08 | 0.16 | 0.19 |
| Yb | 2.01 | 1.02 | 0.48 | 0.99 | 1.20 |
| Lu | 0.33 | 0.16 | 0.08 | 0.15 | 0.18 |
| Hf | 4.44 | 2.60 | 3.26 | 3.56 | 3.24 |
| Ta | 0.41 | 0.42 | 0.92 | 1.62 | 1.14 |
| Th | 5.49 | 9.64 | 9.80 | 7.46 | 5.77 |
| U | 1.83 | 0.70 | 1.91 | 2.21 | 2.15 |
| Pb | 13.8 | 9.99 | 14.2 | 11.6 | 8.30 |

**Table 3.** Whole-rock major and trace element data (*cont.*)

| Crawfish CP13-06A host granodiorite | Crawfish CP13-06B enclave granodiorite | Crawfish CP13-07A host granodiorite | Crawfish CP13-07B enclave diorite | Crawfish CP13-07C enclave granodiorite | Crawfish CP13-07D enclave diorite |
|---|---|---|---|---|---|
| 67.41 | 68.54 | 67.33 | 56.47 | 68.01 | 62.19 |
| 0.43 | 0.34 | 0.41 | 1.05 | 0.39 | 0.76 |
| 16.7 | 16.9 | 16.9 | 16.2 | 16.3 | 16.6 |
| 3.38 | 2.78 | 3.13 | 7.40 | 3.68 | 5.24 |
| 0.06 | 0.05 | 0.07 | 0.14 | 0.07 | 0.11 |
| 1.65 | 1.32 | 1.46 | 4.49 | 1.26 | 2.73 |
| 4.40 | 4.25 | 3.92 | 7.24 | 4.78 | 5.60 |
| 4.08 | 4.56 | 4.16 | 3.48 | 4.04 | 4.05 |
| 1.55 | 1.54 | 2.24 | 1.59 | 0.97 | 1.58 |
| 0.12 | 0.14 | 0.12 | 0.73 | 0.18 | 0.47 |
| 4.19 | 2.79 | 4.62 | 6.44 | 3.69 | 7.97 |
| 532 | 582 | 765 | 433 | 212 | 451 |
| 59 | 45 | 74 | 45 | 28 | 55 |
| 293 | 413 | 367 | 719 | 172 | 721 |
| 10.6 | 8.31 | 9.88 | 20.7 | 19.4 | 17.5 |
| 81 | 114 | 91 | 217 | 149 | 228 |
| 4.15 | 4.30 | 4.44 | 11.0 | 3.68 | 13.5 |
| 57 | 42 | 49 | 196 | 45 | 137 |
| 11 | 6 | 7 | 43 | 6 | 17 |
| 12 | 5 | 7 | 26 | 13 | 13 |
| 25 | 22 | 15 | 66 | 9 | 26 |
| 8 | 6 | 8 | 20 | 8 | 12 |
| 18 | 19 | 19 | 20 | 17 | 20 |
| 60 | 58 | 64 | 119 | 34 | 93 |
| 12.0 | 13.3 | 10.1 | 34.9 | 8.30 | 36.3 |
| 22.7 | 26.2 | 19.4 | 69.1 | 18.3 | 70.9 |
| 2.70 | 3.20 | 2.39 | 8.69 | 2.45 | 8.56 |
| 10.2 | 12.0 | 9.26 | 34.4 | 10.3 | 32.2 |
| 2.19 | 2.42 | 2.14 | 6.35 | 2.67 | 5.52 |
| 0.76 | 0.79 | 0.74 | 1.84 | 0.92 | 1.56 |
| 2.04 | 1.90 | 1.96 | 5.05 | 2.97 | 4.20 |
| 0.32 | 0.28 | 0.30 | 0.73 | 0.51 | 0.59 |
| 1.94 | 1.63 | 1.82 | 4.09 | 3.31 | 3.35 |
| 0.39 | 0.31 | 0.36 | 0.81 | 0.71 | 0.66 |
| 1.08 | 0.83 | 0.99 | 2.14 | 2.00 | 1.78 |
| 0.16 | 0.12 | 0.15 | 0.31 | 0.31 | 0.26 |
| 1.01 | 0.76 | 0.94 | 1.91 | 2.05 | 1.69 |
| 0.17 | 0.13 | 0.15 | 0.31 | 0.35 | 0.28 |
| 2.24 | 2.91 | 2.51 | 5.62 | 3.68 | 5.97 |
| 0.47 | 0.35 | 0.45 | 0.56 | 0.30 | 0.79 |
| 5.29 | 4.23 | 4.71 | 6.72 | 1.26 | 7.71 |
| 1.00 | 1.57 | 1.90 | 2.91 | 0.53 | 3.63 |
| 9.46 | 7.99 | 12.0 | 4.21 | 2.07 | 5.85 |

**Table 3.** Whole-rock major and trace element data (*cont.*)

| Crawfish CP13-09A host granodiorite | Crawfish CP13-09B enclave granite | Crawfish CP13-09C enclave granodiorite | Crawfish CP13-12A host granite | Crawfish CP13-12B enclave granodiorite | Crawfish CP13-12C enclave granodiorite |
|---|---|---|---|---|---|
| 66.70 | 71.96 | 69.31 | 70.25 | 66.49 | 68.47 |
| 0.44 | 0.75 | 0.35 | 0.27 | 0.42 | 0.31 |
| 16.9 | 12.9 | 16.4 | 16.0 | 16.5 | 16.8 |
| 3.60 | 4.10 | 2.83 | 2.59 | 4.17 | 3.09 |
| 0.11 | 0.06 | 0.05 | 0.06 | 0.08 | 0.07 |
| 1.51 | 1.53 | 1.19 | 0.98 | 2.15 | 1.21 |
| 3.97 | 2.64 | 3.90 | 3.25 | 5.06 | 4.21 |
| 4.24 | 3.33 | 4.61 | 4.36 | 3.87 | 4.40 |
| 2.11 | 1.95 | 1.37 | 2.28 | 1.41 | 1.34 |
| 0.12 | 0.17 | 0.11 | 0.09 | 0.18 | 0.08 |
| 2.48 | 2.06 | 1.73 | 3.47 | 6.59 | 4.27 |
| 715 | 774 | 336 | 624 | 384 | 319 |
| 66 | 68 | 49 | 69 | 53 | 66 |
| 342 | 219 | 336 | 329 | 273 | 346 |
| 12.3 | 8.64 | 10.2 | 12.4 | 14.7 | 7.73 |
| 109 | 168 | 97 | 91 | 134 | 87 |
| 5.95 | 7.28 | 4.31 | 6.01 | 6.79 | 6.54 |
| 62 | 77 | 48 | 33 | 62 | 40 |
| 7 | 10 | 6 | 4 | 22 | 1 |
| 6 | 4 | 0 | 2 | 19 | 3 |
| 14 | 14 | 11 | 7 | 50 | 6 |
| 13 | 6 | 7 | 5 | 9 | 6 |
| 19 | 16 | 17 | 17 | 18 | 18 |
| 74 | 73 | 55 | 52 | 64 | 62 |
| 11.4 | 11.6 | 11.8 | 10.7 | 12.3 | 2.33 |
| 21.6 | 21.6 | 22.8 | 20.7 | 24.6 | 4.57 |
| 2.57 | 2.53 | 2.72 | 2.47 | 3.09 | 0.63 |
| 9.81 | 9.67 | 10.5 | 9.50 | 12.4 | 2.95 |
| 2.33 | 1.98 | 2.22 | 2.15 | 2.78 | 1.01 |
| 0.68 | 0.57 | 0.66 | 0.59 | 0.87 | 0.50 |
| 2.33 | 1.74 | 2.08 | 2.03 | 2.73 | 1.23 |
| 0.38 | 0.27 | 0.35 | 0.35 | 0.45 | 0.22 |
| 2.24 | 1.55 | 1.96 | 2.11 | 2.69 | 1.31 |
| 0.45 | 0.32 | 0.38 | 0.43 | 0.54 | 0.27 |
| 1.27 | 0.88 | 1.03 | 1.23 | 1.52 | 0.77 |
| 0.19 | 0.13 | 0.15 | 0.19 | 0.22 | 0.12 |
| 1.34 | 0.87 | 0.92 | 1.27 | 1.44 | 0.80 |
| 0.23 | 0.16 | 0.14 | 0.21 | 0.23 | 0.13 |
| 2.89 | 4.32 | 2.64 | 2.68 | 3.38 | 2.47 |
| 0.59 | 0.48 | 0.34 | 0.75 | 0.55 | 0.71 |
| 4.48 | 2.96 | 4.56 | 5.20 | 3.37 | 1.77 |
| 4.06 | 1.00 | 0.82 | 3.38 | 1.43 | 1.66 |
| 8.36 | 5.27 | 7.79 | 11.5 | 4.33 | 9.52 |

**Table 3.** Whole-rock major and trace element data (*cont.*)

| Crawfish CP13-13 host granite | Krestof KP13-01A host granodiorite | Krestof KP13-01C enclave diorite | Krestof KP13-02A host diorite | Krestof KP13-02B enclave gabbrodiorite | Krestof KP13-02C enclave gabbrodiorite |
|---|---|---|---|---|---|
| 70.07 | 63.14 | 55.56 | 62.19 | 53.63 | 54.66 |
| 0.29 | 0.73 | 0.53 | 0.72 | 0.66 | 0.60 |
| 16.1 | 17.7 | 16.1 | 16.8 | 17.6 | 17.6 |
| 2.26 | 5.41 | 7.69 | 5.56 | 7.54 | 7.17 |
| 0.04 | 0.10 | 0.15 | 0.10 | 0.15 | 0.14 |
| 0.66 | 1.88 | 6.74 | 3.40 | 5.60 | 5.60 |
| 2.98 | 5.49 | 8.64 | 5.97 | 9.25 | 9.40 |
| 4.18 | 4.22 | 3.77 | 3.38 | 3.57 | 3.54 |
| 3.06 | 0.93 | 0.47 | 1.41 | 1.12 | 1.37 |
| 0.07 | 0.16 | 0.11 | 0.15 | 0.11 | 0.09 |
| 3.38 | 1.63 | 0.58 | 2.15 | 1.06 | 1.38 |
| 843 | 411 | 205 | 541 | 444 | 580 |
| 101 | 29 | 12 | 48 | 32 | 39 |
| 204 | 262 | 265 | 231 | 252 | 244 |
| 23.3 | 17.4 | 34.2 | 20.7 | 27.7 | 27.4 |
| 125 | 124 | 63 | 139 | 47 | 57 |
| 7.02 | 4.93 | 4.00 | 6.07 | 3.88 | 3.57 |
| 21 | 87 | 139 | 98 | 136 | 140 |
| 4 | 7 | 78 | 20 | 30 | 28 |
| 4 | 7 | 189 | 24 | 50 | 49 |
| 9 | 10 | 289 | 51 | 52 | 63 |
| 7 | 12 | 24 | 17 | 27 | 26 |
| 19 | 19 | 17 | 16 | 16 | 16 |
| 49 | 79 | 107 | 75 | 96 | 88 |
| 26.0 | 10.1 | 13.8 | 14.4 | 12.9 | 12.6 |
| 50.1 | 20.4 | 32.7 | 28.8 | 25.8 | 25.9 |
| 5.92 | 2.64 | 4.62 | 3.60 | 3.50 | 3.48 |
| 22.3 | 10.9 | 19.4 | 14.4 | 15.1 | 15.0 |
| 4.72 | 2.70 | 4.93 | 3.44 | 4.16 | 4.14 |
| 0.74 | 0.98 | 1.07 | 0.93 | 1.04 | 1.01 |
| 4.28 | 2.86 | 5.14 | 3.54 | 4.57 | 4.46 |
| 0.72 | 0.49 | 0.93 | 0.60 | 0.83 | 0.80 |
| 4.36 | 3.18 | 6.02 | 3.80 | 5.30 | 5.21 |
| 0.88 | 0.66 | 1.30 | 0.81 | 1.11 | 1.08 |
| 2.52 | 1.89 | 3.75 | 2.26 | 3.01 | 2.94 |
| 0.38 | 0.28 | 0.58 | 0.34 | 0.44 | 0.43 |
| 2.46 | 1.79 | 3.67 | 2.11 | 2.67 | 2.67 |
| 0.39 | 0.30 | 0.60 | 0.34 | 0.42 | 0.42 |
| 3.95 | 3.18 | 2.13 | 3.66 | 1.33 | 1.57 |
| 0.65 | 0.34 | 0.27 | 0.44 | 0.25 | 0.24 |
| 10.89 | 2.74 | 2.05 | 4.28 | 0.93 | 1.73 |
| 2.84 | 0.96 | 0.79 | 1.15 | 0.41 | 0.59 |
| 19.7 | 6.40 | 6.51 | 8.54 | 9.80 | 9.32 |

CIPW normative compositions for albite (Ab), anorthite (An), orthoclase (Or), and quartz (Q) were calculated for all Crawfish and Krestof samples (Table 4). Ab-An-Or normative mineralogies were used in conjunction with the classification scheme of Barker (1979) for the host granitoid rocks. Krestof Island samples are classified as tonalites, and Crawfish Inlet samples are classified as tonalites and granodiorites (Figure 10). This is consistent with the observation that potassium feldspar is an accessory phase and/or completely absent from most Crawfish and Krestof plutonic samples.

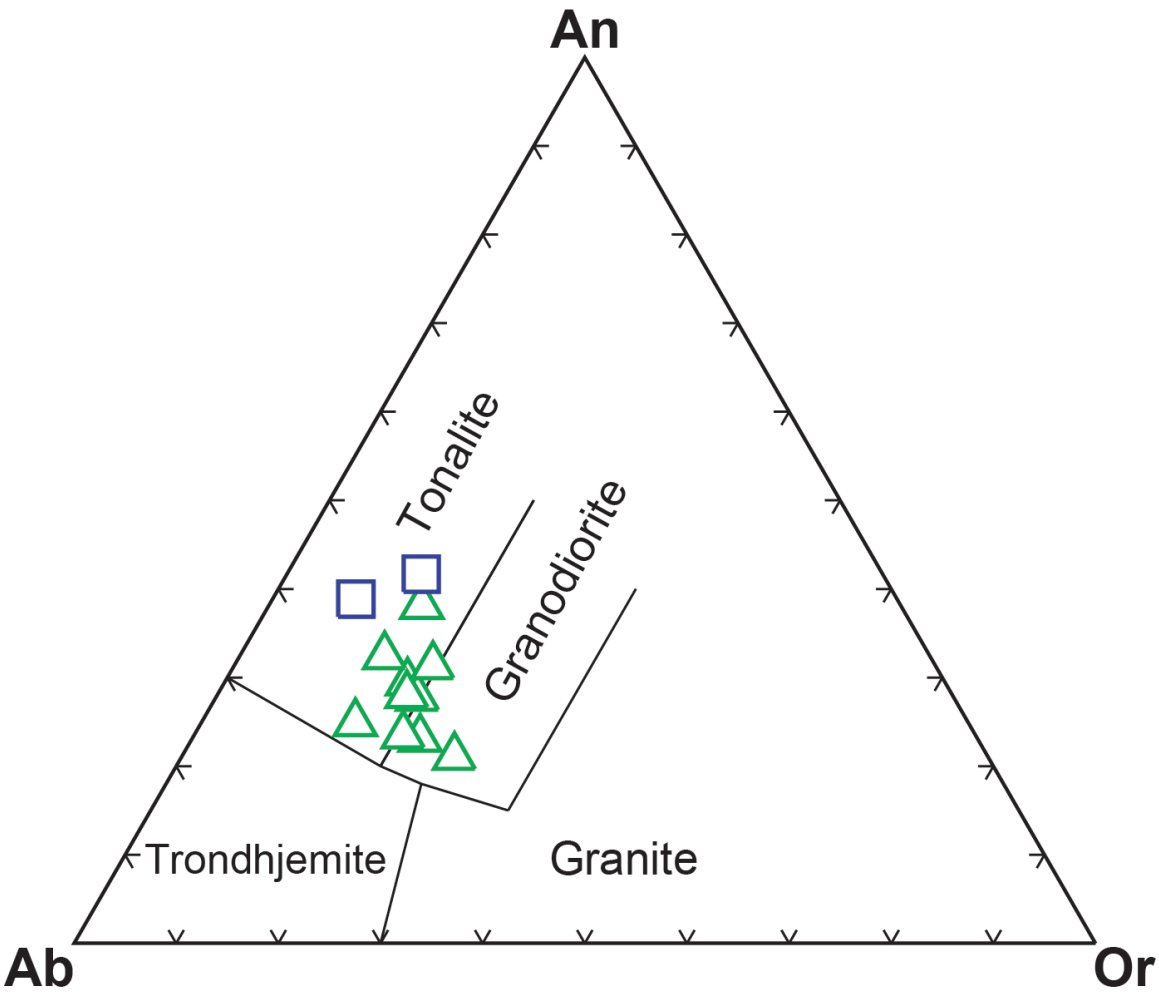


**Figure 10.** Plot of CIPW normative albite (Ab), anorthite (An), and orthoclase (Or) compositions for Crawfish and Krestof host granodiorites/tonalites. Petrographic fields defined by Barker (1979) are show. Symbols as in Figure 6.

**Table 4.** CIPW normative mineralogy for Crawfish and Krestof samples

| Sample | Q | Or | Ab | An |
|---|---|---|---|---|
| KP13-01A | 16.9 | 5.5 | 35.7 | 26.2 |
| KP13-01C | 1.0 | 2.8 | 31.9 | 25.5 |
| KP13-02A | 16.0 | 8.3 | 28.6 | 26.4 |
| KP13-02B | - | 6.6 | 30.2 | 28.7 |
| KP13-02C | - | 8.1 | 30.0 | 28.2 |
| CP13-01 | 22.3 | 12.9 | 32.6 | 20.8 |
| CP13-03A | 22.1 | 12.0 | 35.3 | 19.8 |
| CP13-03B | 29.0 | 14.7 | 37.7 | 11.9 |
| CP13-03C | 28.2 | 9.6 | 38.3 | 16.0 |
| CP13-03D | 23.8 | 8.6 | 38.4 | 18.2 |
| CP13-06A | 23.6 | 9.2 | 34.5 | 21.0 |
| CP13-06B | 23.3 | 9.1 | 38.6 | 20.2 |
| CP13-07A | 22.0 | 13.2 | 35.2 | 18.7 |
| CP13-07B | 6.0 | 9.4 | 29.5 | 24.0 |
| CP13-07C | 26.3 | 5.7 | 34.2 | 22.5 |
| CP13-07D | 14.4 | 9.3 | 34.3 | 22.5 |
| CP13-09A | 20.8 | 12.5 | 35.9 | 18.9 |
| CP13-09B | 34.8 | 11.5 | 28.2 | 12.0 |
| CP13-09C | 25.3 | 8.1 | 39.0 | 18.6 |
| CP13-12A | 26.0 | 13.5 | 36.9 | 15.5 |
| CP13-12B | 21.9 | 8.3 | 32.8 | 23.6 |
| CP13-12C | 24.7 | 7.9 | 37.2 | 20.4 |
| CP13-13 | 25.2 | 18.1 | 35.4 | 14.3 |

All Crawfish and Krestof samples plot within the calc-alkaline field on an AFM diagram after Irvine and Baragar (Figure 11). Figure 12 shows Crawfish and Krestof samples on a diagram of aluminum saturation index (ASI) versus $SiO_2$. ASI is defined as the molecular ratio of $Al_2O_3/[CaO + Na_2O + K_2O]$ (Shand, 1951). All Krestof samples (both enclaves and host tonalites) are metaluminous, meaning they display ASI < 1. The majority of Crawfish samples are peraluminous (ASI > 1), with the exception of enclaves containing less than 66 wt % $SiO_2$ (samples CP13-07B, -07D, and -12B). None of the Crawfish or Krestof rocks plot in the S-type field for ASI > 1.1 defined by White et al. (1986).

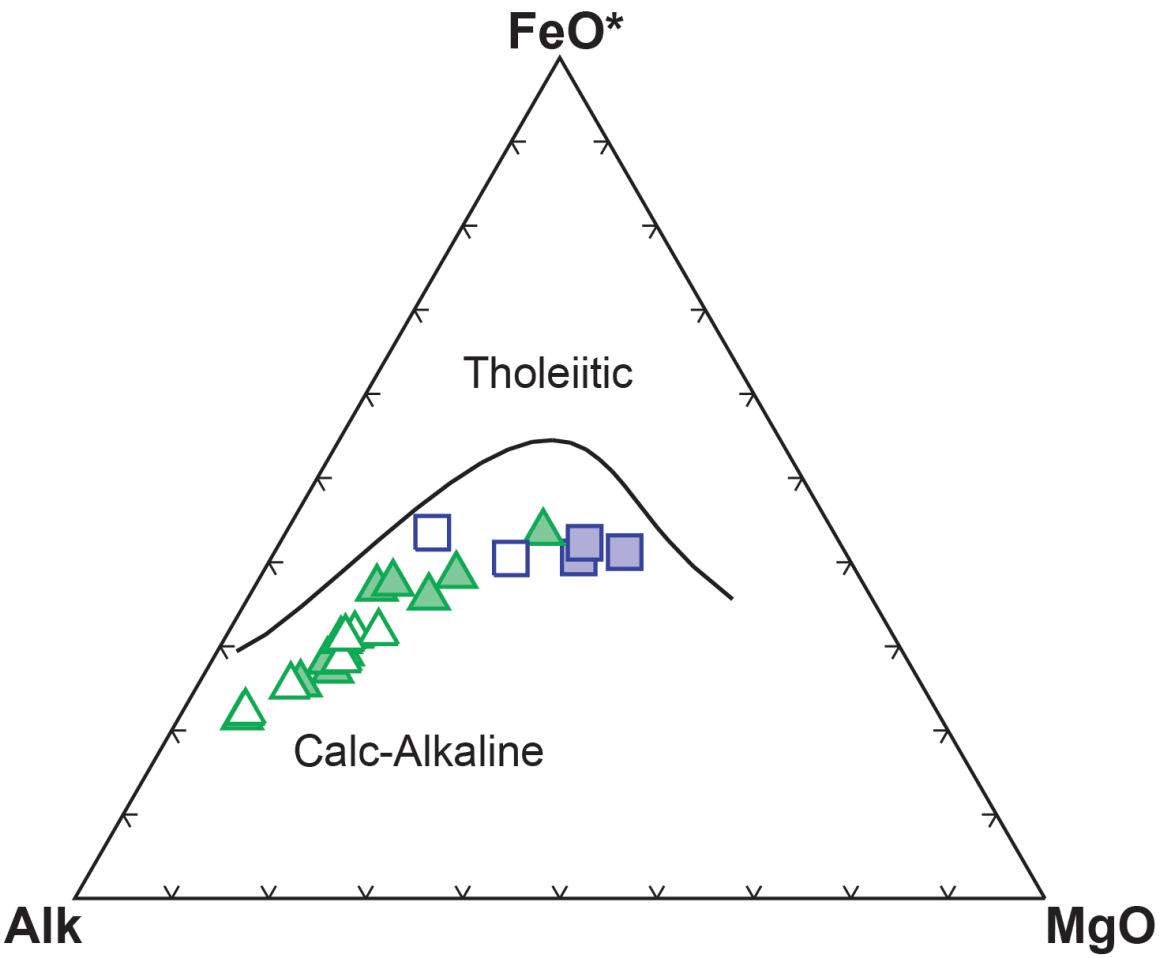


**Figure 11.** AFM diagram (after Irvine and Baragar, 1971) showing Crawfish Inlet and Krestof Island samples. Alk = $Na_2O + K_2O$. Symbols as in Figure 6.

Major element Harker diagrams for all Crawfish and Krestof samples (enclaves and host granodiorites/tonalities) are shown in Figure 13. FeO*, MgO, and CaO exhibit negative correlations with wt % $SiO_2$. $Al_2O_3$ exhibits a broad negative correlation with $SiO_2$, while $K_2O$ and $Na_2O$ display broadly positive correlations with $SiO_2$. Krestof enclaves and host granodiorites are significantly lower in $SiO_2$ than samples from the Crawfish pluton, excluding least evolved Crawfish enclaves CP13-07B and 07D. Crawfish enclave CP13-09B is notably higher in FeO and $TiO_2$ and lower in $Al_2O_3$ and $Na_2O$ compared to other high silica (>70 wt%) enclaves sampled from the Crawfish pluton. Least evolved Crawfish enclaves CP13-07B and 07D are notably enriched in

$TiO_2$ compared to all Crawfish samples except CP13-09B. Host tonalite samples from the Krestof pluton fall along similar trends defined by the Crawfish granodiorites/tonalites. The low $SiO_2$ enclaves from the Krestof pluton have notably lower abundances of $TiO_2$ and $P_2O_5$ compared to those from the Crawfish.

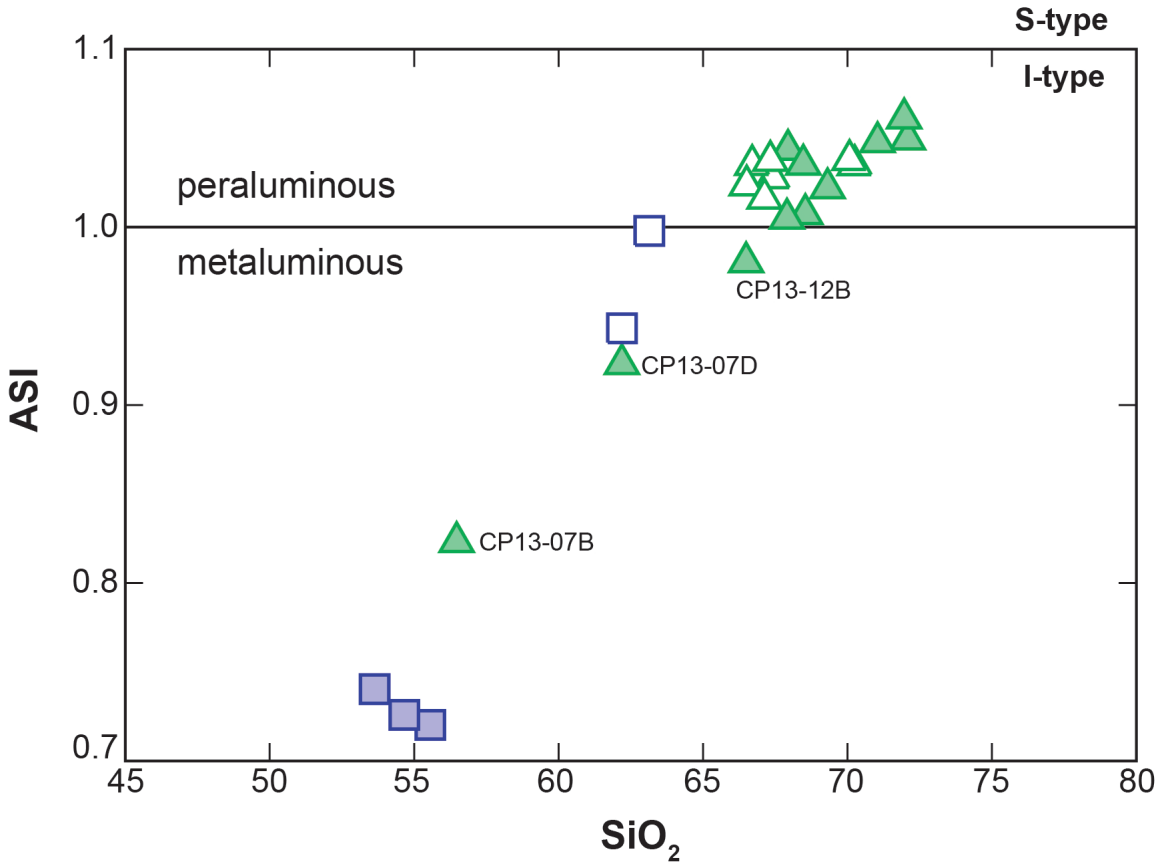


**Figure 12.** Discrimination plot of $Al_2O_3/(K_2O + Na_2O + CaO)$, commonly referred to as the aluminum saturation index, versus $SiO_2$ for enclaves and host granodiorites/tonalites from the Crawfish and Krestof plutons. Peraluminous-metaluminous boundary from Shand (1951); S-type/I-type boundary at ASI = 1.1 from White et al. (1986).

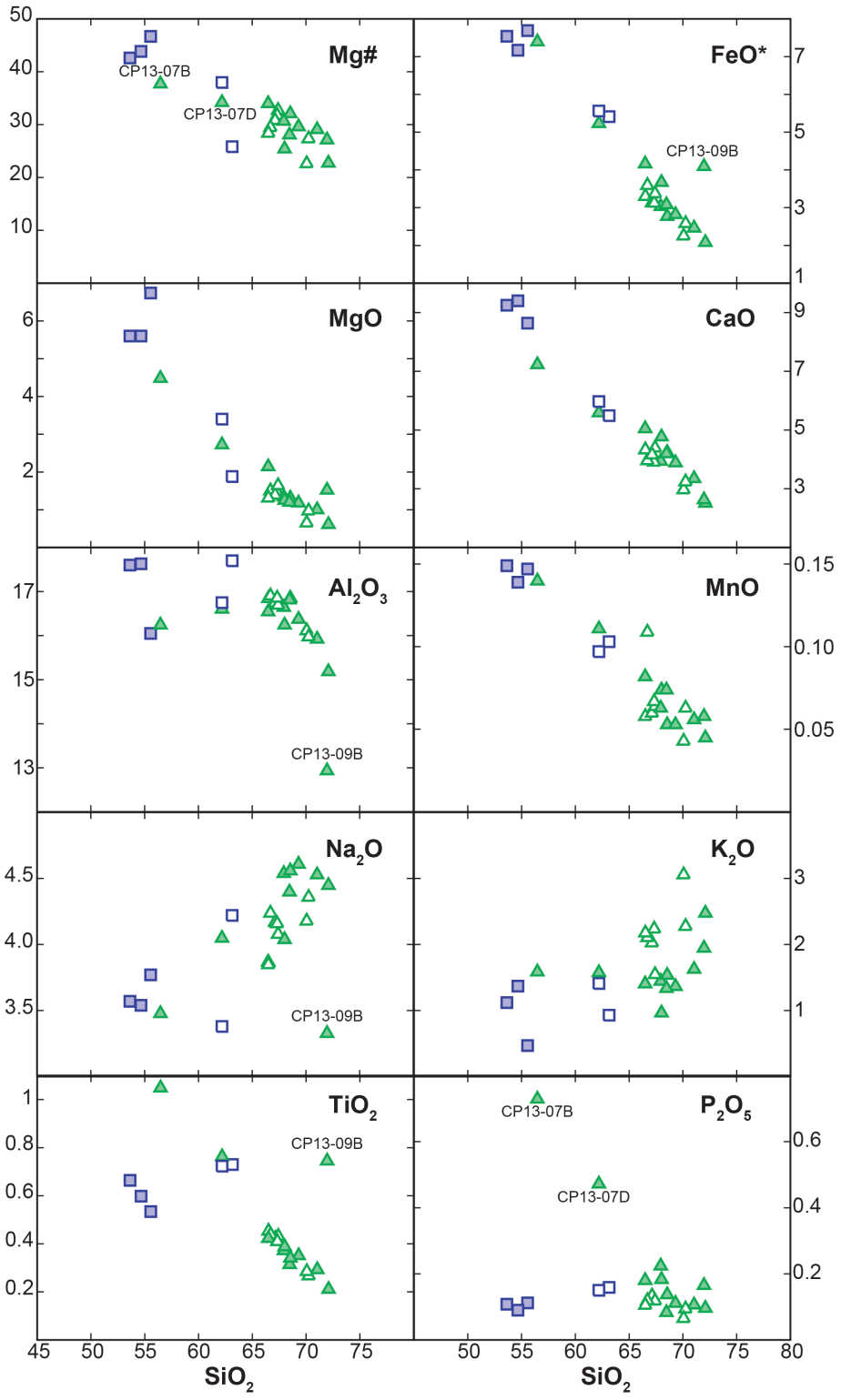


**Figure 13.** Major element Harker diagrams for Crawfish and Krestof samples. Mg# corresponds to 100 × (MgO/MgO + FeO*) where FeO* is representative of total Fe (i.e. FeO* = FeO + 0.9$Fe_2O_3$). All values are normalized to 100%. Major element compositions and Mg# are given in wt% oxides. Symbols as in Figure 6.

*Whole-rock trace element geochemistry*

Table 3 gives whole-rock trace element data for Crawfish and Krestof samples. Harker diagrams for transition metals (Ni, Cr, Sc, and V) are shown in Figure 14. Krestof enclave KP13-01C is significantly higher in Ni, Cr, and Cu (not shown) than all other Crawfish and Krestof samples (Figure 14). Crawfish enclaves 07B, 07D, and 09B are enriched in V relative to other samples.

Figure 15 shows other trace elements plotted versus wt% $SiO_2$. In contrast to major elements, there is less systematic variation between trace elements and $SiO_2$. Once again, geochemical distinctions are seen between the least evolved Crawfish and Krestof enclaves. The Krestof enclaves are depleted in Ta, Nb, Sr, and La but enriched in Y and Yb compared to least evolved Crawfish enclaves CP13-07B and -07D.

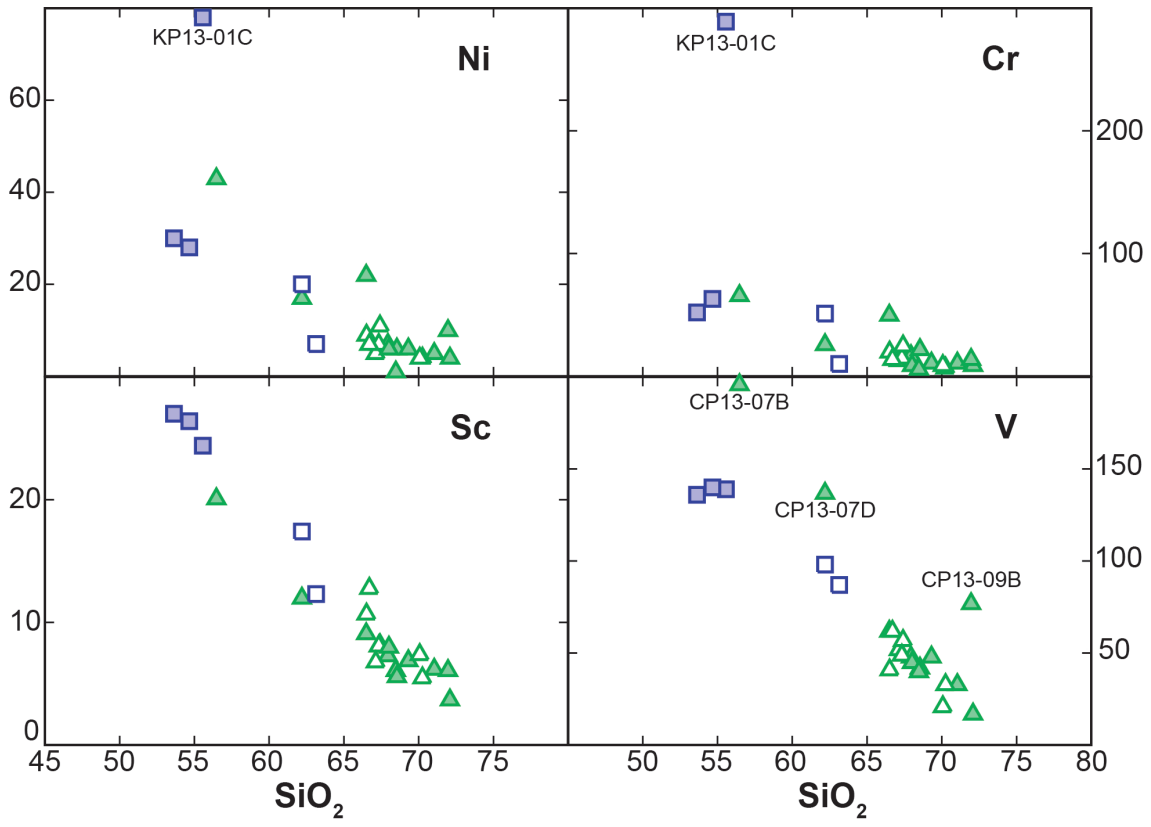


**Figure 14.** Transition metal elements plotted versus $SiO_2$ for all Crawfish and Krestof samples. All trace element abundances are in ppm. Symbols as in Figure 6.

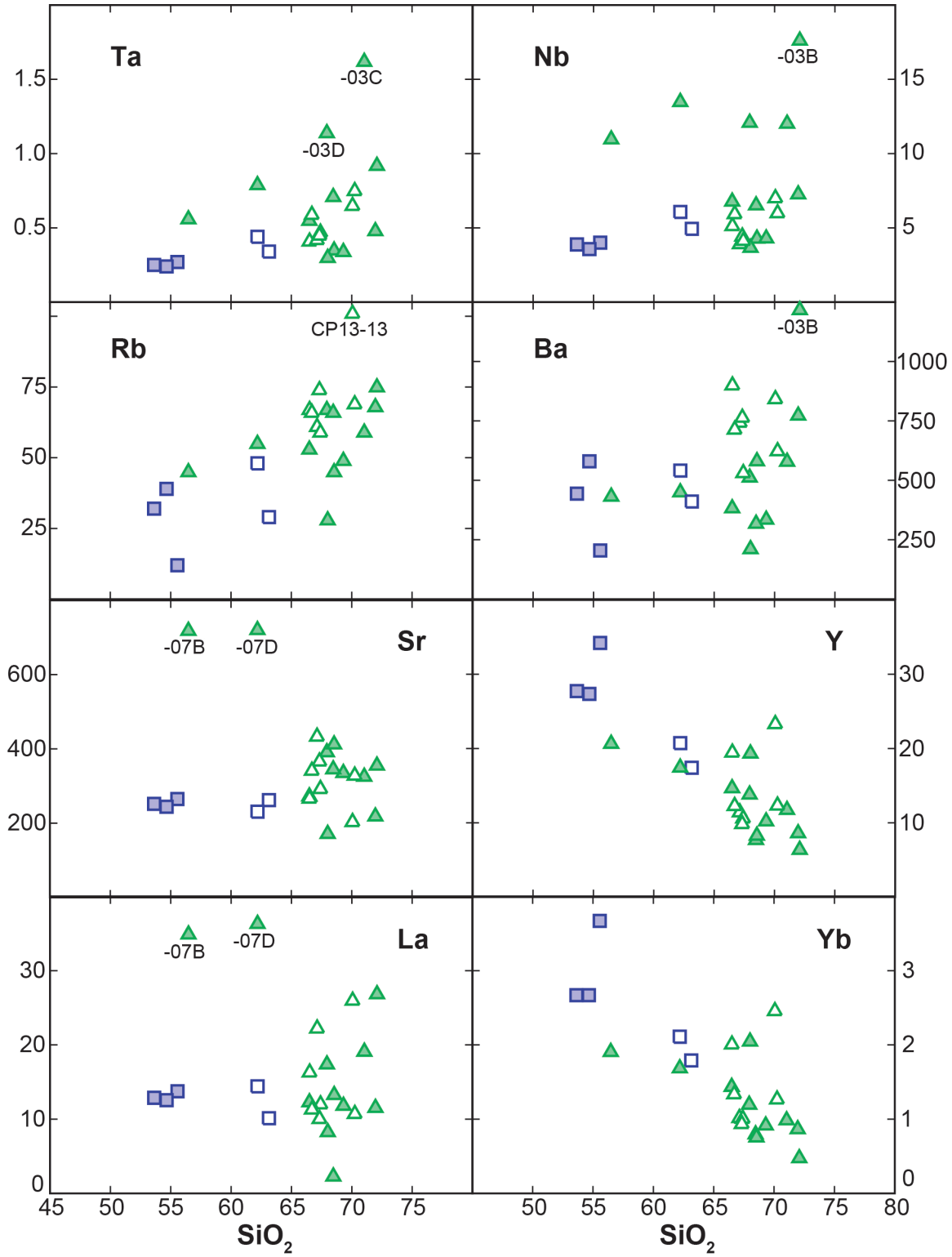


**Figure 15.** Select trace elements plotted versus $SiO_2$. All trace element abundances are in ppm. Symbols as in Figure 6.

The majority of Crawfish and Krestof samples plot within the field defined for volcanic arc granites (VAG) on various trace element discrimination diagrams for plutonic systems (Pearce et al., 1984). Figure 16 illustrates the discrimination diagram for Yb versus Ta.

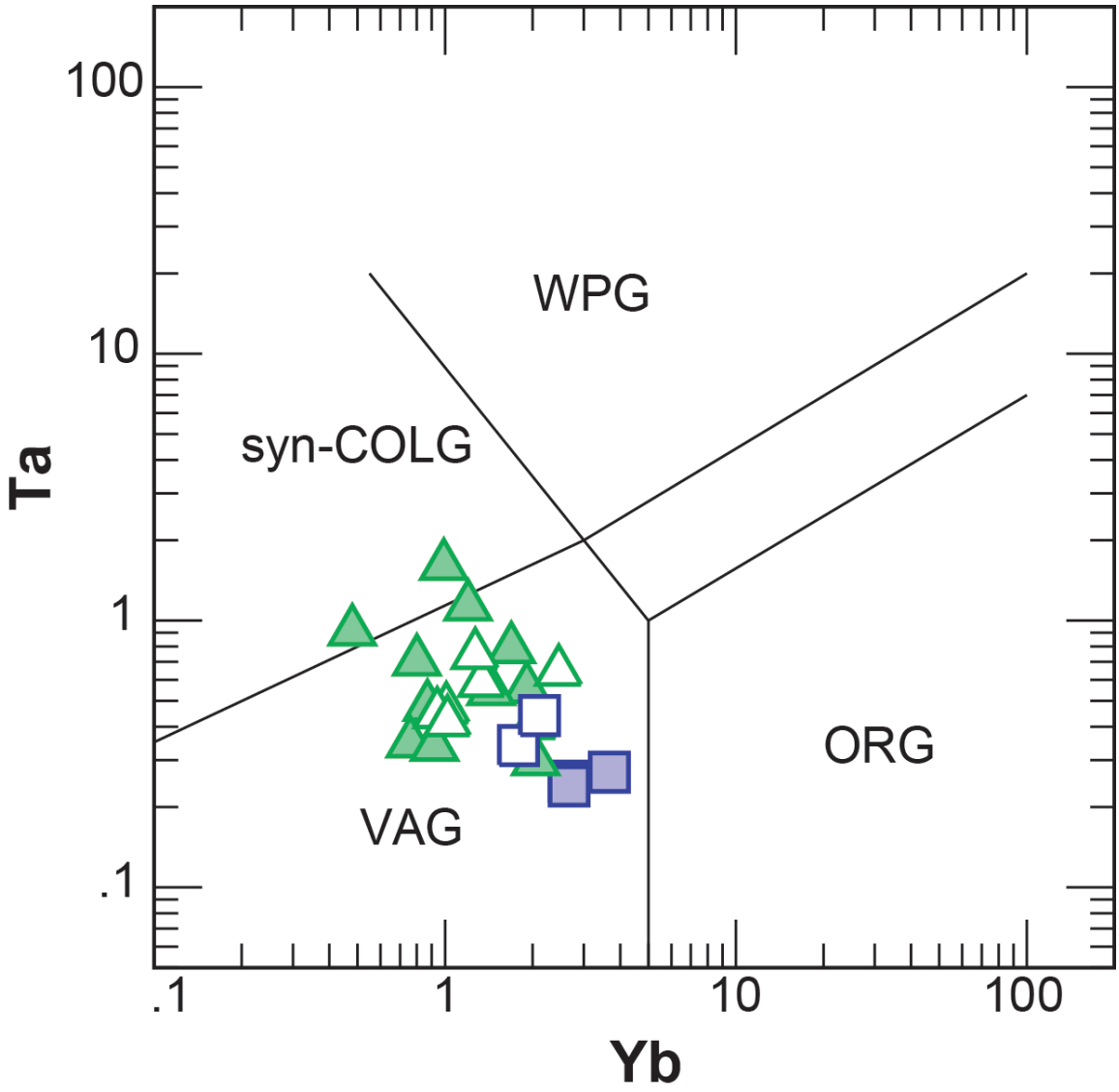


**Figure 16.** Ta versus Yb discrimination diagram after Pearce et al. (1984) showing all Crawfish and Krestof samples. Abbreviations as follows: WPG = within-plate granites; ORG = ocean-ridge granites; VAG = volcanic arc granites; syn-COLG = syn-collisional granites.

Chondrite-normalized rare earth element (REE) diagrams for enclaves and their host granodiorites/tonalites from the Krestof and Crawfish pluton are shown in the Figure 17. With one exception (CP13-12C), all samples are light rare earth element (LREE) enriched. However, the steepness of the profiles is variable. Krestof Island samples display relatively flat REE profiles, and most exhibit slight Eu anomalies. REE profiles of low-$SiO_2$ Krestof enclaves closely resemble those of their host tonalites (Figure 17D). In contrast, least evolved ($SiO_2$ < 62 wt%) Crawfish enclaves are more enriched in all REEs relative to their host (Figure 17C). More evolved enclaves are similar to their hosts in exhibiting LREE-enrichment, but show greater variability in their profiles (Figure 17B). Sample CP13-12C is unusual, with its relatively flat profile and positive Eu anomaly. Enclave CP13-03B has the steepest REE pattern among samples considered here (Figure 17B).

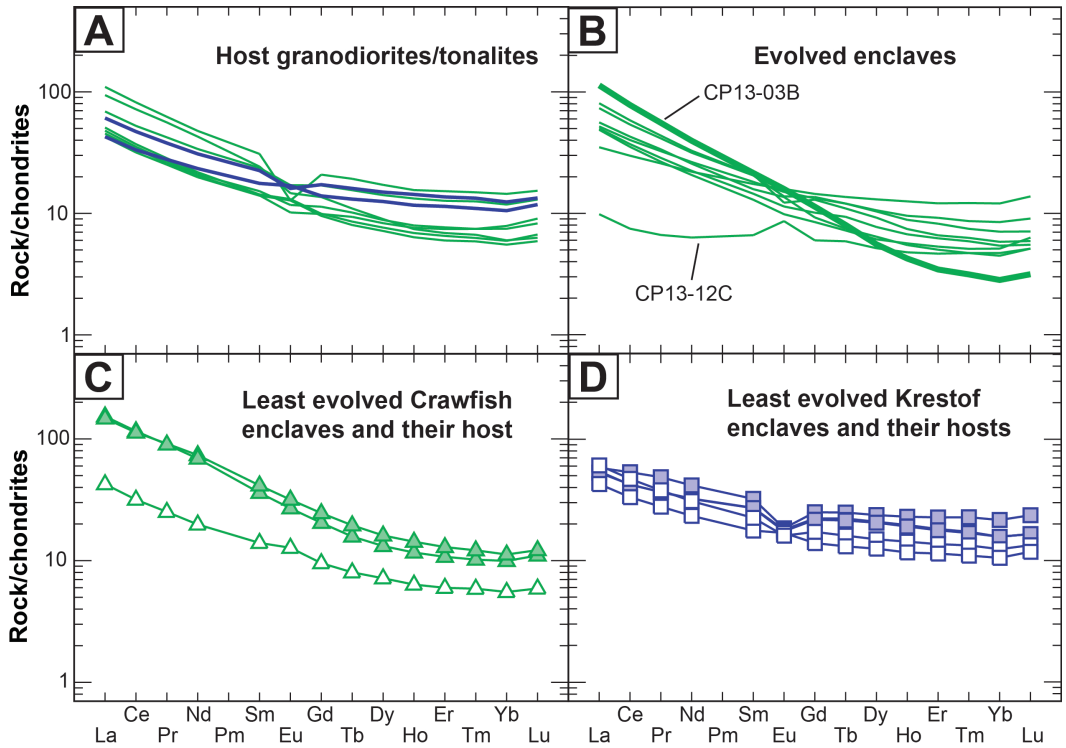


**Figure 17.** Chondrite-normalized REE diagrams for samples from the Crawfish Inlet and Krestof Island: (A) host granodiorites/tonalites and (B) least evolved enclaves. Green

lines and blue lines represent data for Crawfish and Krestof samples, respectively. Panel (C) displays the least evolved Crawfish enclaves and their host, and (D) shows the Krestof enclaves and their hosts. Symbols for (C) and (D) as in Figure 6. Chondrite normalization values from Sun and McDonough, 1989.

Figure 18 shows Crawfish and Krestof samples on a $(La/Yb)_{CN}$ versus $Yb_{CN}$ diagram. Sample CP13-03B plots well above all others in the adakite field as a result of steep REE profile. Crawfish enclaves and their hosts plot in both the adakite and island arc basalt fields (Figure 18). In contrast, all Krestof samples (both enclaves and hosts) have $(La/Yb)_{CN}$ values < 5 and plot within the island arc basalts field (Figure 18). The Krestof enclaves are enriched in Yb relative to all other enclaves Figures 15 and 18).

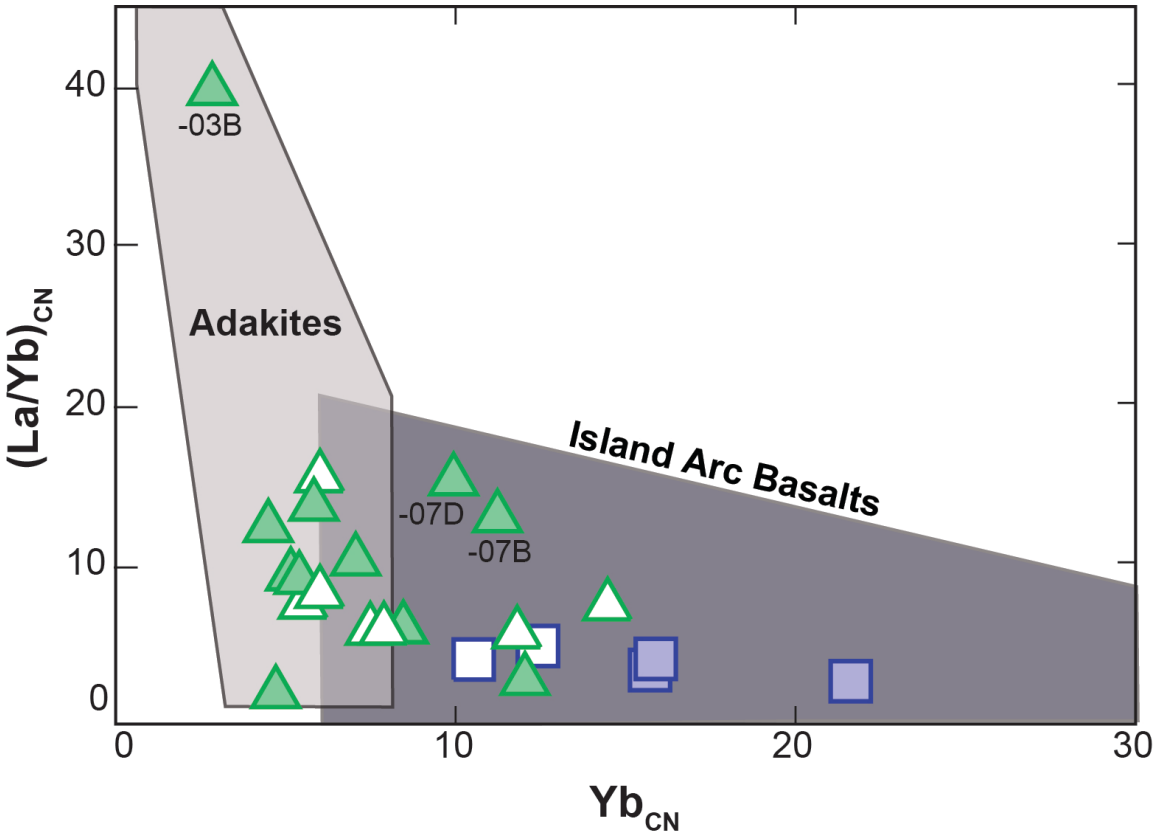


**Figure 18.** $(La/Yb)_{CN}$ versus $Yb_{CN}$ variation diagram for all Crawfish and Krestof samples. LREE-enriched enclave CP13-03B plots well above all other samples. Fields for island arc basalts and adakites are from Drummond and Defant (1990) and Martin (1999). Symbols as in Figure 6.

Spider diagrams, using normalization values for normal MORB (NMORB; Sun and McDonough, 1989) for CPW accretionary wedge sediments and all Crawfish and Krestof samples excluding the least enclaves are shown in Figure 19. Patterns for Crawfish and Krestof host granodiorites/tonalites are broadly similar to each other and the accretionary wedge sediments they intrude. Notable characteristics for the hosts include negative Nb anomalies and Pb 'spikes' (Figure 19B). The suite of evolved enclaves from the Crawfish pluton displays larger variations in trace element compositions than the host granodiorites/tonalites (Figure 19C).

Figure 20 exhibits spider diagrams for the least evolved enclaves from the Crawfish and Krestof plutons and their hosts. Krestof enclaves have similar spider diagrams relative to their hosts with the exception of lower Zr and higher HREEs (Figure 20A). In contrast, Crawfish enclaves are enriched in most trace elements and have a notably smaller Pb spike compared to their host (Figure 20B). In comparison to the Krestof enclaves, the least evolved Crawfish samples are enriched in most elements except for HREEs, Y, and Pb (Figure 20C). In addition, Krestof enclaves exhibit larger Pb spikes and negative anomalies for P, Zr, and Ti (Figure 20C).

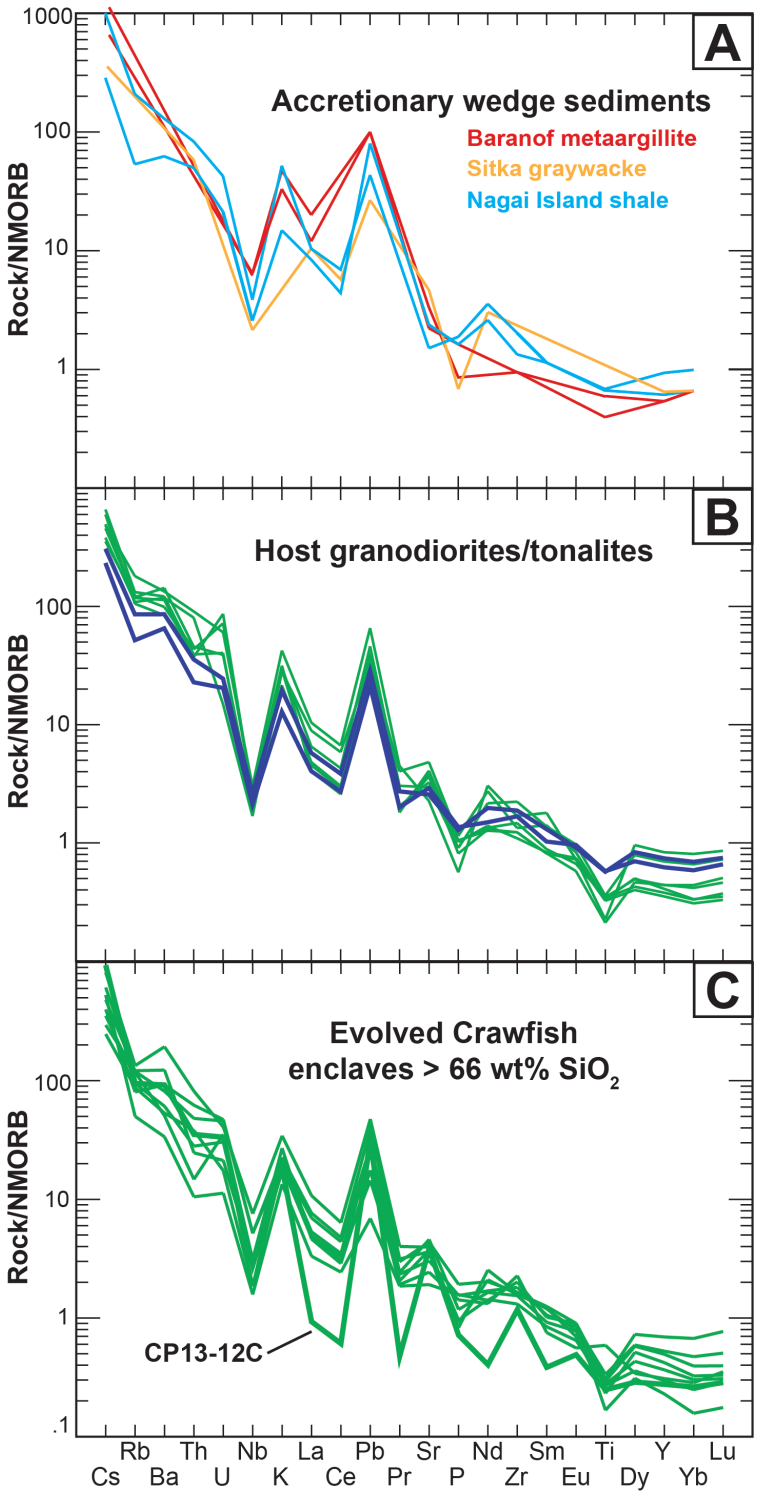


**Figure 19.** NMORB normalized spider diagrams: (A) accretionary wedge sediments from across the SBPB; (B) Crawfish and Krestof host granodiorites/tonalites; (C) more evolved Crawfish enclaves. Data for Crawfish samples are shown by green lines and Krestof samples by blue lines. NMORB normalization values from Sun and McDonough, 1989. Nagai Island sediment compositions taken from Short et al. (2013). Baranof metaargillite and Sitka graywacke sediment compositions are from EarthChem.

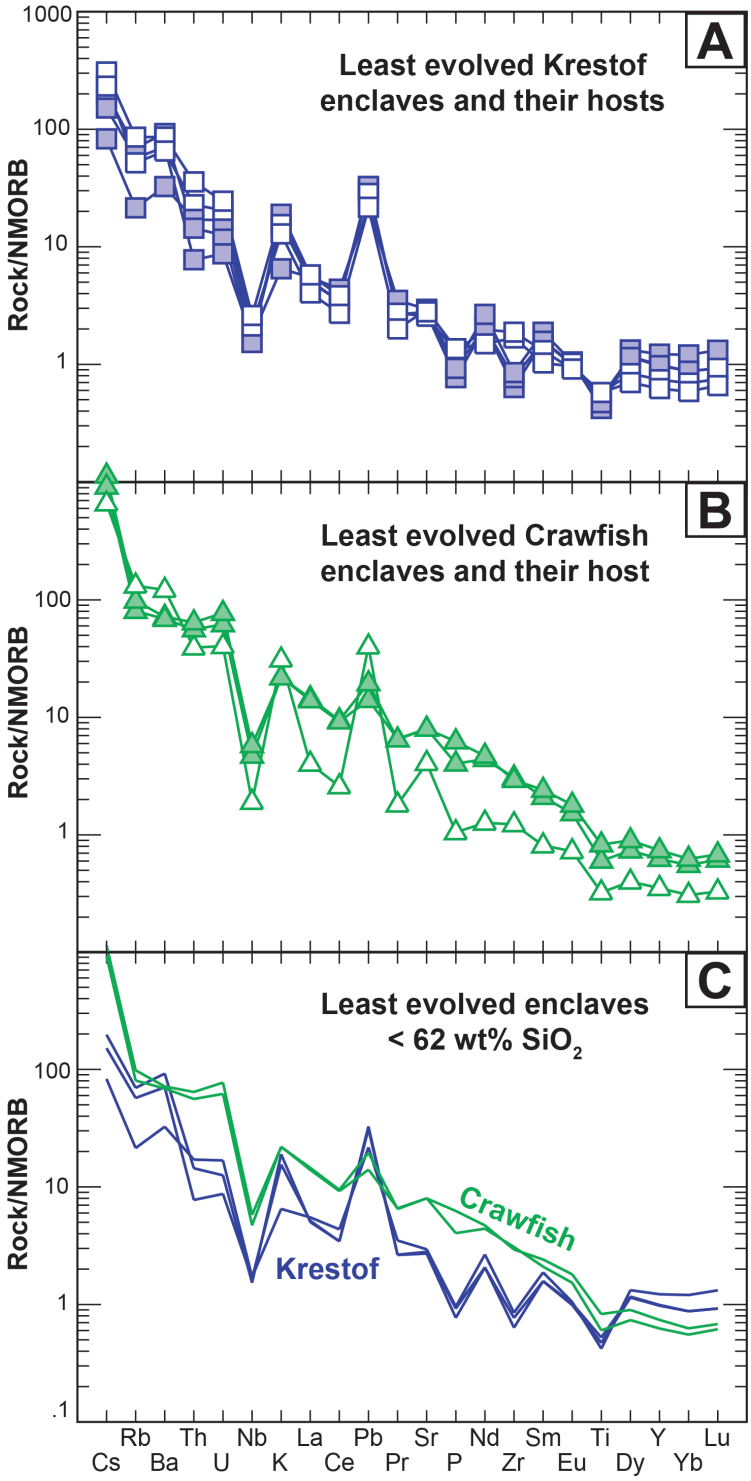


**Figure 20.** NMORB normalized spider diagrams for: (A) Low $SiO_2$ Krestof enclaves and their host tonalites, (B) Low $SiO_2$ Crawfish enclaves (CP13-07B and -07D) and their host plutonic rocks, and (C) overlay of the least evolved (< 62% $SiO_2$) enclaves from the Crawfish and Krestof plutons. Data for Crawfish samples are shown by green lines and Krestof samples by blue lines. Symbols in (A-B) are as in Figure 6. NMORB normalization values from Sun and McDonough, 1989.

Most enclaves from the Crawfish pluton exhibit high Sr/Y ratios (> 25; Figure 21). As a result, many of these samples plot within the adakite field. Crawfish enclave CP13-03B, which plotted well above all other Crawfish and Krestof samples on the $(La/Yb)_{CN}$ versus $Yb_{CN}$ diagram (Figure 18), also displays the highest Sr/Y ratio. In contrast, none the Krestof samples have Sr/Y ratios exceeding 20, and these samples plot within the MORB and island arc basalt fields (Figure 21).

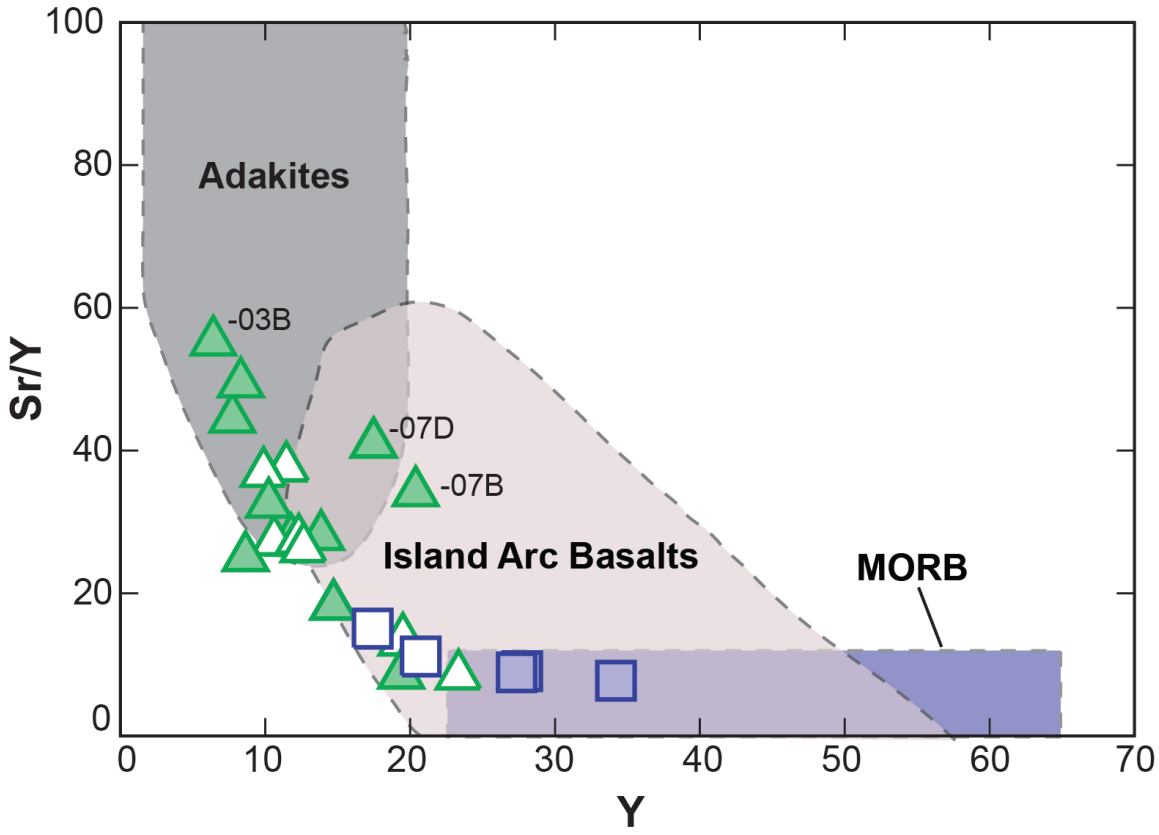


**Figure 21.** Sr/Y versus Y for all Crawfish and Krestof samples. Most enclaves and host granodiorites/tonalites from the Crawfish pluton plot within the adakite field. Fields for island arc basalts and adakites are from Drummond and Defant (1990) and Martin (1999). Symbols as in Figure 6.

To further examine the Pb spikes seen in spider diagrams for the host granodiorites/tonalites, CPW sediments, and evolved Crawfish enclaves (Figure 19), the Pb/La is plotted versus La and $SiO_2$ in Figure 22. The Crawfish samples show a general increase in Pb/La with increasing $SiO_2$ content (Figure 22B). In contrast, Pb/La ratios are similar in the Krestof enclaves and their hosts. Figure 22A includes a 'mantle array' defined by numerous analyses of OIB and MORB. The only samples plotting in the mantle array are least evolved Crawfish enclaves CP13-07B and -07D. Most other Crawfish and all Krestof samples plot within the CPW sediment field. This suggests the possibility of significant sedimentary contributions during the genesis of most Crawfish and Krestof magmas.

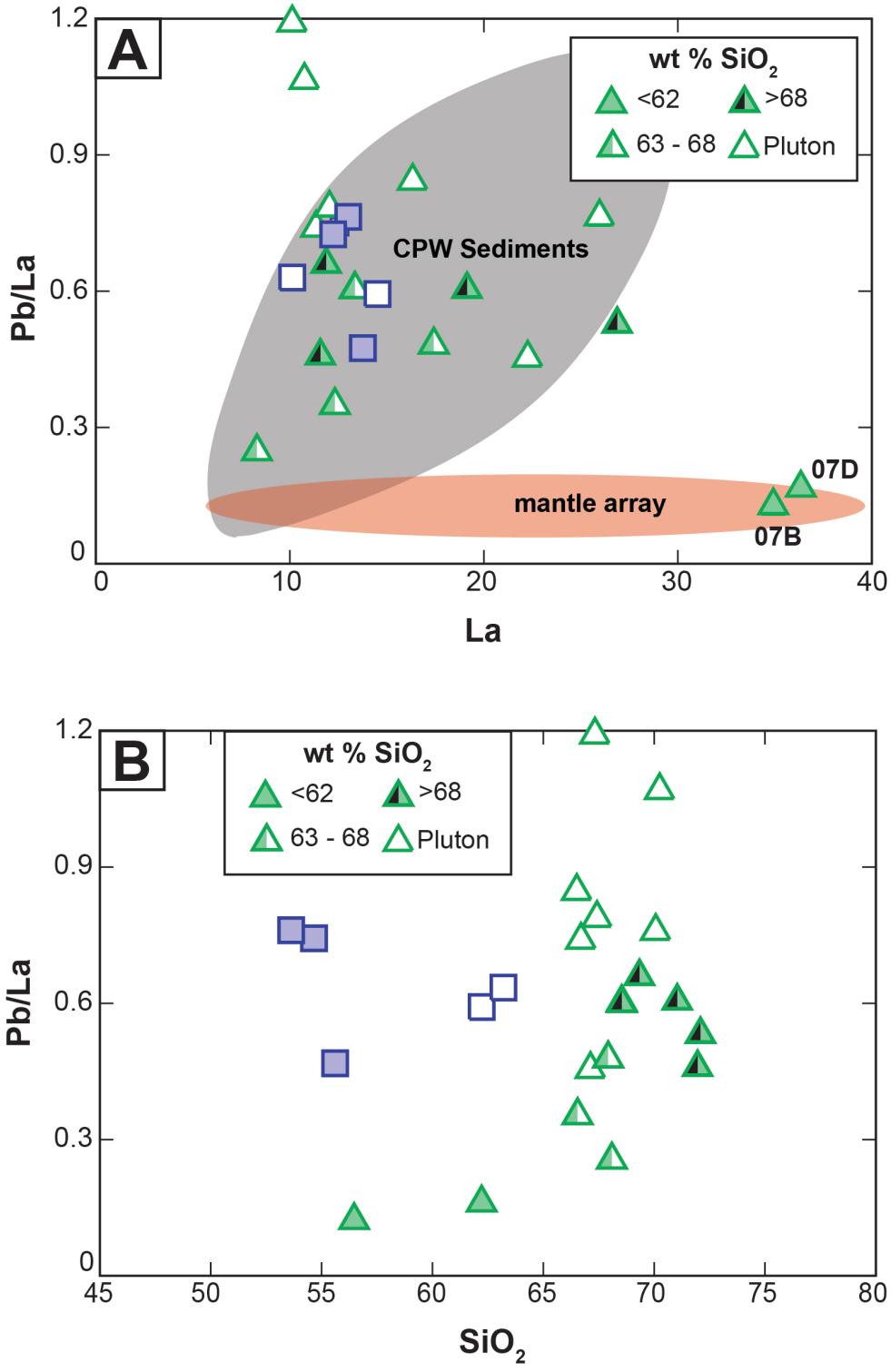


**Figure 22.** (A) Pb/La versus La for Crawfish and Krestof host plutons and their least evolved enclaves. The fields for SBPB sediments are defined by data from Hill et al. (1981), Barker et al. (1992), Lytwyn et al. (2000), Short et al. (2013), and EarthChem. Mantle array defined using numerous MORB and OIB analyses from GEOROC and EarthChem. Symbols as in Figure 6 and in legend (inset) for Crawfish rocks.

*Summary of whole-rock geochemical data*

Despite their spatial and temporal proximity, there are geochemical differences between Crawfish and Krestof igneous rocks. Krestof granodiorite/tonalite samples are systematically lower in $SiO_2$ (62-64 wt%) than their Crawfish counterparts (66-70 wt%: Figures 12 and 13). All Krestof samples are metaluminous while most Crawfish samples are peraluminous, with the exception of the least evolved enclaves and CP13-12B (Figure 12). The least evolved Crawfish enclaves are chemically distinct from the Krestof enclaves. For example, they have distinct spider diagram patterns (Figure 20C), Sr/Y and $(La/Yb)_{CN}$ ratios (Figure 18 and 21). These observations suggest that the magmas emplaced in the Crawfish and Krestof plutons were derived from either different sources and/or parental magmas.

*Sr and Nd isotopic compositions*

Various radiogenic isotope systems offer insights into the chemical nature of mantle sources, as well as differentiation processes. Two isotopic systems were examined as a part of this study: Rb-Sr and Sm-Nd. These two isotope systems differ markedly with respect to their behavior during melt/rock interactions, which makes their dual assessment particularly useful in constraining differentiation processes and magmatic sources during igneous petrogenesis (DePaolo and Wasserburg, 1976; Zindler et al., 1982; Zindler and Hart, 1986; Rollinson, 1993).

**Table 5.** Sr and Nd isotope data for Baranof Island samples

| Sample | Rock Type | Concentration (ppm) | | Ratio | Measured | Initial | Concentration (ppm) | | Ratio | Measured | Initial | $\varepsilon_{Nd}$ |
|---|---|---|---|---|---|---|---|---|---|---|---|---|
| | | Rb | Sr | $^{87}Rb/^{86}Sr$ | $^{87}Sr/^{86}Sr$ | $^{87}Sr/^{86}Sr$ | Sm | Nd | $^{147}Sm/^{144}Nd$ | $^{143}Nd/^{144}Nd$ | $^{143}Nd/^{144}Nd$ | |
| KP13-01A | host | 29 | 262 | 0.322 | 0.70533 | 0.70509 | 2.70 | 10.55 | 0.1549 | 0.512728 | 0.512676 | 2.0 |
| KP13-01C | enclave | 12 | 265 | 0.128 | 0.70521 | 0.70511 | 4.93 | 19.32 | 0.1541 | 0.512701 | 0.512649 | 1.5 |
| KP13-02A | host | 48 | 231 | 0.602 | 0.70580 | 0.70537 | 3.44 | 14.31 | 0.1451 | 0.512645 | 0.512596 | 0.5 |
| KP13-02B | enclave | 32 | 252 | 0.363 | 0.70565 | 0.70539 | 4.16 | 14.53 | 0.1730 | 0.512655 | 0.512598 | 0.5 |
| KP13-02C | enclave | 39 | 244 | 0.465 | 0.70575 | 0.70541 | 4.14 | 14.43 | 0.1734 | 0.512658 | 0.512601 | 0.5 |
| CP13-03A | host | 61 | 434 | 0.406 | 0.70483 | 0.70454 | 3.71 | 20.36 | 0.1102 | 0.512768 | 0.512732 | 3.1 |
| CP13-03C | enclave | 59 | 326 | 0.523 | 0.70459 | 0.70422 | 3.19 | 15.09 | 0.1276 | 0.512802 | 0.512759 | 3.6 |
| CP13-03D | enclave | 67 | 392 | 0.497 | 0.70456 | 0.70420 | 3.14 | 13.31 | 0.1426 | 0.512794 | 0.512747 | 3.4 |
| CP13-07A | host | 74 | 367 | 0.582 | 0.70529 | 0.70487 | 2.14 | 8.40 | 0.1537 | 0.512737 | 0.512686 | 2.2 |
| CP13-07D | enclave | 55 | 721 | 0.220 | 0.70370 | 0.70354 | 5.52 | 29.73 | 0.1123 | 0.512996 | 0.512958 | 7.5 |
| CP13-09A | host | 66 | 342 | 0.560 | 0.70481 | 0.70440 | 2.33 | 9.89 | 0.1424 | 0.512816 | 0.512769 | 3.8 |
| CP13-09C | enclave | 49 | 336 | 0.425 | 0.70468 | 0.70437 | 2.22 | 9.59 | 0.1399 | 0.512676 | 0.512629 | 1.1 |
| CP13-12A | host | 69 | 329 | 0.611 | 0.70474 | 0.70430 | 2.15 | 8.33 | 0.1562 | 0.512827 | 0.512775 | 3.9 |
| CP13-12C | enclave | 66 | 346 | 0.548 | 0.70451 | 0.70411 | | | | | | |

Table 5 gives whole-rock Sr and Nd isotopic and elemental data. Figure 23 shows Nd and Sr isotopic data for Crawfish and Krestof samples (both enclaves and host granodiorites/tonalites), as well as fields for the SBPB, CPC and CPW sediments. All Crawfish and Krestof samples plot near or within the mantle array. Enclaves from the Krestof pluton have isotopic compositions nearly identical to their hosts. In contrast, Crawfish enclaves show greater isotopic variation relative to their hosts. The isotopic compositions of the Krestof enclaves are distinct from those of the Crawfish. Enclave CP13-07D has the most primitive isotopic composition of the rocks analyzed here and, furthermore, is more primitive than other SBPB granitoids (Figure 23). With the exception of enclave CP13-07D, the Crawfish and Krestof samples are isotopically similar to other eastern SBPB intrusive rocks. Relative to other SBPB and CPC granitoids, Sr and Nd isotopic compositions of Crawfish and Krestof samples suggest smaller amounts of accretionary wedge sedimentary material.

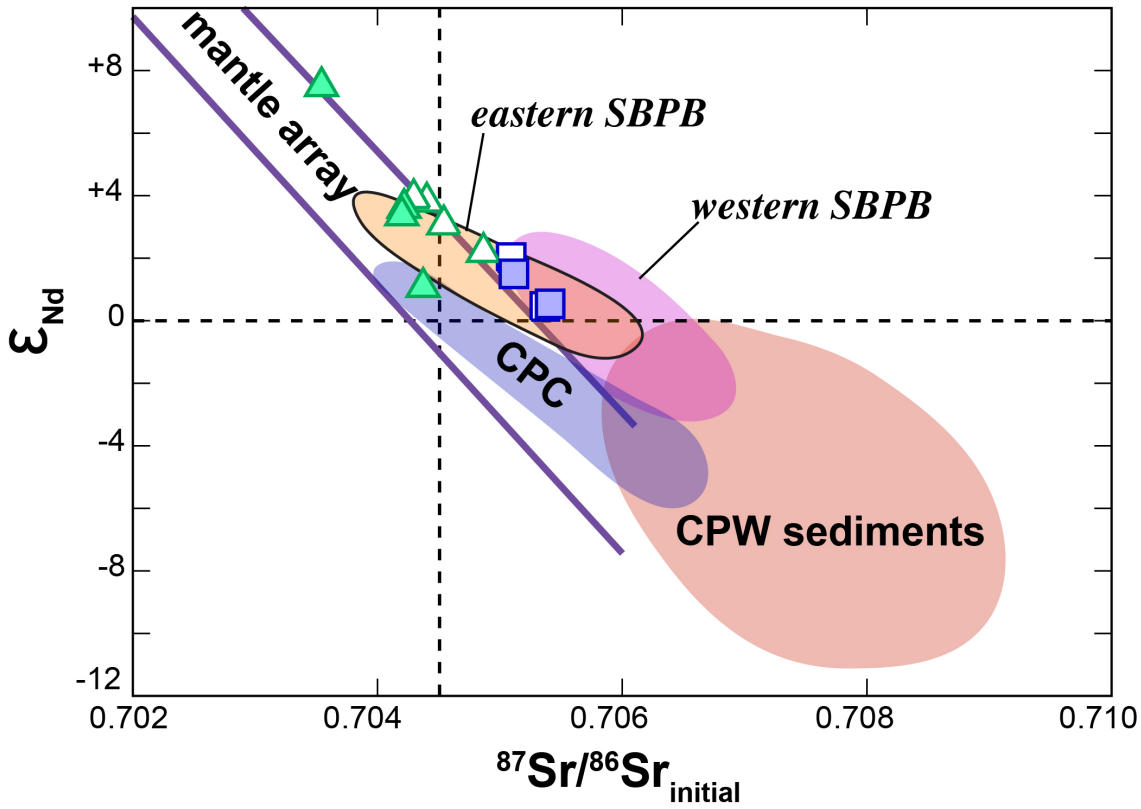


**Figure 23.** $\varepsilon_{Nd}$ vs. $^{87}Sr/^{86}Sr_{initial}$ diagram for enclaves and tonalites/granodiorites from the Crawfish and Krestof plutons. Fields for eastern SBPB, western SBPB, northern Coast Plutonic Complex (CPC), and CPW sediments are shown for comparison and are referenced as follows: eastern SBPB – Sisson et al., 2003; western SBPB – Barker et al., 1992; northern CPC – Arth et al., 1988; CPW sediments – EarthChem and references therein. Dashed lines indicate estimated Bulk Earth composition (DePaolo and Wasserburg, 1976). Mantle array after McCulloch and Perfit (1981). Symbols as in Figure 6.

*Correlation of isotopic data with U/Pb ages*

As reported in Roig et al. (2014), magmatic zircon from the Crawfish Inlet pluton shows a strong relationship between $\varepsilon_{Hf}$ and U-Pb age (Figure 24). Host granitoid samples from the Crawfish and Krestof plutons were processed to isolate zircons, and they were also analyzed for U-Pb age dating and $\varepsilon_{Hf}$. See Roig et al. (2014) for details on the isolation, preparation, and collection of zircon data.

U/Pb ages for the Crawfish Inlet pluton range from ~ 47-53 Ma (Figure 2), which correlate with $\varepsilon_{Hf}$ (Figure 24). The oldest zircons have $\varepsilon_{Hf}$ ~5, which plots relatively close to CHUR. Alternatively, the younger zircons have $\varepsilon_{Hf}$ values approaching 15, plotting close to the depleted mantle boundary (Figure 24). Average sedimentary materials typically record $\varepsilon_{Hf}$ values between 0 and -15 (Chauvel et al., 2008). This suggests the earliest magmas emplaced in the Crawfish pluton underwent more assimilation and/or mixing with crust/sediment (resulting in lower $\varepsilon_{Hf}$ values) than magmas that were emplaced during later stages (with higher $\varepsilon_{Hf}$).

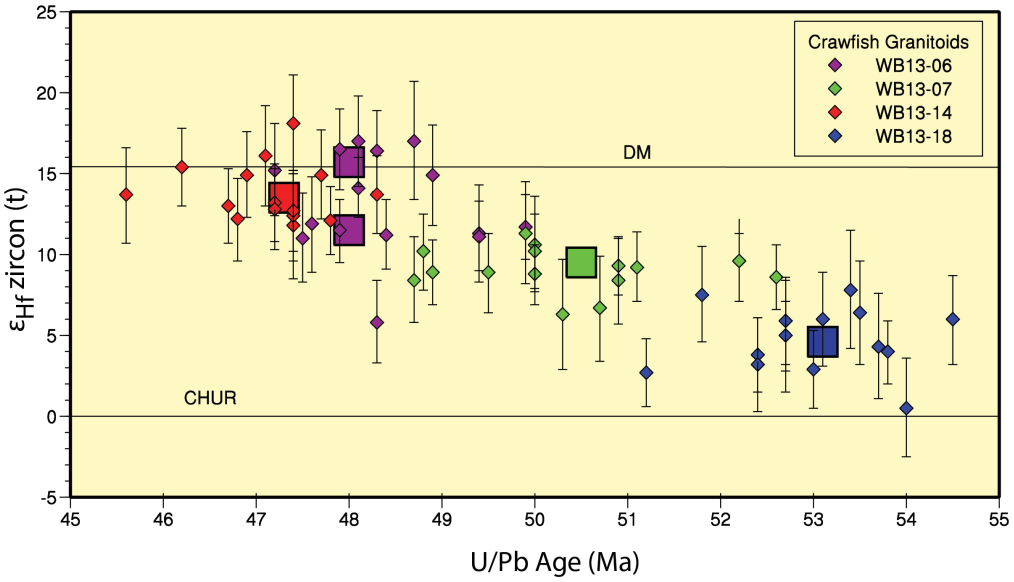


**Figure 24.** $\varepsilon_{Hf}$ in magmatic zircons versus U/Pb ages for Crawfish granitoids (Roig et al., 2014). Crawfish magmatic zircons show a consistent correlation of decreasing $\varepsilon_{Hf}$ with increasing age. CHUR = chondritic uniform reservoir and DM = depleted mantle.

A similar relationship between U-Pb age and $\varepsilon_{Hf}$ is seen between U/Pb ages and $\varepsilon_{Nd}$ and $^{87}Sr/^{86}Sr_{initial}$ in Crawfish and Krestof granodiorites/tonalites. Figure 25 illustrates the increase in $\varepsilon_{Nd}$ and decrease in $^{87}Sr/^{86}Sr_{initial}$ with decreasing age. The higher

$^{87}Sr/^{86}Sr_{initial}$ and lower $\varepsilon_{Nd}$ suggest a greater involvement of isotopically evolved material in older magmas, and magmatic compositions became progressively more juvenile with time (Figure 25).

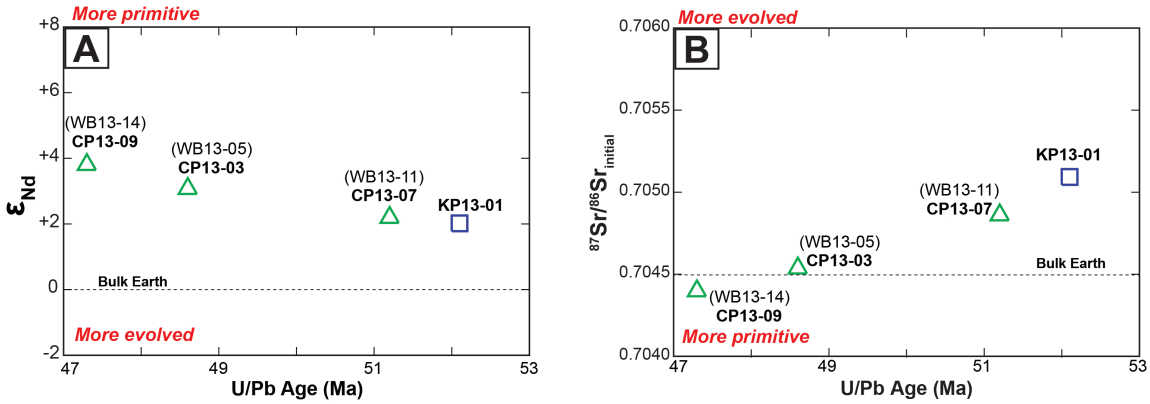


**Figure 25.** (A) $\varepsilon_{Nd}$ and (B) $^{87}Sr/^{86}Sr_{initial}$ versus U/Pb ages for Crawfish and Krestof host granitoids. Symbols as in Figure 6.

*Geochemical Variations across the SBPB*

Most previous studies of the SBPB have focused on reconciling the time-transgressive nature and spatial distribution of SBPB intrusive rocks into comprehensive plate tectonic models (Bradley et al., 2003; Cowan, 2003; Haeussler et al., 2003; Farris and Paterson, 2009). In focusing on the big picture of tectonic reconstructions, few of these studies have carefully examined the SBPB from a geochemical perspective. Those that do have suggested that systematic geochemical variations are present across the SBPB. For example, Farris and Paterson (2009) related geochemical variations across the belt into a comprehensive plate tectonic model. They divided the belt into three discrete segments from west to east: (1) Sanak-Kodiak, (2) Kenai-Prince William Sound, and (3) Yakutat-Baranof. Farris and Paterson assert that the western and eastern portions of the belt of the exhibit distinct geochemical characteristics, with the Kenai-Prince William Sound segment displaying some characteristics of both the western and eastern

segments. They (2009) found that plutons of the western segment have LREE-enriched profiles with well-developed negative Eu anomalies and Sr/Y (< 25) ratios that plot well outside of the adakitic field (Hill et al, 1981; Moore et al, 1983; Farris and Paterson, 2009). In contrast, rocks of the eastern segment were found to exhibit flatter REE profiles lacking Eu anomalies, higher Sr/Y (> 25) ratios, and $Al_2O_3$ >15 wt% (Harris et al., 1996; Sisson et al., 2003b).

In this study, geochemical data from multiple studies of SBPB intrusions were compiled and compared to data for the Crawfish and Krestof plutons to assess the validity of these proposed spatial relationships. Geochemical data for coeval (~50 Ma) plutons of the CPC were also evaluated in relation to the Paleocene intrusive rocks on Baranof Island.

Figure 26 shows major element Harker diagrams for the Crawfish and Krestof Island plutons and igneous rocks from across the SBPB. Compositions of Crawfish and Krestof host granitoids generally plot alongside other SBPB rocks. The least evolved enclaves are significantly more mafic than all other SBPB samples considered here. In general, plutons of the western SBPB are more peraluminous than those of the eastern SBPB, particularly samples from the Sanak and Shumagin Islands (Hill et al., 1981; red circles in Figure 26). Many of the Sanak samples, as well as felsic dikes from the Seldovia Quadrangle (Lytwyn et al., 2000; blue crosses in Figure 26), plot well into the S-type field on an ASI versus $SiO_2$ diagram (Figure 26). This is in contrast to Crawfish and Krestof rocks, which are predominantly I-type (ASI < 1.1) and peraluminous to metaluminous. The $Al_2O_3$ Harker diagram shows that Crawfish enclave CP13-07B and the Krestof enclaves plot off the trend observed for other SBPB rocks. The Krestof

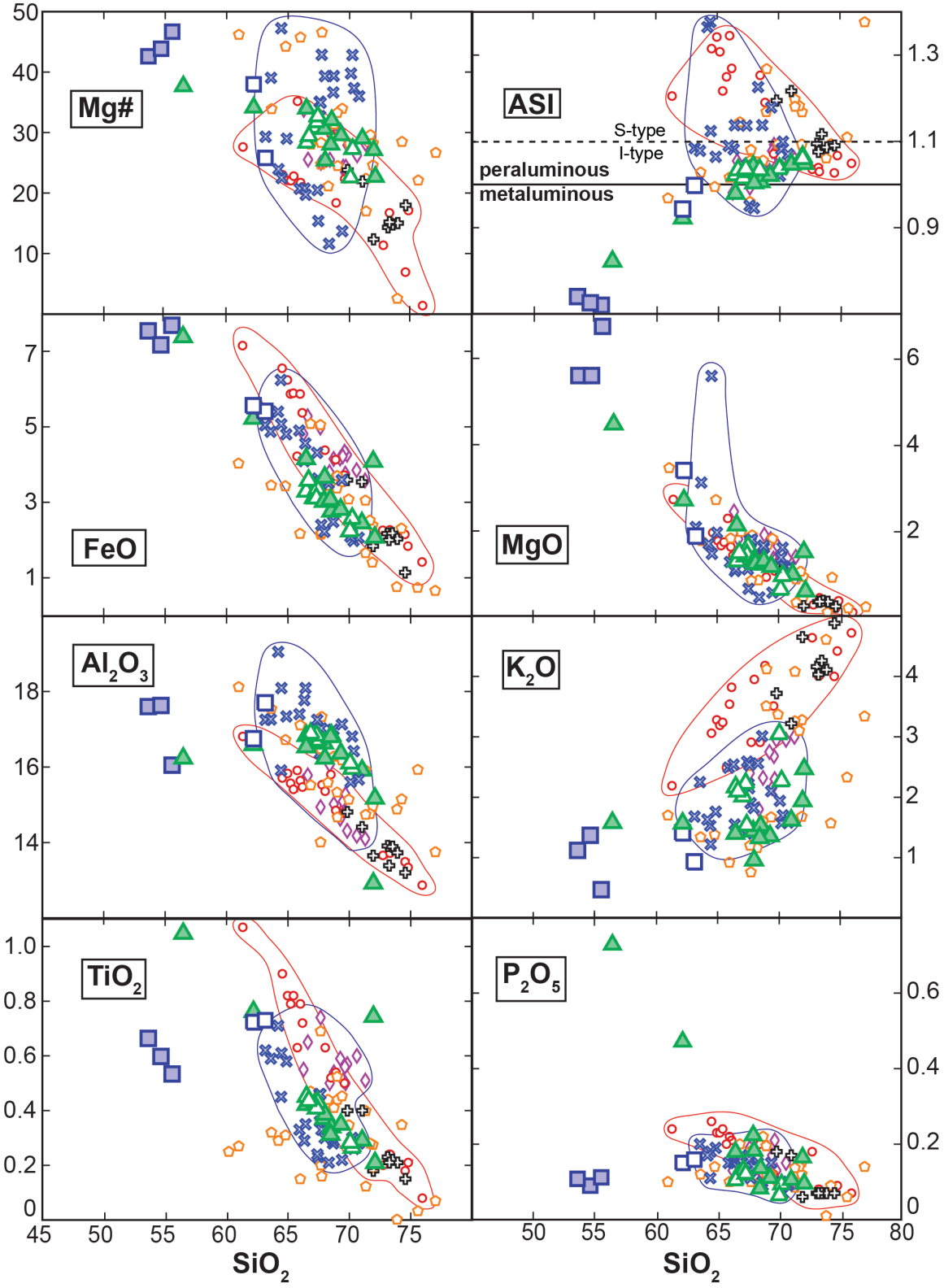


**Figure 26.** Comparison of Crawfish and Krestof major element compositions with rocks from across the SBPB. Red outlines represent western SBPB compositions and the blue lines outline middle SBPB intrusive rocks. Symbols are the same as in Figures 1 and 6.

enclaves have $TiO_2$ and $P_2O_5$ abundances distinct from other SBPB rocks. Least evolved Crawfish enclaves are notably enriched in $P_2O_5$. These observations suggest that the least evolved Crawfish and Krestof enclaves are distinct from other more evolved SBPB intrusive rocks, in addition to the two enclave types being distinct from one another.

Farris and Paterson (2009) outlined systematic variations in the extent of LREE-enrichment across the SBPB. However, when all of the data from the SBPB is considered, such systematic variations are not obvious (Figure 27). Whereas Farris and Paterson proposed that only SBPB rocks in the western segment displayed LREE-enrichment, samples from the Crawfish and Krestof plutons in the eastern segment exhibit LREE-enrichment (Figures 17 and 27C). In particular, SBPB plutons emplaced within the Chugach metamorphic complex (CMC) display wide variations in REE chemistry that complicate spatial geochemical relationships across the SBPB.

Adakites were originally proposed to be products of direct slab melting (Drummond and Defant, 1990), but others have since demonstrated that adakitic compositions can be generated through lower crustal melting and other processes involving garnet and/or hornblende fractionation (Smith and Leeman, 1982; Dawes, 1993; Garrison and Davidson, 2003; Girardi et al., 2012). Other T-R-T and trench-transform-ridge encounters preserved in the geologic record as a result of proposed forearc magmatism above a slab window also contain adakites: namely the Cocos-Nazca-Caribbean triple junction in Panama (Drummond et al., 1995; Johnston and Thorkelson, 1997) and Chilean triple junction (Forsythe and Nelson, 1985; Kay et al., 1993)

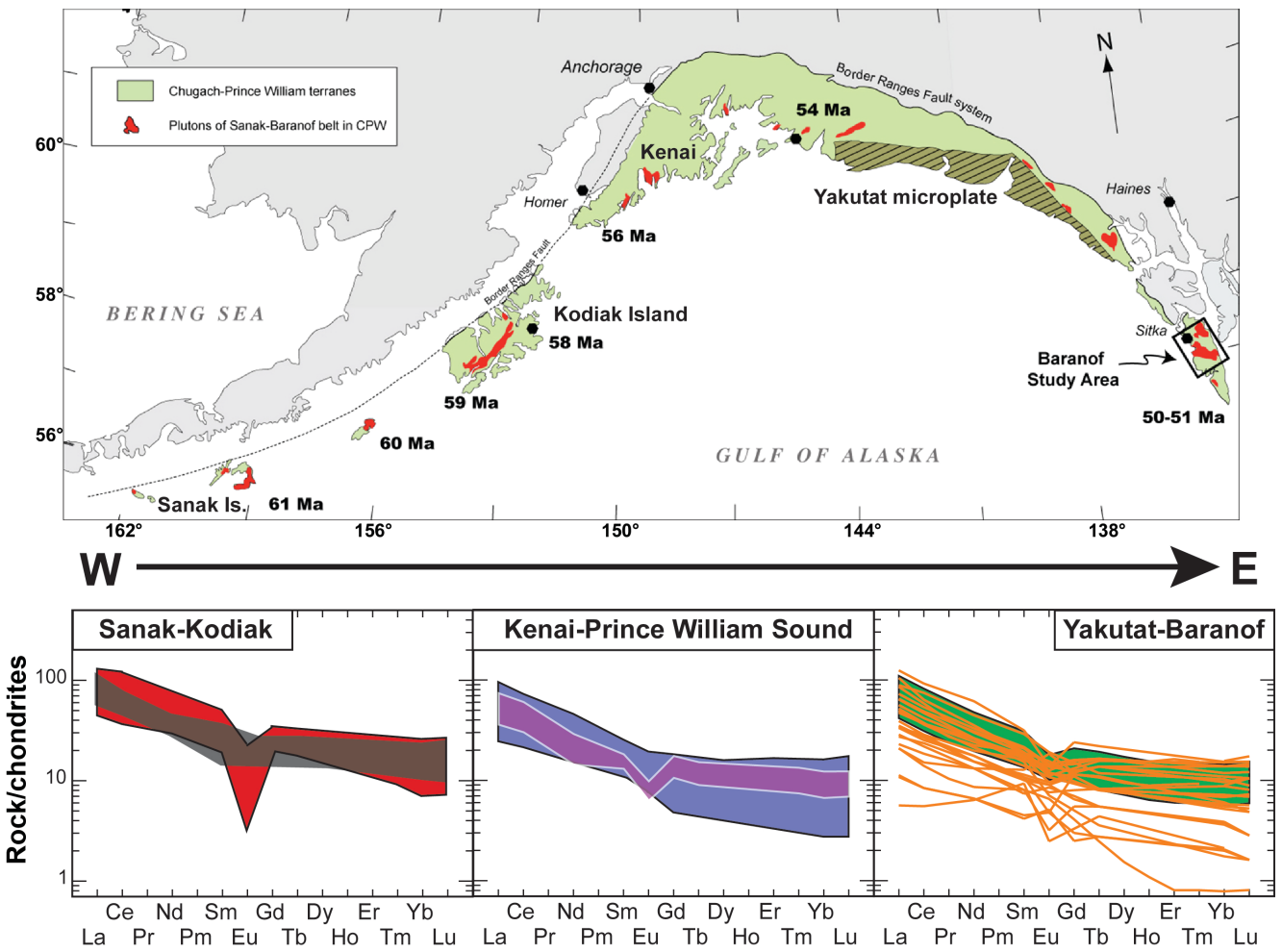


**Figure 27.** Chondrite-normalized REE diagrams for plutons across the SBPB. The regional map from Figure 2 is shown to orient the REE diagrams with their respective location in the belt. REE abundances for (A) Sanak-Kodiak (Hill et al., 1981; Short et al., 2013); (B) Kenai-Prince William Sound (Lytwyn et al., 2000; Bradley et al., 2003; Barker et al., 1992); (C) Yakutat-Baranof (this study) are shown as fields. Data for individual samples from plutons intruding the Chugach metamorphic complex (Sisson et al., 2003b) are shown as orange lines.

Many plutonic rocks of the eastern SBPB exhibit adakitic characteristics, including high Sr/Y and $(La/Yb)_{CN}$ ratios (Figure 28). This is in contrast to the western segment of the SBPB, where the majority of samples from that region have low Sr/Y and $(La/Yb)_{CN}$ compositions. The primary exception to this is the coeval near-trench felsic dikes of the Seldovia Quadrangle (Lytwyn et al., 2000; Bradley et al., 2003; blue crosses in Figure 28), which exhibit similar Sr/Y and $(La/Yb)_{CN}$ compositions to younger SBPB plutons emplaced in the eastern portions of the belt.

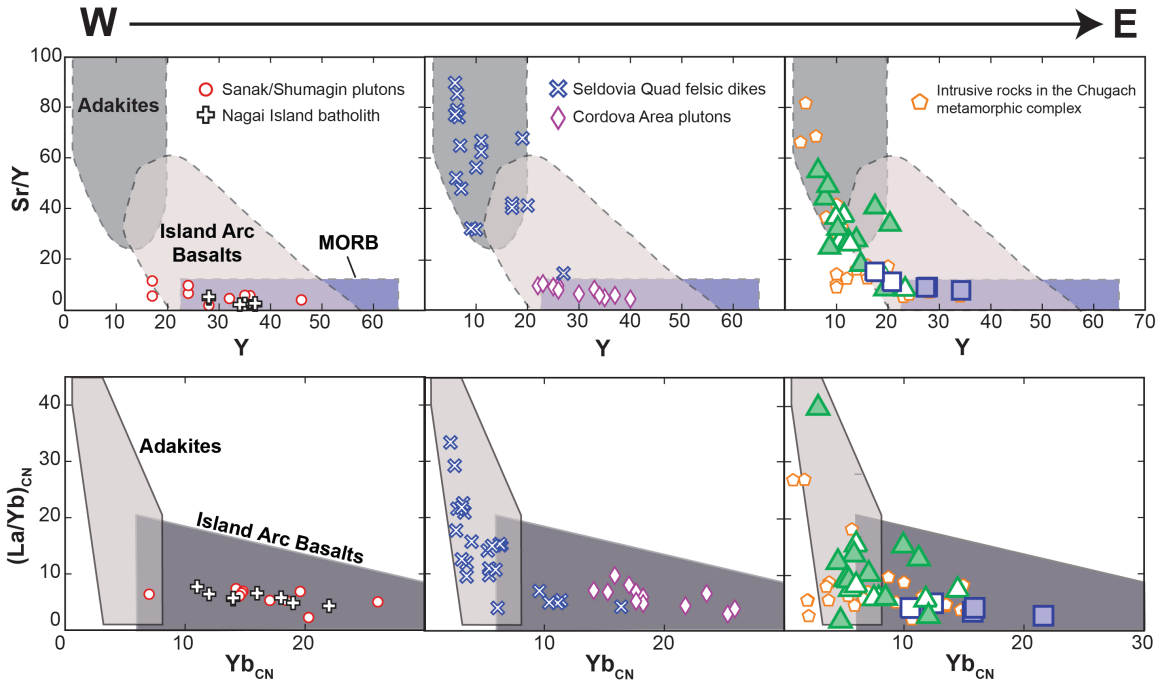


**Figure 28.** Diagrams showing Sr/Y vs. Y and $(La/Yb)_{CN}$ vs. $Yb_{CN}$ compositions for SBPB plutons, arranged from west to east. CN indicates values have been chondrite-normalized based on Sun and McDonough (1989). Symbols as in Figures 1 and 6, and fields as in Figures 18 and 21.

*Comparison of Baranof Island plutons with coeval CPC intrusions*

It is important to consider the possible relationship between the Crawfish and Krestof plutons and igneous rocks of the Southern CPC and Coast Range province in British Columbia/Washington, because the Baranof-Leech River model of Cowan makes these units contiguous at 48 °N when forearc magmatism was active over a slab window ~50 Ma (Figure 3). Therefore, Crawfish and Krestof compositions were compared with coeval igneous rocks spanning the length of the CPC (Figure 1).

Chondrite-normalized (Sun and McDonough, 1989) REE profiles for three CPC localities (Figure 1) are shown in Figure 29. All CPC samples exhibit LREE enrichment similar to many SBPB intrusive rocks. Samples from the Northern CPC (Arth and Plafker, 1988) exhibit a smaller range in REE compositions than intrusions to the south. Figure 30 shows that the coeval CPC suites exhibit similar geochemical characteristics to Crawfish samples. In particular, samples from the northern CPC and Coast Mountain batholith are the only ones that have compositions similar to the least evolved Crawfish enclaves CP13-07B and -07D (Figures 30), whereas none of the other SBPB samples share these characteristics (Figure 28).

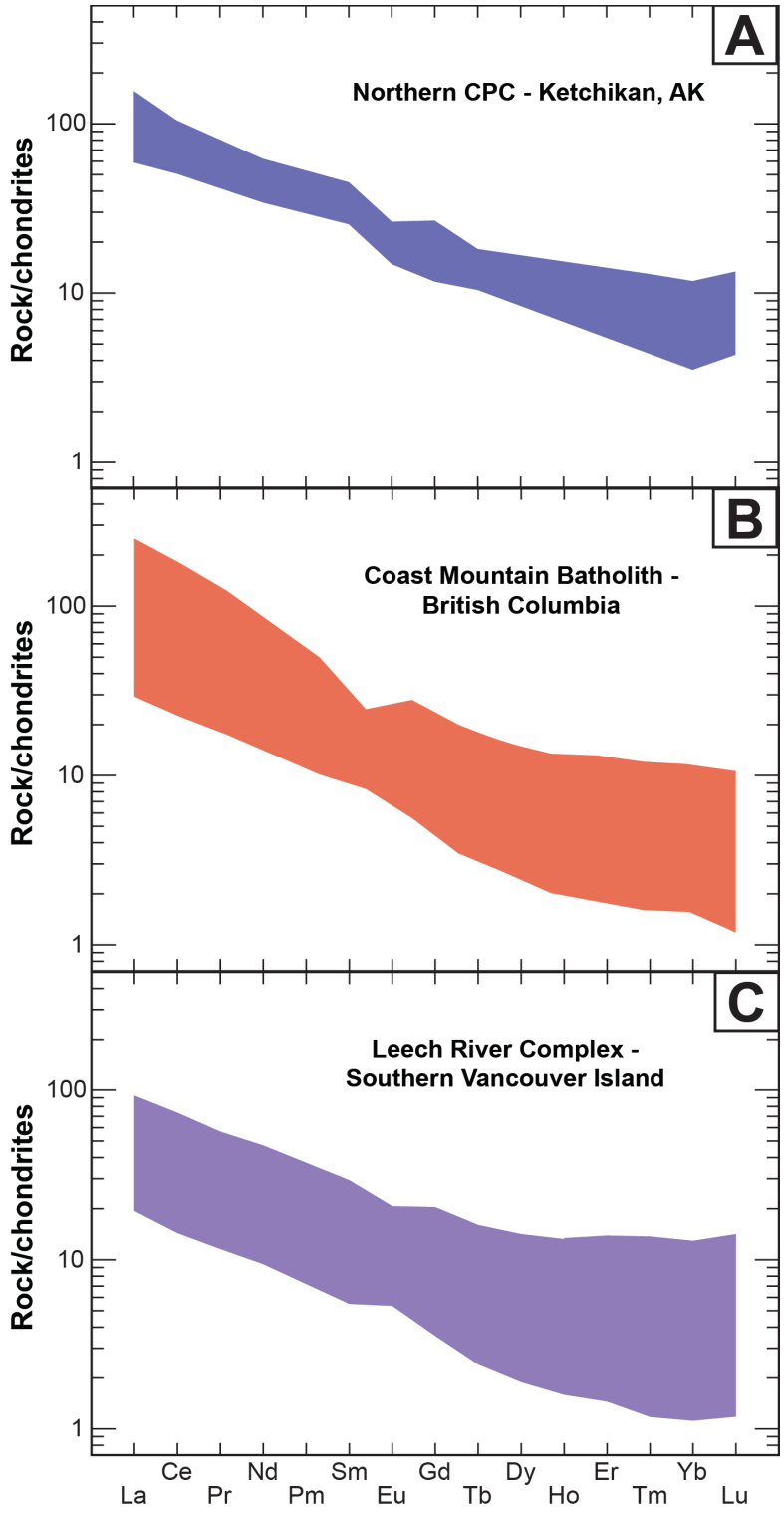


**Figure 29.** Chondrite-normalized (Sun and McDonough, 1989) REE abundances for three ~50 Ma intrusive suites of the CPC shown in Figure 5. Panel (A) shows REE compositions from the Northern CPC i.e., Coast batholith near Ketchikan, AK, (B) is from the Coast Mountains in British Columbia, and (C) shows REE compositions for intrusive rocks in the Leech River complex on Southern Vancouver Island (Figure 5).

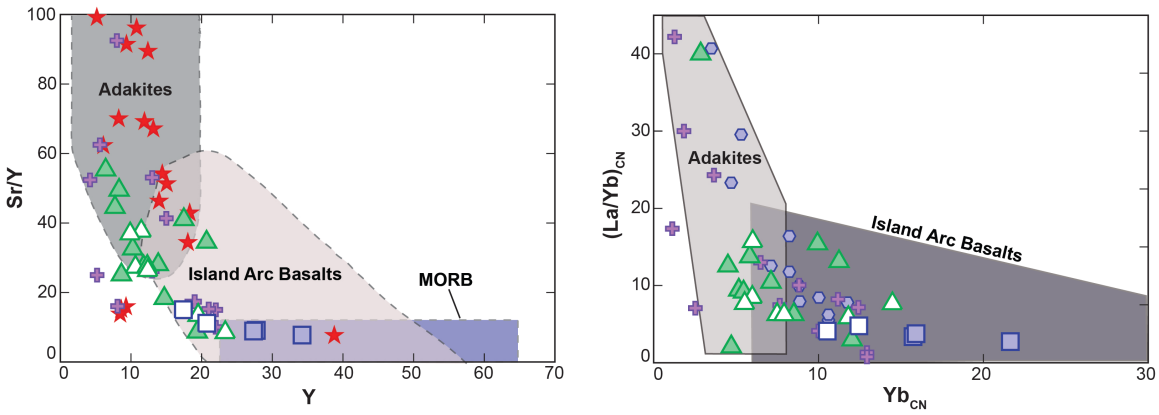


**Figure 30.** (A) Sr/Y versus Y and (B) $(La/Yb)_{CN}$ versus $Yb_{CN}$ diagrams for Crawfish and Krestof samples along with coeval intrusive rocks from the CPC. CPC symbols from Figure 1, Baranof Island symbols from Figure 6, and fields from Figures 18 and 21.

*Petrogenesis of SBPB and CPC Magmas*

Despite geochemical variations across the SBPB, all studies considering the petrogenesis of SBPB intrusive rocks have proposed that the magmas contained some combination of anatectic sedimentary melt with a mantle-derived MORB component. These studies have explained the observed geochemical variations by variable differentiation processes and/or variable amounts of sedimentary versus mantle contributions in different SBPB magmas.

Hudson et al. (1979) and Hill (1979) were the first studies to focus on characterizing the geochemistry of SBPB near-trench intrusive rocks. Hill (1979) reported mixed results, which were followed by another paper presenting better isotopic data used in petrogenetic models (Hill et al., 1981). The results led Hill et al. to conclude that some combination of assimilation-fractional crystallization (AFC) processes and crustal anatexis were important in generating melts in the far western SBPB (Sanak and Shumagin Islands). They assumed a MORB parental magma and sedimentary assimilant in their AFC models. Similar results were reported by Barker et al. (1992) for three

SBPB plutons in the Cordova area, although Barker et al. proposed that the Cordova melts contained very little MORB/mantle component and were largely a product of partial melting of accretionary wedge sediments. Geochemical variations observed within the Kodiak batholith have led to various petrogenetic models (Hill et al., 1981; Moore et al., 1983; Ayuso et al., 2009). Lytwyn et al. (2000) and Bradley et al. (2003) suggested AFC processes were the most plausible explanation for compositions of near-trench dikes in the Seldovia Quadrangle. Some studies of igneous rocks in the Chugach metamorphic complex have suggested that underplating by mafic magmas induced crustal anatexis that generated adakitic magmas (Harris et al., 1996). Others have attributed the eastern SBPB adakites to subduction of a transform fault offsetting the ridge and the initiation of a trench-transform-ridge (Sisson et al., 2003b), analogous to the proposed historic trench-transform-ridge encounter in Panama (Drummond et al., 1995; Johnston and Thorkelson, 1997; Sisson et al., 2003a). Similarly diverse petrogenetic processes have been proposed for the origin of CPC magmas (Mahoney et al., 2009; Girardi et al., 2012)

# PETROGENETIC MODELING

*Modeling magma differentiation processes*

Granitoid magmas can be generated through a variety of differentiation processes involving a mafic parental magma. Fractional crystallization (FC) has long been recognized as a possible mechanism for generating high $SiO_2$ melts from a mafic parent (e.g. Bowen, 1928). Crawfish and Krestof magmas cannot be the product of fractional FC because of their variable isotopic compositions, which require open system processes such as AFC (e.g. DePaolo, 1981) and/or magma mixing (Frost and Mahood, 1987;

Wenner and Coleman, 2004). Another possibility is partial melting of crustal rocks (Hudson et al., 1979; Barker et al., 1992).

*Assimilation-fractional crystallization modeling*

As noted above, other studies have invoked AFC and partial melting as the petrogenetic processes that generated SBPB forearc intrusive rocks. The equations that model AFC processes given by DePaolo (1981) were utilized to evaluate the relative role of sediments and mantle-derived mafic magmas in the genesis of magmas emplaced in the Crawfish and Krestof plutons. Endmember bulk mixing was also assessed for its potential to generate compositions observed for Crawfish Inlet and Krestof Island enclaves and their host granodiorites/tonalites.

Three mafic parental magmas were assumed in the models: MORB (Kelemen, 2004), average OIB (Zindler and Hart, 1986; Sun and McDonough, 1989), and the least evolved Crawfish enclave CP13-07D (Tables 6-8). The models used three different sediment compositions from the Valdez and Orca groups of the CPW accretionary wedge (Farmer et al., 1993; Tables 6 and 7).

Figure 31 illustrates the $^{87}Sr/^{86}Sr_{initial}$ and $\varepsilon_{Nd}$ compositions produced via AFC processes involving a MORB parental magma and three endmember accretionary wedge assimilants (Table 6). The models suggest that if AFC processes are responsible for generating Crawfish and Krestof compositions from magma derived from a depleted mantle (MORB) source, it requires either assimilation of the most isotopically evolved (p€ Orca) sediments at low $R_a/R_c$ (0.2) *or* high $R_a/R_c$ (0.5) if less isotopically evolved sediments (Valdez greywacke) were assimilated. Although the $R_a/R_c$ modeled curves fit the Crawfish/Krestof data, they require unreasonably high degrees of fractionation.

When $R_a/R_c = 0.5$, models using any of the assumed assimilants produce isotopic compositions similar to granodiorite/tonalite samples. These models intersect Crawfish and Krestof compositions at more reasonable *F* values (*F* = 0.5-0.8).

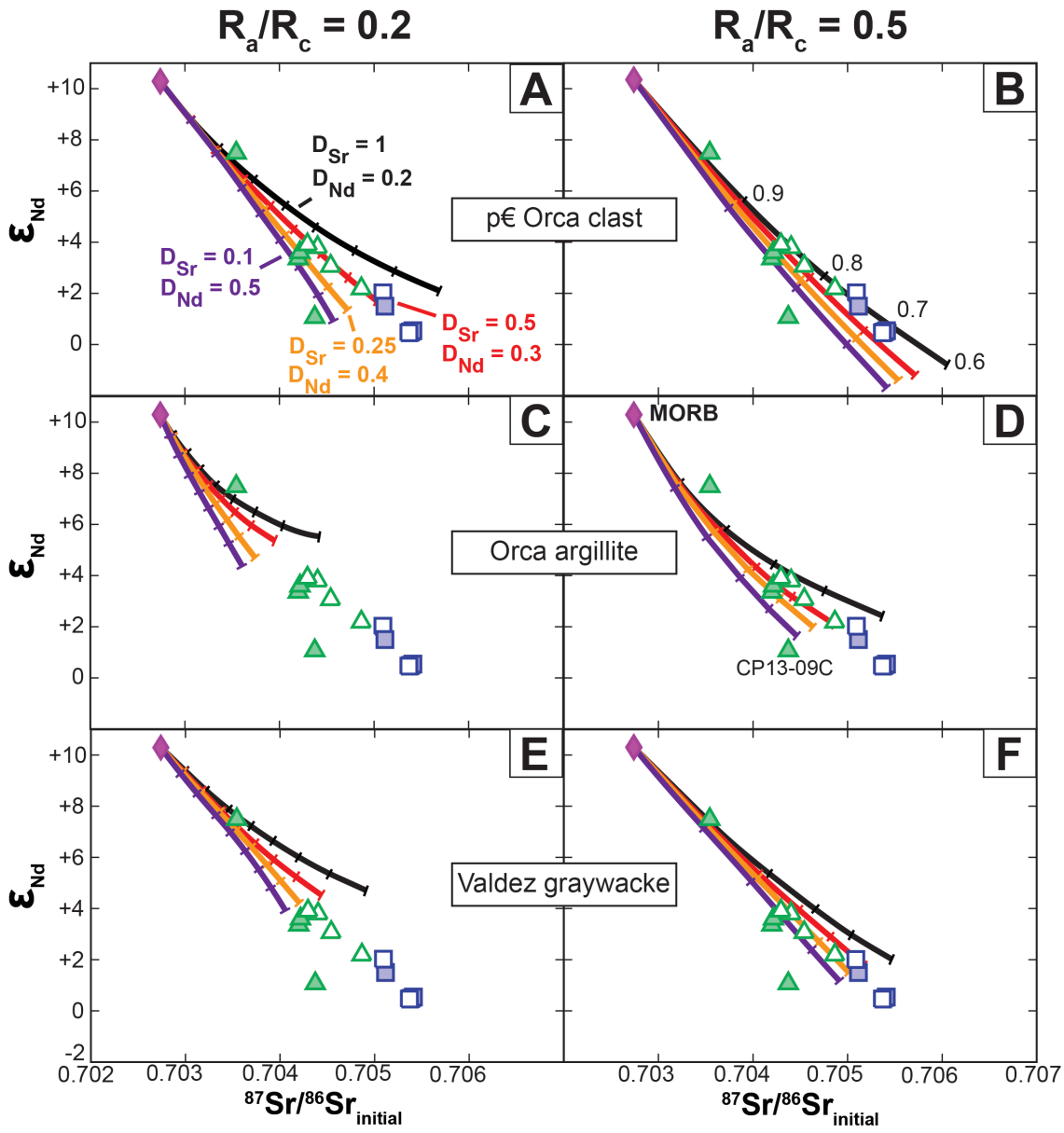


**Figure 31.** AFC models involving MORB as a parental magma. Table 6 gives the parameters used in the models. Tick marks represent 10% intervals of total F (0.9, 0.8, etc.). Different colored curves indicate different bulk distribution coefficients (D) for Sr and Nd, which are labled in panel (A). Symbols as in Figure 6.

**Table 6.** Parameters used in AFC models displayed in Figure 31

| Panel | $R_a/R_c$ | Parent Magma | Rb | Sr | Sm | Nd | $\varepsilon_{Nd}$ | $^{87}Sr/^{86}Sr_{initial}$ |
|---|---|---|---|---|---|---|---|---|
| A-F | 0.2/0.5 | MORB | 2.93 | 141 | 2.96 | 9.30 | 10.29 | 0.70274 |
| **Panel** | **$R_a/R_c$** | **Assimilant** | **Rb** | **Sr** | **Sm** | **Nd** | **$\varepsilon_{Nd}$** | **$^{87}Sr/^{86}Sr_{initial}$** |
| A | 0.2 | p€ Orca clast | 69.3 | 334 | 5.04 | 29.5 | -9.4 | 0.70816 |
| B | 0.5 | p€ Orca clast | 69.3 | 334 | 5.04 | 29.5 | -9.4 | 0.70816 |
| C | 0.2 | Orca argillite | 40 | 128 | 4.71 | 22.7 | -3.8 | 0.70804 |
| D | 0.5 | Orca argillite | 40 | 128 | 4.71 | 22.7 | -3.8 | 0.70804 |
| E | 0.2 | Valdez graywacke | 57.4 | 362 | 5.36 | 27.6 | -3.3 | 0.70641 |
| F | 0.5 | Valdez graywacke | 57.4 | 362 | 5.36 | 27.6 | -3.3 | 0.70641 |

Varying the bulk distribution coefficients for Sr and Nd alters the shape and length of the modeling curve (Figure 31A). In general, models using $D_{Sr} = 1$ and $D_{Nd} = 0.2$ (black curves; Figures 31-33) or $D_{Sr} = 0.5$ and $D_{Nd} = 0.3$ (red curves; Figures 31-33) better fit the isotopic compositions of Crawfish and Krestof host granodiorites/tonalites. However, for some of the Crawfish enclaves (most notably CP13-09C), models with $D_{Sr} = 0.25$ and $D_{Nd} = 0.1$ (purple curves: Figure 31-33) give the closest matches. This observation suggests that plagioclase, for which the distribution coefficient for Sr is 1.6 – 5 (Rollinson, 1993), was not an important fractionating phase during the evolution of melts emplaced as enclaves.

Models assuming enclave CP13-07D as the parental magma are shown in Figure 32, with model parameters reported in Table 7. No matter how isotopically evolved the assimilant is, AFC processes involving low assimilation rates cannot generate any of the Crawfish and Krestof compositions. When high rates of assimilation ($R_a/R_c = 0.5$) are assumed, only assimilation of the most evolved sediment can produce the Crawfish and Krestof compositions (Figure 32).

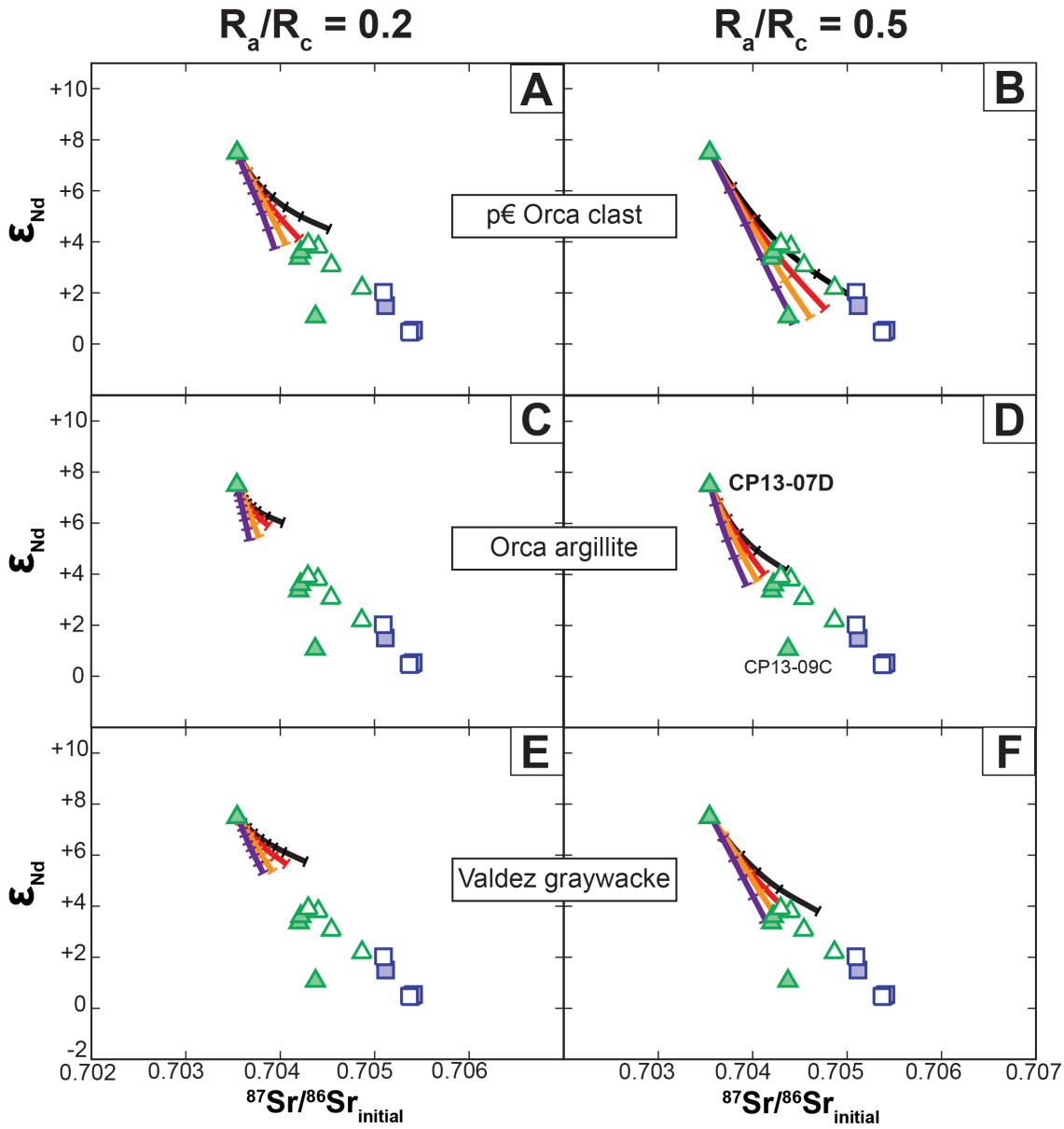


**Figure 32.** AFC models involving enclave CP13-07D as a parental magma. Table 7 gives the parameters used in the models. Tick marks represent 10% intervals of total F (0.9, 0.8, etc.). Different colored curves represent different bulk distribution coefficients for Sr and Nd as defined in Figure 31A. Symbols as in Figure 6.

**Table 7.** Parameters used in AFC models displayed in Figure 32

| Panel | $R_a/R_c$ | Parent Magma | Rb | Sr | Sm | Nd | $\varepsilon_{Nd}$ | $^{87}Sr/^{86}Sr_{initial}$ |
|---|---|---|---|---|---|---|---|---|
| A-F | 0.2/0.5 | CP13-07D | 54.9 | 721 | 5.52 | 32.2 | 7.52 | 0.70354 |
| **Panel** | **$R_a/R_c$** | **Assimilant** | **Rb** | **Sr** | **Sm** | **Nd** | **$\varepsilon_{Nd}$** | **$^{87}Sr/^{86}Sr_{initial}$** |
| A | 0.2 | p€ Orca clast | 69.3 | 334 | 5.04 | 29.5 | -9.4 | 0.70816 |
| B | 0.5 | p€ Orca clast | 69.3 | 334 | 5.04 | 29.5 | -9.4 | 0.70816 |
| C | 0.2 | Orca argillite | 40 | 128 | 4.71 | 22.7 | -3.8 | 0.70804 |
| D | 0.5 | Orca argillite | 40 | 128 | 4.71 | 22.7 | -3.8 | 0.70804 |
| E | 0.2 | Valdez graywacke | 57.4 | 362 | 5.36 | 27.6 | -3.3 | 0.70641 |
| F | 0.5 | Valdez graywacke | 57.4 | 362 | 5.36 | 27.6 | -3.3 | 0.70641 |

Figure 33 compares AFC models using three different mafic parental magmas and the most evolved sedimentary assimilant compositions (Table 8). For models where low rates of assimilation are assumed, neither OIB nor enclave CP13-07D are plausible parents. In contrast, models involving MORB can produce the Crawfish and Krestof compositions, especially when high rates of assimilation are assumed. For models using $R_a/R_c = 0.5$, all three mafic magmas seem to be plausible parents for the Crawfish samples. Only models assuming a MORB parent can generate the Krestof compositions.

The discrepancy between MORB and OIB/CP13-07D models illustrates the importance of the difference in Rb, Sr, Sm, and Nd elemental abundances between the parental magma and assimilant (Figure 33 and Table 8). Although OIB and CP13-07D are more isotopically evolved than MORB (Table 8), the lengths of the AFC curves are shorter because of their enriched character (Figure 33). The high concentrations of Sr and Nd in OIB and CP13-07D dilute the effects of assimilating isotopically evolved sediment (DePaolo, 1981).

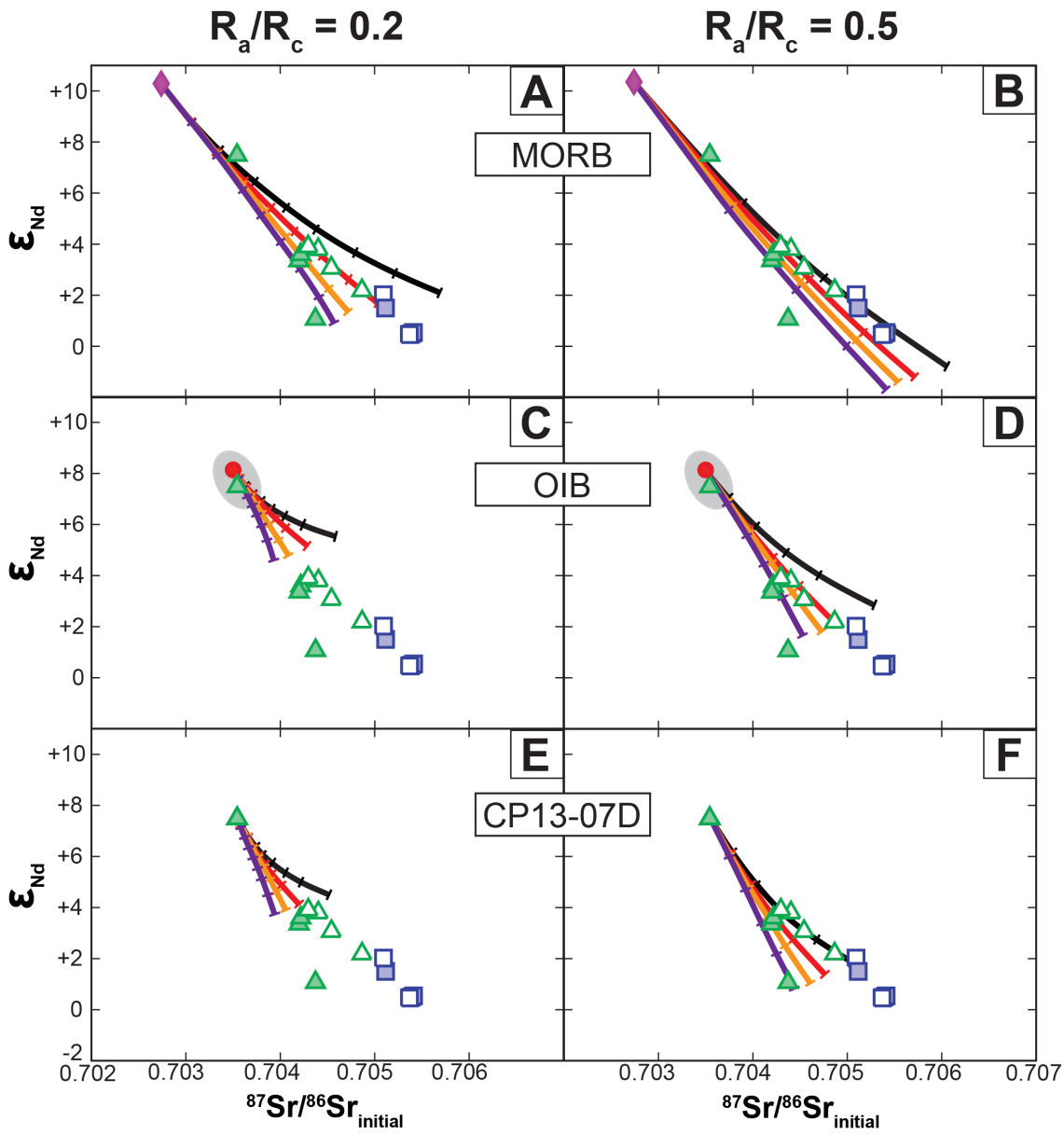


**Figure 33.** Comparison of AFC models when different mafic parental magmas are assumed (Table 8). All models shown involve assimilation of the most evolved Orca group sediment composition (Table 8). Tick marks represent 10% intervals of F, which indicates the total melt fraction remaining (0.9, 0.8, etc.). Different colored curves represent different bulk distribution coefficients for Sr and Nd as defined in Figure 31A. Symbols as in Figure 6.

**Table 8.** Parameters used in AFC models displayed in Figure 33

| Panel | $R_a/R_c$ | Parent Magma | Rb | Sr | Sm | Nd | $\varepsilon_{Nd}$ | $^{87}Sr/^{86}Sr_{initial}$ |
|---|---|---|---|---|---|---|---|---|
| A | 0.2 | MORB | 2.93 | 141 | 2.96 | 9.30 | 10.29 | 0.70274 |
| B | 0.5 | MORB | 2.93 | 141 | 2.96 | 9.30 | 10.29 | 0.70274 |
| C | 0.2 | OIB | 31 | 660 | 10.0 | 38.5 | 8.14 | 0.70350 |
| D | 0.5 | OIB | 31 | 660 | 10.0 | 38.5 | 8.14 | 0.70350 |
| E | 0.2 | CP13-07D | 54.9 | 721 | 5.52 | 32.2 | 7.52 | 0.70354 |
| F | 0.5 | CP13-07D | 54.9 | 721 | 5.52 | 32.2 | 7.52 | 0.70354 |
| **Panel** | **$R_a/R_c$** | **Assimilant** | **Rb** | **Sr** | **Sm** | **Nd** | **$\varepsilon_{Nd}$** | **$^{87}Sr/^{86}Sr_{initial}$** |
| A-F | 0.2/0.5 | p€ Orca clast | 69.3 | 334 | 5.04 | 29.5 | -9.4 | 0.70816 |

To further evaluate the models based on Sr and Nd isotopes, the Rb and Sm elemental compositions produced in the AFC models are shown in Figure 34. These models show that the only way to generate Krestof compositions via AFC processes requires a MORB parental magma. The Sm-$\varepsilon_{Nd}$ systematics rule out OIB and CP13-07D as parents to the Crawfish and Krestof magmas.

AFC models indicate that a MORB parental magma and high rates of assimilation of evolved sediment might be an explanation for the origin of the Krestof Island pluton. Although some modeled compositions for Sr and Nd isotopes fit the Crawfish compositions, the variations in elemental abundances for Rb and Sm rule out those models.

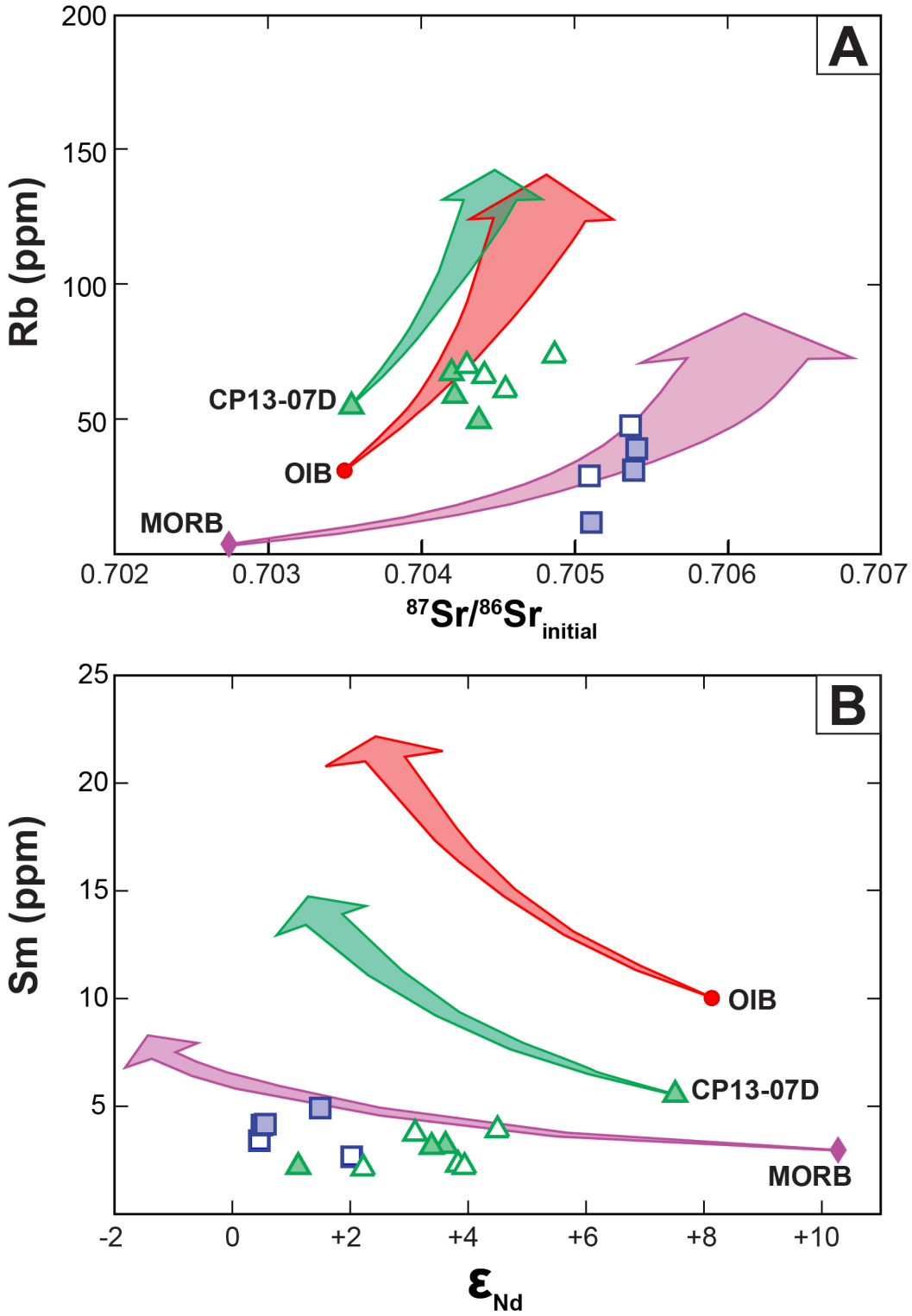


**Figure 34.** (A) Rb versus $^{87}Sr/^{86}Sr_{initial}$ diagram and (B) Sm versus $\varepsilon_{Nd}$ diagram showing AFC models and Crawfish/Krestof compositions. Model parameters are the same as in Figure 33 and Table 7, but $R_a/R_c$ was limited to 0.5. Symbols as in Figure 6.

*Bulk mixing models*

Bulk mixing models were constructed to further evaluate the petrogenetic processes responsible for producing the compositions observed in Crawfish and Krestof samples. All mixing models were calculated using IgPet for Mac: 2013, and assumed the same three parental magmas considered in AFC models (MORB, OIB, and CP13-07D).

Endmember mixing between the MORB (Kelemen, 2004) parental magma and two CPW sediments is shown on a Sr/Y versus Y diagram (Figure 35). The best fit for Crawfish compositions requires mixing with the most Sr/Y-enriched CPW sediment. Krestof compositions can be generated through mixing involving either the Sr/Y-enriched sediment or average Orca group (Plafker et al., 1989). Typical OIB and least evolved enclave CP13-07D have too high of Sr/Y ratios to be plausible endmembers of mixing. In addition, these models do not account for any known physical mechanism to melt the sediments before mixing with the mantle-derived endmember. Partial melting of sediment is complicated by fractionating and/or residual phases that significantly alter the chemistry of the partial melt, leading to magmas with very different compositions than the sediments themselves.

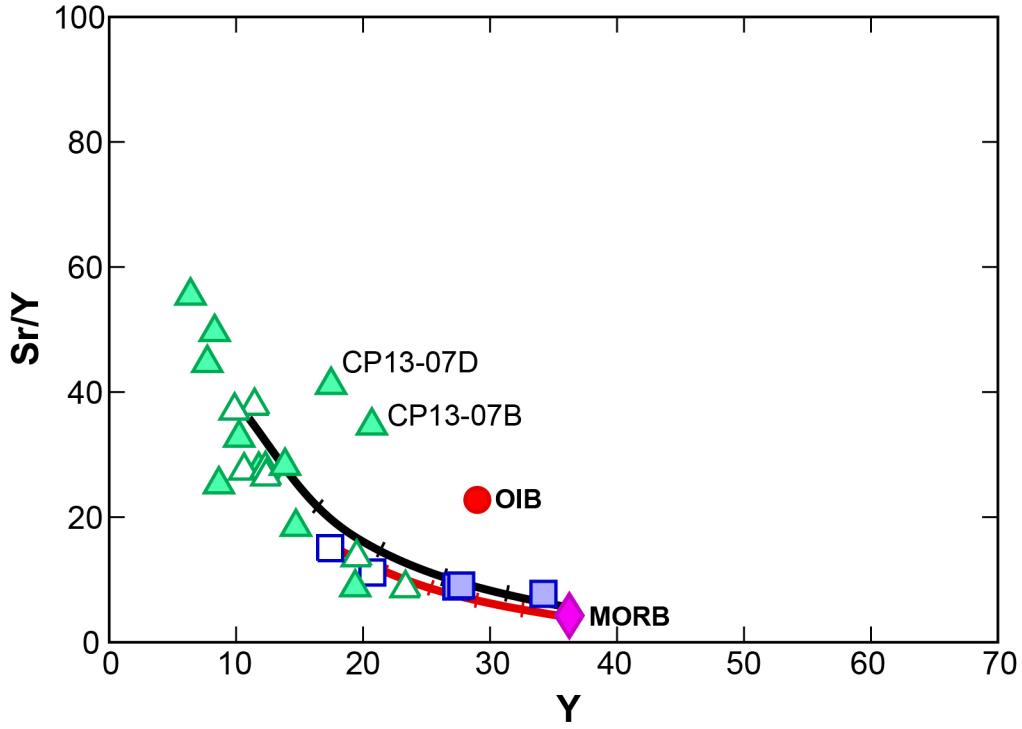


**Figure 35.** Calculated mixing curves for Sr/Y versus Y assuming simple bulk mixing between MORB and sedimentary endmember compositions. The black curve shows mixing with Sr/Y enriched sedimentary sample (Sitka greywacke D512687 from EarthChem). The red curve represents mixing with average Orca group sediment from Plafker et al. (1989). MORB and OIB compositions from Kelemen et al. (2004) and Sun and McDonough (1989), respectively. Tick marks represent 20% mixing intervals.

Figure 36 illustrates the Sr and Nd isotopic mixing lines between a MORB endmember and a range of CPW sedimentary compositions. With the exception of Crawfish enclave CP13-09C, the broad mixing field overlaps Crawfish and Krestof compositions. Mixing lines produced using OIB or enclave CP13-07D would likewise provide reasonable fits to the Crawfish and Krestof data. Endmember mixing models of isotopic compositions are superior to those for trace elements (Figure 35), because the isotopes are not susceptible to fractionation during partial melting.

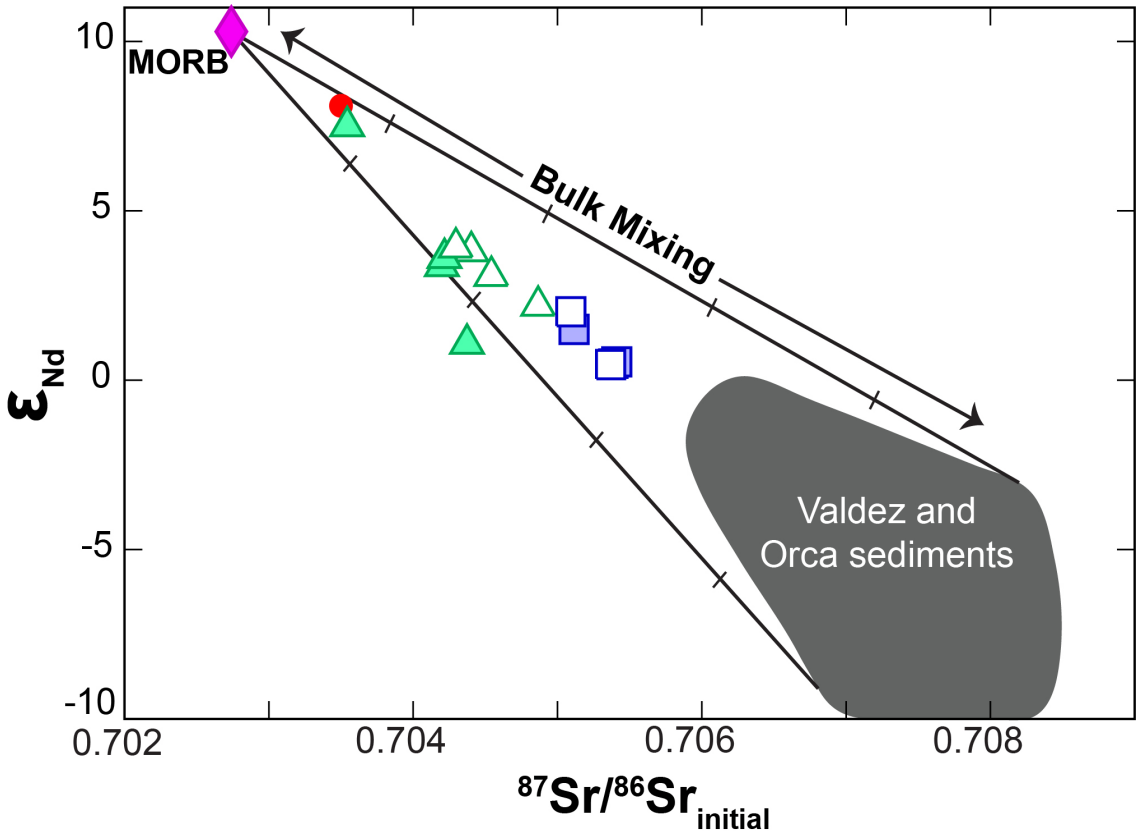


**Figure 36.** Generalized mixing curve for an $\varepsilon_{Nd}$ vs. $^{87}Sr/^{86}Sr_{initial}$ diagram using MORB as the mantle parent and the complete range of isotopic composition from Farmer et al., 1993 as possible assimilants. MORB and OIB compositions from Kelemen et al. (2004) and Sun and McDonough (1989), respectively. Tick marks represent 20% mixing intervals.

# DISCUSSION

The Crawfish and Krestof plutons, emplaced 53-47 Ma in the eastern SBPB, are composed of granodiorites and tonalites that host a suite of magmatic enclaves, which range in composition from gabbrodiorite to granite (Figure 9). With regards to major elements, Crawfish and Krestof host granodiorites/tonalites are broadly similar to other SBPB granitoids, however, the least evolved enclaves (< 62 wt% $SiO_2$) from both plutons are distinct (Figure 26). Many enclaves and host tonalites/granodiorites from the Crawfish Inlet pluton exhibit trace element characteristics typical of adakites, as observed for other intrusions in the eastern SBPB (Figures 18, 21, and 28). Approximately 50 Ma intrusive rocks of the CPC also display adakitic characteristics (Figure 30). Krestof samples do not possess adakitic characteristics (Figures 18, 21, and 28), despite their coeval nature and spatial proximity to the Crawfish pluton (Figure 2). In addition, Sr and Nd isotopic data for Crawfish/Krestof samples are similar to those observed for other eastern SBPB intrusive rocks (Figure 23).

Magmatic zircons isolated from the Crawfish pluton exhibits correlations between U/Pb age and $\varepsilon_{Hf}$, with older samples appearing to have a more evolved nature (Figure 24). The same relationship is observed for a small set of whole-rock Sr and Nd isotopic analyses of host granitoid samples (Figure 25).

The least evolved enclaves from the Crawfish and Krestof plutons have distinct trace element and Sr-Nd isotopic characteristics (Figures 15, 20, and 23). These distinctive characteristics preclude a common source rock and/or parental magma for the two enclave suites.

Trace element characteristics of the host granodiorites/tonalites suggest a significant involvement of sedimentary material in the Crawfish and Krestof plutons (Figures 19 and 22). AFC models assuming a MORB parental magma can explain both isotopic and selected trace element characteristics of the Krestof samples (Figures 31, 33, and 34). However, AFC models involving MORB were generally unsuccessful in producing the isotopic characteristics of Crawfish samples. AFC models involving OIB or Crawfish enclave CP13-07D appear to fit the isotopic compositions observed for Crawfish samples, but only when high rates of assimilation are assumed (Figures 32 and 33). In addition, those models predict trace element characteristics that do not match the observed Crawfish compositions (Figure 34).

Bulk mixing between MORB and CPW sedimentary endmembers generally provide good fits for the trace element and isotopic characteristics of Crawfish/Krestof samples. However, the physical mechanism through which mixing is taking place is unclear. Mixing models of trace elements are unreliable, because they may be affected substantially by fractionation during partial melting. Sr and Nd isotopic compositions are compatible for use with bulk mixing, because their compositions are not altered by partial melting and/or fractionation processes.

Trace element and isotopic compositions of least evolved Crawfish enclaves suggest the presence of localized OIB-type magmas within the Crawfish Inlet pluton. This result expands on prior studies characterizing the petrogenesis of SBPB intrusive rocks, all of which only considered MORB as parental to SBPB magmas. This suggests that future studies on the SBPB should explore the geochemistry of both host granitic rocks *and* their least-evolved enclaves.

In order to definitively comment on the proposed tectonic models of Cowan (2003) and Haeussler et al. (2003), more detailed geochemical comparisons across the SBPB, CPC, and Coast Range basaltic terrane are required. In particular, geochemical comparisons between the ~ 50 Ma plutons on Baranof Island and the Coast Range basaltic terrane may be key to distinguishing between possible tectonic reconstructions, because Cowan (2003) suggests Baranof Island and the Coast Range basaltic terrane were contiguous at the time the intrusions were emplaced.

To summarize, findings of this study suggest that compositions of two 53-47 Ma forearc plutons on Baranof Island were the result of petrogenetic processes involving some combination of mantle-derived mafic magma interacting with lower crustal and/or accretionary wedge sedimentary material. Mantle sources appear to include both OIB and MORB type sources. Lower crustal melting induced by underplating of mafic magmas, followed by mixing with the mantle-derived parent and/or potential AFC processes involving accretionary wedge sediments, offers one explanation for adakitic compositions observed in the Crawfish Inlet pluton. The chemically distinct, non-adakitic Krestof Island pluton may be the result of AFC processes involving a MORB parent and high rates of assimilation of isotopically evolved accretionary wedge sediments. Bulk mixing between mantle-derived magmas and sediments is an alternative explanation for generating the compositions observed in the Crawfish and Krestof plutons.

# ACKNOWLEDGEMENTS

I would like to thank Cameron Davidson and John Garver for making this project possible. I acknowledge NSF EAR 1116554 (to John Garver, Union College) and EAR 1116536 (to Cameron Davidson, Carleton College: Collaborative Research: Provenance and Thermal Evolution of the Chugach-Prince William Terrane Flysch, Southern Alaska) for funding. Sample collection and field studies were permitted by the Tongass National Forest. I'd also like to acknowledge the Keck Geology Consortium for funding and support. I thank Trinity University for the Semmes Distinguished Science scholarship for additional funding. I thank the Washington State University GeoAnalytical laboratory for providing XRF and ICP-MS analyses, and Staci Loewy at the Jackson School of Geosciences (UT-Austin) for Sr and Nd isotopic analyses. I'd like to thank and recognize the rest of the KECK Alaska 2013 field team: Meghan Riehl, Kate Kaminski, Bri Rick, Brian Frett, and Claudia Roig. Lastly, I would like to thank my research advisor Diane Smith at Trinity University for her guidance and hard work.

# REFERENCES


Arth, J.G., Barker, F. and Stern, T.W., 1988, Coast Batholith and Taku plutons near Ketchikan, Alaska: Petrography, geochronology, geochemistry, and isotopic character: American Journal of Science, v. 288-A, p. 461-489.

Ayuso, R., Haeussler, P., Bradley, D., Farris, D., Foley, N., and Wandless, 2009, The role of ridge subduction in determining the geochemistry and Nd-Sr-Pb isotopic evolution of the Kodiak batholith in southern Alaska: Tectonophysics, v. 464, p. 137-163.

Barker, F., 1979, Trondhjmite: Definition, environment and hypotheses of origin, *in* Barker, F., ed., Trondhjemites, dacites, and related rocks: Elsevier Scientific, New York, p. 1-12.

Barker, F., Farmer, G.L., Ayuso, R.A., Plafker, G., and Lull, J.S., 1992, The 50 Ma granodiorite of the eastern Gulf of Alaska: Melting in an accretionary prism in the forearc: Journal of Geophysical Research, v. 97, p. 6,757-6,778.

Bowen, N.L., 1928, The evolution of igneous rocks: Princeton, New Jersey, Princeton University Press, 332 p.

Bradley, D., Kusky, T., Haeussler, P., Goldfarb, R., Miller, M., Dumoulin, J., Nelson, S.W., and Karl, S.M., 2003, Geologic signature of early Tertiary ridge subduction in Alaska: Geological Society of America Special Papers 371, p. 19-49.

Chauvel, C., Lewin, E., Carpentier, M., Arndt, N.T., and Marini, J.-C., 2008, Role of recycled oceanic basalt and sediment in generating the Hf-Nd mantle array: Nature, v. 1, p. 64-67.

Cowan, D.S., 2003, Revisiting the Baranof-Leech River hypothesis for early Tertiary coastwise transport of the Chugach-Prince William Terrane: Earth and Planetary Science Letters, v. 213, p. 463–475.

Cox, K.G., Bell, J.D., and Pankhurst, R.J., 1979, The interpretation of igneous rocks: Allen & Unwin, London, 450 p.

Dawes, R.L., 1994, Mount St. Helens: Potential example of the partial melting of the subducted lithosphere in a volcanic arc: Comments and Reply: Geology, v. 22, p. 187-188.

DePaolo, D.J., 1981, Trace element and isotopic effects of combined wallrock assimilation and fractional crystallization: Earth and Planetary Science Letters, v. 53, p. 189-202.

DePaolo, D.J., and Wasserburg, G.J., 1976, Nd isotopic variations and petrogenetic models: Geophysical Research Letters, v. 3, p. 249-252.

Drummond, M.S., and Defant, M.J., 1990, A model for trondhjemite-tonalite-dacite genesis and crustal growth via slab melting Archean to modern comparisons: Journal of Geophysical Research, v. 95, p. 21,503-21,521.

Drummond, M.S., Bordelon, M., Deboer, J.Z., Defant, M.J., Bellon, H., and Feigenson, M.D., 1995, Igneous petrogenesis and tectonic setting of plutonic and volcanic rocks of the Cordillera de Talamanca, Cost Rica Panama, Central American arc: American Journal of Science, v. 295, p. 875-919.

Farmer, G.L., Ayuso, R., and Plafker, G., 1993, A Coast Mountains provenance for the Valdez and Orca groups, southern Alaska, based on Nd, Sr, and Pb isotopic evidence: Earth and Planetary Science Letters, v. 116, p. 9-21.

Farris, D. W., and Paterson, S. R., 2009, Subduction of a segmented ridge along a curved continental margin: Variations between the western and eastern Sanak–Baranof belt, southern Alaska: Tectonophysics, v. 464, p. 100-117.

Flood, R.H., and Vernon, R.H., 1988, Microstructural evidence of orders of crystallization in granitoid rocks: Lithos, v. 21, p. 237-245.

Forsythe, R., and Nelson, E., 1985, Geological manifestations of ridge collision: Evidence from the Golfo de Penas-Tatio Basin, southern Chile: Tectonics, v. 4, p. 477-495.

Frost, T.P., and Mahood, G.A., 1987, Field, chemical, and physical constraints on mafic-felsic magma interaction in the Lamarck Granodiorite, Sierra Nevada, California: Geological Society of America Bulletin, v. 99, p. 272-291.

Garrison, J.M., and Davidson, J.P., 2003, Dubious case for slab melting in the northern volcanic zone of the Andes: Geology, v. 31, p. 565-568.

Girardi, J.D., Patchett, P.J., Ducea, M.N., Gehrels, G. E., Robinson Cecil, M., Rusmore, M.E., Woodsworth, G.J., Pearson, D.M., Manthei, C., and Wetmore, P., 2012, Elemental and isotopic evidence for granitoid genesis from deep-seated sources in the Coast Mountains Batholith, British Columbia: Journal of Petrology, v. 53, p. 1505-1536.

Groome, W.G., Thorkelson, D.J., and Friedman, R.M., 2003, Magmatic and tectonic history of the Leech River Complex, Vancouver Island, British Columbia: Evidence for ridge-trench intersection and accretion of the Crescent terrane: Geological Society of America Special Papers 371, p. 327-353.

Haeussler, P., Bradley, D.C., Wells, R.E., and Miller, M.L., 2003, Life and death of the Resurrection plate: Evidence for its existence and subduction in the northeastern Pacific in the Paleocene–Eocene time: Geological Society of America Bulletin, v. 115, p. 867–880.

Hammarstrom, J.M., and Zen, E., 1986, Aluminum in hornblende: An empirical igneous geobarometer: American Mineralogist, v. 71, p. 1297-1313.

Harris, N.R., Sisson, V.B., Wright, J.E., and Pavlis, T.L., 1996, Evidence of Eocene mafic underplating during forearc intrusive activity, eastern Chugach Mountains, Alaska: Geology, v. 24, p. 263–266.

Hill, M.D., 1979, Volcanic and plutonic rocks of the Kodiak-Shumagin shelf, Alaska:

subduction deposits and near-trench magmatism: Ph.D. thesis, University of California-Santa Cruz, 274 p.

Hill, M., Morris, J., and Whelan, J., 1981, Hybrid granodiorites intruding the accretionary prism, Kodiak, Shumagin and Sanak Islands, Southwest Alaska: Journal of Geophysical Research, v. 86, 10,569-10,590.

Holland, J.E., Surpless, B., Smith, D.R., Loewy, S. L., and Lackety J.S., 2013, Intrusive history and petrogenesis of the Ash Mountain Complex, Sierra Nevada batholith: Geosphere, v. 9, p. 691-717.

Hudson, T.L., Plafker, G., and Peterman, Z.E., 1979, Paleogene anatexis along the Gulf of Alaska margin: Geology, v. 7, p. 573–577.

Irvine, T.N., and Baragar, W.R.A., 1971, A guide to the chemical classification of the common volcanic rocks: Canadian Journal of Earth Sciences, v. 8, p . 523-548.

Johnston, S.T., and Thorkelson, D.J., 1997, Cocos-Nazca slab window beneath Central America: Earth and Planetary Science Letters, v. 146, p. 465-474.

Karl, S.M., Haeussler, P.J., Zumsteg, C.L., Himmelberg, G.R., Layer, P.W., Friedman, R.F., Roeske, S.M., and Snee, L.W., 2014, Geologic map of Baranof Island, Southeast Alaska: U.S. Geological Survey Investigations Map, 14-xxx, *in press*.

Kay, S.M., Ramos, V.A., and Marquez, M., 1993, Evidence in Cerro Pampa volcanic rocks for slab-melting prior to ridge-trench collision in southern South America: Journal of Geology, v. 101, p. 703–714.

Kelemen, P.B., Yogodzinski, G.M., and Scholl, D.W., 2004, Along-strike variation in lavas of the Aleutian island arc: Implications for the genesis of high Mg# andesite and the continental crust, *in* Inside the Subduction Factory, AGU Monograph, v. 138, p. 223-276.

Loney, R.A, Brew, D.A., Muffler, P., and Pomeroy, J.S., 1975, Reconnaissance geology of Chichagof, Baranof, and Kruzof Islands, southeastern Alaska: U.S. Geological Survey Professional Paper 792, p. 46-54.

Lull, J.S., and Plafker, G., 1985, Petrography of sandstone from the Yakutat Group, Malaspina district, southern Alaska, *in* Bartsch-Winkler, S., and Reed, K.M., eds., The U.S. Geological Survey in Alaska: Accomplishments during 1983: U.S. Geological Survey Circular 945, p. 73-77.

Lytwyn, J., Casey, J., Gilbert, S., and Kusky, T., 1997, Arc-like mid-ocean ridge basalt formed seaward of a trench-forearc system just prior to ridge subduction: An example from subaccreted ophiolites in southern Alaska: Journal of Geophysical Research, v. 102, p. 10,225–10,243.

Lytwyn, J., Gilbert, S., Casey, J., and Kusky, T.M., 2000, Geochemistry of near-trench intrusives associated with ridge subduction, Seldovia quadrangle, Southern Alaska: Journal of Geophysical Research, v. 105, p. 27,957–27,978.

Madsen et al., J.K., Thorkelson, D.J., Friedman, R.M., and Marshall, D.D., 2006,

Cenozoic to Recent plate configurations in the Pacific Basin: Ridge subduction and slab window magmatism in western North America: Geosphere, v. 2, p. 11-34.

Mahoney, B.J., Gordee, S.M., Haggart, J.W., Friedman, R.M., Diakow, L.J. and Woodsworth, G.J., 2009, Magmatic evolution of the eastern coast plutonic complex, Bella Coola region, west-central British Columbia: Geological Society of America Bulletin, v. 121, p. 1362-1380.

Martin, H., 1999, Adakitic magmas: modern analogues of Archaean granitoids: Lithos, v. 46, p. 411-429.

McCulloch, M.T., and Perfit, M.R., 1981, $^{143}$/Nd/$^{144}$Nd, $^{87}$Sr/$^{86}$Sr and trace element constraints on the petrogenesis of Aleutian island arc magmas: Earth and Planetary Science Letters, v. 56, p. 167-179.

Moore, J.C., Byrne, T., Plumley, P.W., Reid, M., Gibbons, H., and Coe, R.S., 1983, Paleogene evolution of the Kodiak Islands, Alaska: Consequences of ridge-trench interaction in a more southerly latitude: Tectonics, v. 2, p. 265–293.

Murphy, J.B., Hynes, A.J., Johnston, S.T., and Keppie, J.D., 2003, Reconstructing the ancestral Yellowstone plume from accreted seamounts and its relationship to flat-slab subduction: Tectonophysics, v. 365, p. 185-194.

Pavlis, T.L., and Sisson, V.B., 2003, Development of a subhorizontal decoupling horizon in a transpressional system, Chugach metamorphic complex, Alaska; evidence for rheological stratification of the crust: Geological Special Papers 371, p. 191-216.

Pearce, J.A., Harris, N.B.W., and Tindle, A.J., 1984, Trace element discrimination diagrams for the tectonic interpretation of granitic rocks: Journal of Petrology, v. 25, p. 956-983.

Plafker, G., Nokleberg, W.J., and Lull, J.S., 1989, Bedrock geology and tectonic evolution of the Wrangellia, Peninsular and Chugach terraces along the Trans-Alaska Crustal Transect in the Chugach Mountains and southern Copper River basin, Alaska: Journal of Geophysical Research, v. 94, p. 4255-4295.

Plafker, G., Moore, J.C., Winkler, G.R., 1994, Geology of the southern Alaska margin, *in* Plafker, G., and Berg, H.C., eds., The Geology of Alaska: Boulder, Colorado, Geological Society of America, The Geology of North America, v. G-1, p. 389-426.

Rick, B.J., Frett, B.K., Davidson, C.M., and Garver, J.I., 2014, U/Pb dating of detrital zircon from Seward and Baranof Island provides depositional links across the Chugach-Prince William terrane and Southeastern Alaska: Cordilleran Tectonics Workshop, University of British Columbia – Okanagan, Abstracts with program, p. 35-36.

Roig, C.I., Casovie, A.J., Davidson, C.M., Garver, J.I., and Valley, J.W., 2014, Oxygen and Hafnium isotope geochemistry of zircon, quartz, and garnet from the Crawfish Inlet and Krestof Island plutons, Baranof Island, Alaska: KECK Symposium Volume 2014, p. xx-xxxx.

Rollinson, H.R., 1993, Using geochemical data: Routledge, New York, 352 p.

Shand, S.J., 1951, Eruptive rocks: John Wiley, New York, 488 p.

Short, A.K., 2013, Age and petrogenesis of the Shumagin batholith in western Chugach-Prince William terrane, Alaska: Short contribution, Keck Geology Consortium, 26th annual symposium volume, p. 26-31.

Sisson, V.B., Pavlis, T.L., Roeske, S.M., and Thorkelson, D.J., 2003a, Introduction: An overview of ridge-trench interactions in modern and ancient settings: Geological Society of America Special Papers 371, p. 1–18.

Sisson, V.B., Poole, P.R., Harris, N.R., Burner, H.C., Pavlis, T.L., Copeland, P., Donelick, R.A., and McLelland, W.C., 2003b, Geochemical and geochronologic constraints for genesis of a tonalite–trondhjemite suite and associated mafic intrusive rocks in the eastern Chugach Mountains, Alaska: A record of ridge-transform subduction: Geological Society of America Special Papers 371, p. 293–326.

Sun, S.-s., and McDonough, W.F., 1989, Chemical and isotopic systematics of oceanic basalts: Implications for mantle composition and processes: Geological Society Special Publication 42, p. 313-345.

Thorkelson, D.J., and Taylor, R.P., 1989, Cordilleran slab windows: Geology, v. 17, p. 833-836.

Vernon, R.H., 1990, Crystallization and hybridism in microgranitoid enclave magmas: Microstructural evidence: Journal of Geophysical Research, v. 95, p. 17,849-17,859.

Wenner, J.M., and Coleman, D.S., 2004, Magma mixing and Cretaceous crustal growth: geology and geochemistry of granites in the central Sierra Nevada batholith, California: International Geology Review, v. 46, p. 880-903.

White, A.J.R., Clemens, J.D., Holloway, J.R., Silver, L.T., Chappell, B.W., and Wall, V.J., 1986, S-type granites and their probable absence in southwestern North America: Geology, v. 14, p. 115-118.

Wilson, M., Igneous petrogenesis: A global tectonic approach: Unwin Hyman, London, 466 p.

Zindler, A., Jagoutz, E., and Goldstein, S., 1982, Nd, Sr and Pb isotopic systematics in a three component mantle: a new perspective: Nature, v. 298, p. 519-523.

Zindler, A. and Hart, S., 1986, Chemical geodynamics: Annual Reviews in Earth and Planetary Science, v. 14, p. 493-57.

# APPENDIX I

## *Field Methods and Sampling*

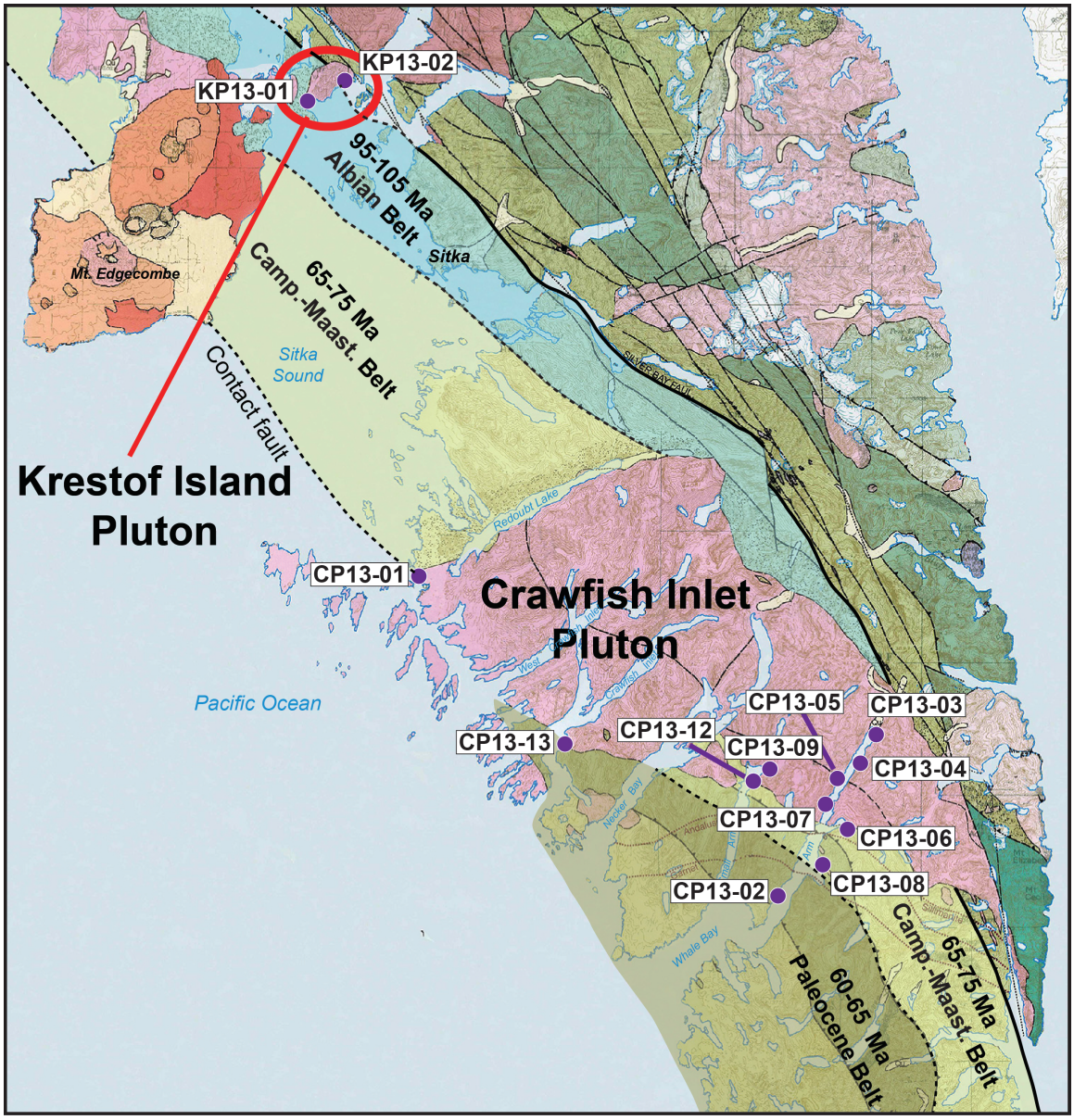


**Figure I-a.** Terrane map of Baranof Island with Paleocene intrusive bodies marked in pink. All sample localities from this study are marked by purple circles with their corresponding sample name boxed nearby.

## *Krestof Pluton*

**KP13-01**
*Host granitoid and enclaves:* 57.15755° N – 135.52324° W

Enclaves/xenoliths were extremely abundant, with many of the enclaves exhibiting 'pillowy' textures. Evidence for heterogeneity in both composition and grains size within the enclaves was noticeable across the outcrop. Some evidence for cuspate/lobate (co-magmatic) textures observed, including wavy contacts along enclave rims. Also evidence of the greywacke xenoliths hosted in both the pluton as well as in magmatic inclusions (photo below). The host pluton is noticeably higher in ferromagnesian (CI = ~ 30) minerals and is finer-grained than the Crawfish pluton. Enclaves (*01B*) and (*01C*) were notably more aphanitc than surrounding granitoid body, with sample *01C* appearing the most mafic. This sample (01C) appeared porphyritic-aphanitic with plagioclase phenocrysts significantly larger than the surrounding groundmass.

**Figure I-b:** Xenolith of Sitka greywacke hosted within a magmatic inclusion found in the float at locality *KP13-01*. This location displayed evidence for active magma mixing (enclaves) and assimilation (xenoliths) processes.

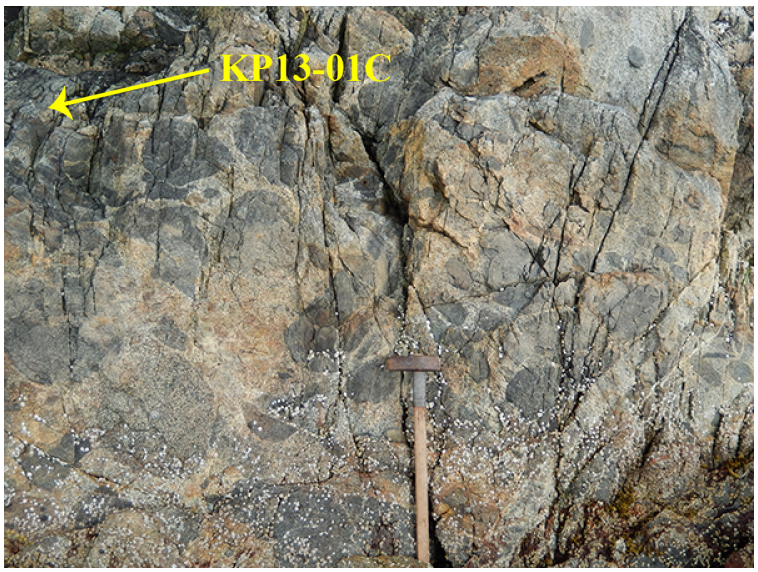


**Figure I-c.** Outcrop photo showing the abundance of mafic inclusions at sample locality KP13-01. Enclave KP13-01C was taken from the large enclave in the upper left corner.

**KP13-02**

*Host granitoid and enclaves:* 57.16589° N – 135.48474° W

Outcrop appeared very similar to *KP13-01* exposure with fewer enclaves present. Enclaves present appeared homogeneous. Host pluton was nearly identical to *KP13-01* sample.

**Figure I-d.** Characteristic enclave sampled at locality KP13-02 approximately 500 m East of previous sample location. Again, evidence for heterogeneous magmas was preserved by magmatic inclusions of seemingly more mafic nature.

## *Crawfish Pluton*

**CP13-01**
*Host granitoid:* 56.84694° N – 135.38065° W

Sample collected adjacent to the northern contact with Sitka greywacke. Very sharp contacts but large zones of mixed granitic/greywacke observed. Very few smaller xenoliths of greywacke were observed, and no enclaves were present. Low abundance of ferromagnesian minerals, with those present appearing to be almost exclusively biotite. The lack of aphanitic textures in the pluton and growth of metamorphic minerals in the greywacke near the contact suggests minimal contact metamorphism effects.

**Figure I-e:** Sharp contact at northwestern edge of Crawfish pluton with Sitka greywacke country rock. Multiple large blocks of apparent greywacke 'xenoliths' were observed near the sampling locality.

**CP13-02**
*Host granitoid (Leucogranite):* 57.16589° N – 134.94612° W

Small intrusive body exposed at the western edge of the Whale Bay's Great Arm. Extremely muscovite-rich leucogranite with no ferromagnesian silicates. Significant pyrite observed, possibly result of large-scale melting of pyrich-rich mudstone such as the Sitka Greywacke (personal communication, Cam Davidson). Sharp contact with adjacent greywacke, and no zones of mixed granite/greywacke were observed along shoreline.

**CP13-03**
*Host granitoid and enclaves:* 56.74030° N – 134.83032° W

Samples collected at the end of the Great Arm, Whale Bay. Similar outcrop to sample *CP13-01* although the pluton appears to contain higher ferromagnesian content at this locality (CI = 12-15). The abundance of enclaves as well as 'schliering' textures within dikes/coeval magma injections suggests magma mixing/mingling processes were active. Large enclaves contain inclusions of the surrounding granitoid body; possibly suggesting injection of intermediate/mafic magma occurred following significant crystal fractionation (> 20 %) of pluton. Other enclaves contained xenoliths of greywacke country rock. Enclave samples (*03B*), (*03C*), and (*03D*) were all drilled from different phases of the same large magmatic inclusion. Sample (*03D* – presumably most mafic) was collected from the core of the inclusion with (*03C*) and (*03B*) collected increasingly close to the rim.

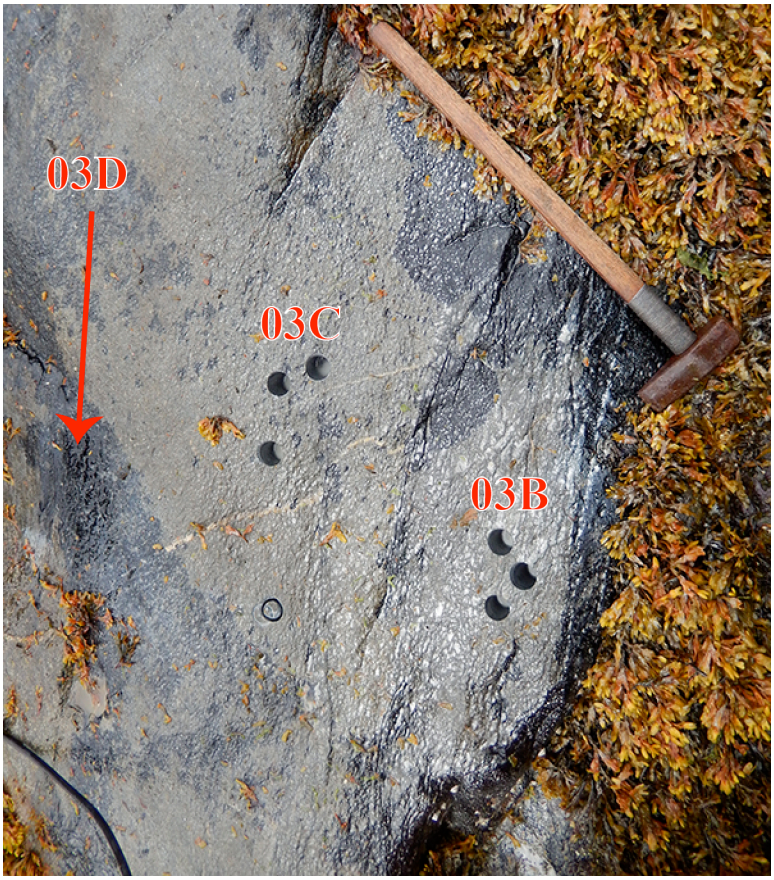


**Figure I-f.** Large magmatic inclusion with variable compositions that was drilled to obtain enclave samples at locality *CP13-03*. Paleomagnetic cores were also sampled at this location within the same inclusion.

**CP13-04**

*Host granitoid:* 56.72392° N – 134.84612° W

Pluton is significantly more homogenous than at *CP13-03* exposure. Little evidence of different magma injections in the form of enclaves and/or greywacke xenoliths, but some banding textures were observed (possibly crystal fractionation and layered settling of more ferromagnesian minerals). Fresh surface was collected with biotite appearing as dominant ferromagnesian mineral with CI ~15. Documented on site as biotite granodiorite/tonalite.

**CP13-05**

*Host granitoid and 'hybrid' inclusion:* 56.71241° N – 134.87527° W

Granitoid sample recorded as granodiorite/tonalite with similar appearance to other Crawfish granitoid samples (CI = 12). Hybrid magma/inclusion *CP13-05B* contains higher percentage of ferromagnesian minerals (CI = ~25) with notably more hornblende. Hybrid magma displays porphyritic texture with large (~ 5 mm) biotite crystals surrounded by finer-grained phaneritic matrix. The inclusion was sampled near a possible fracture zone which could have contributed to its differing texture/composition. Numerous examples of mafic 'schliering' textures cross-cut by later-forming leucocratic dikes likely representative of the last melt in the system. However, none of the zones exhibiting these textures were available to sampling.


**Figure I-g.** Schliering textures and cross-cutting leucocratic dike adjacent to sample site CP13-05.

**CP13-06**
*Host pluton and inclusion:* 56.68570° N – 134.86272° W

Sample obtained very close to the contact with the Sitka greywacke. Considerable evidence for co-magmatic inclusions present here, although only one large inclusion was accessible for sampling. This 'hybrid' inclusion appeared tabular in nature, suggesting possible relation to andesite dikes mapped in the area (Source….). This sampled inclusion exhibited porphyritic texture, with large (~5 – 6 mm) hornblende crystals in an aphanitic, dark-grey groundmass. Numerous leucocratic aplite dikes were observed in the area, suggestive of similar magmatic activity as observed nearby at sample site *CP13-05* (photo above). Country rocks with abundant andalusite porphyroblasts were observed close to this locality, suggesting a relatively shallow-depth of emplacement and a steep geothermal gradient (low-pressure, high-temperature) during emplacement of the Crawfish.

**CP13-07**
*Host granitoid and enclaves:* 56.70158° N – 134.88554° W

This location exhibited the largest abundance of co-magmatic inclusions of any of the Crawfish pluton sample sites. Similar to outcrop *KP13-01*, with cuspate-lobate margins suggesting the hotter, more mafic material was flowing around the more competent blocks of granodiorite (photo below). Host pluton was similar to other sample sites, although it appears to contain slightly larger phenocrysts relative to other samples. Hybrid inclusion *07B* was characterized as a 'plag-hybrid' because of large porphyritic plagioclase phenocrysts in a dark-grey groundmass. This composition was generally observed in tabular features but the collected sample came from a 'bleb-like' feature. Sample *07C* appeared similar to the andesite collected at *CP13-06*, with large rod-like

hornblende grains in a light-grey groundmass. Finally, sample *07D* displayed the most promise as a co-magmatic inclusion because of the cuspate-lobate margins (below) at its contacts with the pluton. The mafic inclusion exhibited porphyritic texture with small (~ 1 mm) plagioclase phenocrysts in an extremely fine-grained, dark-grey groundmass.

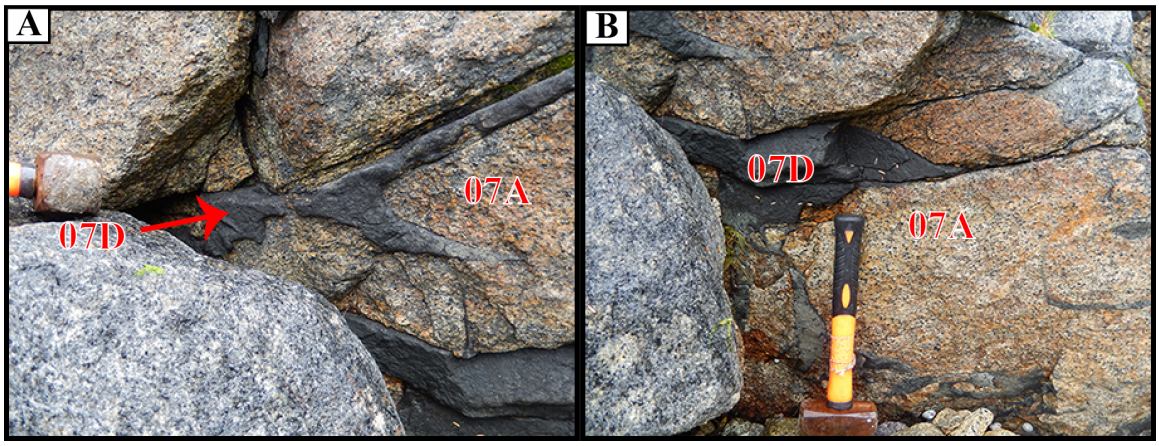


**Figure I-h.** Examples of crenulated (cuspate-lobate) margins suggesting interaction of co-magmatic bodies during emplacement of the Crawfish pluton. The less competent (more viscous) mafic magma flowed around and through the considerably cooler host pluton, producing these distinct textures at the contact.

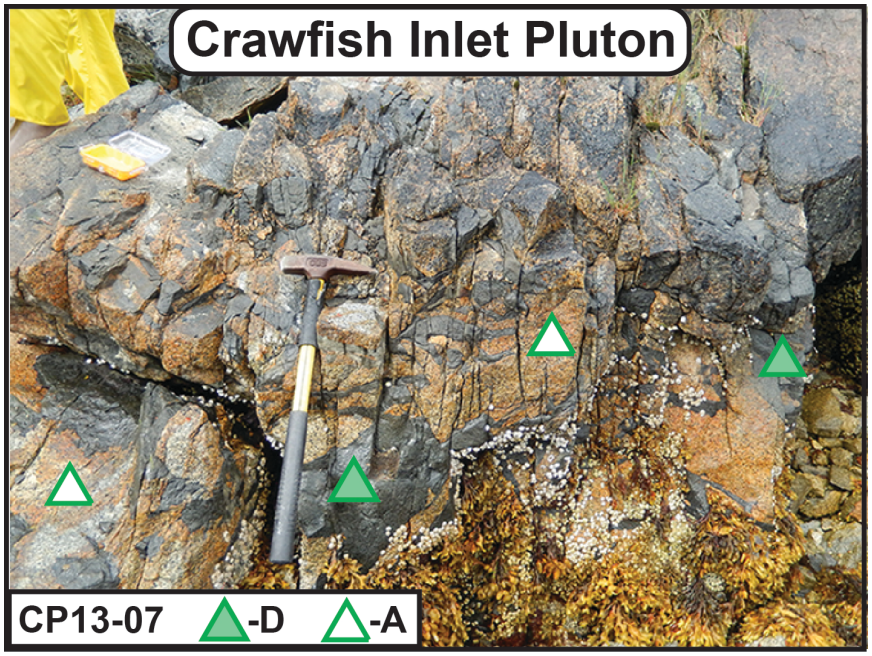


**Figure I-i.** Photo displaying the abundance of enclaves at sample site CP13-07. Note the presence of quenching textures from Figure I-f above. Rock hammer used for scale.

**CP13-08**

*Host granitoid (Leucogranite):* 56.66555° N – 134.89749° W

Small, 'finger-like' intrusive body within the Sitka greywacke, just SW of the major contact between the Crawfish and Sitka greywacke. The pluton appeared very similar to the leucocratic sample (*CP13-02*), although this sample does contain some biotite. Characterized in the field as a biotite-muscovite leucogranite, with considerable pyrite. The pluton displayed significant compositional heterogeneity across the outcrop, with some zones rich in biotite and other areas lacking ferromagnesian minerals altogether. Other areas of the outcrop displayed foliation, and small garnet porphyroblasts were found in greywacke country rocks adjacent to the contact.

**CP13-09**

*Host granitoid and enclaves:* 56.71754° N – 134.95419° W

Sample collected at the end of the Small Arm of Whale Bay. The host pluton at this site appeared to have a slightly lower percentage of ferromagnesian minerals, and no hornblende was observed (CI ~ 8-10). The inclusion sampled for *09B* appeared tabular and exhibited cuspate-lobate textures along the margin of the feature, suggesting the surrounding pluton was still behaving like a liquid (i.e. capable of flow) during the injection of the dike. The tabular body had a CI ~ 50, and was notably biotite dominant. Sample *09C* came from a presumably more mafic 'bleb' feature with plagioclase phenocrysts in dark-grey groundmass. This inclusion displayed considerable heterogeneity (see photo), including small fragments of the host pluton (presumably) within the magmatic inclusion.

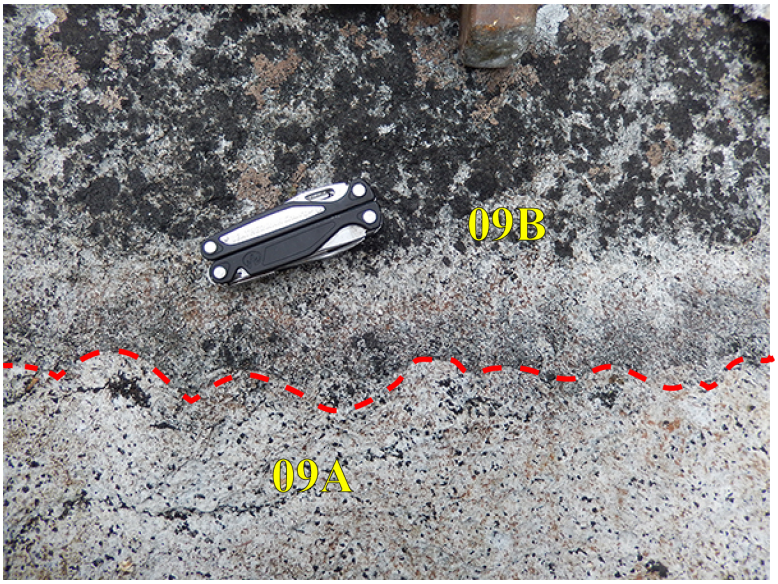


**Figure I-j.** Highlighting the co-magmatic texture observed along the contact between samples CP13-09A and -09B. The crenulated contact is outlined in red and units are labeled in yellow.


**Figure I-k.** Illustrating heterogeneity and possible assimilation of host pluton fragments in magmatic inclusion 09C. Note the crenulated nature of the contacts. The fragments of host pluton (09A) were separated from the inclusion sample prior to sending for geochemistry and isotope analyses.

**CP13-12**
*Host granitoid and enclaves:* 56.71511° N – 134.97520° W

Sample collected near the end of the Small Arm of Whale Bay. Notable evidence of magma mixing/mingling here in the form of large, tabular-like aphanitic body (12B) as well as small magmatic 'blebs' appearing to be magmatic enclaves (12C). Both were sampled for geochemical analysis, with -12A and -12C also selected for Sr and Nd isotope analysis.

**CP13-13**
*Host granitoid:* 56.74250° N – 135.19786° W

Sample collected towards the northern portion of the pluton near Crawfish Inlet. The pluton appeared to exhibit a lower CI here. Sample collected immediately adjacent to contact with Sitka greywacke. Pegmatitic quartz veins were abundant here. Some enclaves were present, but all of those found were in float and therefore were not sampled.

# APPENDIX II

**Table II-a.** Petrographic descriptions of Crawfish Inlet and Krestof Island granitoid lithologies

| Sample | Texture | Minerals | Other | Uncrossed Polars Image | Crossed Polars Image |
|---|---|---|---|---|---|
| CP13-01 | porphyritic phaneritic; hypidio-morphic; 0.5-3.5 mm; avg. grain 0.75 ***or*** 2 mm | plg, qtz, bt, opq | many plg grains heavily zoned; some large euhedral plg exhibit resorbed cores; locally poikilitic w/in ferromagnesian clusters | 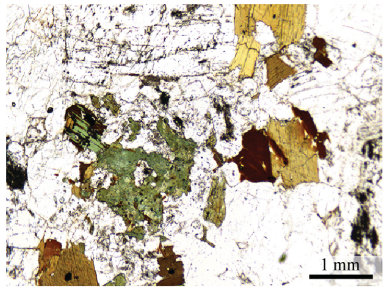  | 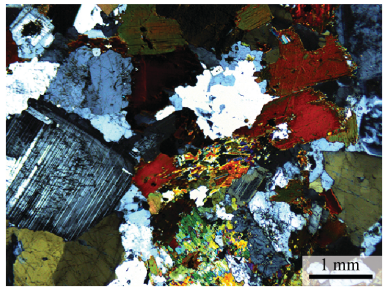  |
| CP13-03A | seriate; hypidio-morphic; 0.3-3.0 mm; avg. grain 1.0 mm | plg, qtz, bt, hbl, chl, opq | plg less resorbed than other samples, poikil-itc texture with bt oikocrysts enclosing small qtz grains; bt locally altered to chl | 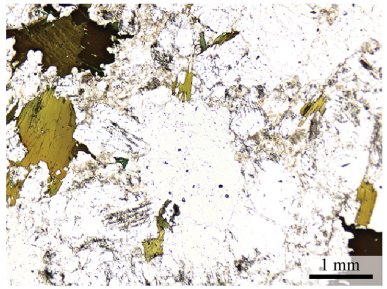  | 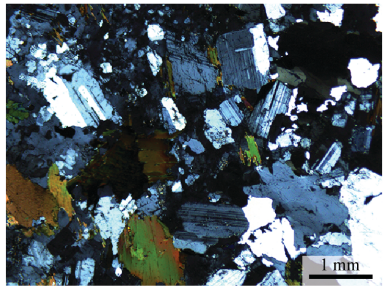  |
| CP13-04 | phaneritic; 0.5-2.5 mm; avg. grain 1.25 mm | plg, qtz, bt, chl, hbl | many grains heavily altered; 'shreddy' textures common; bt commonly replaced by chl; plg zonations common | 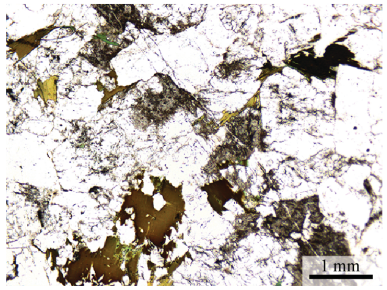  | 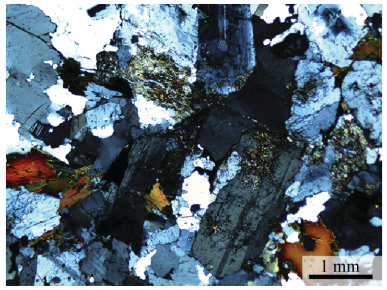  |

Minerals are given in order of decreasing abundance using the following abbreviations: qtz = quartz; plg = plagioclase; bt = biotite; hbl = hornblende; chl = chlorite; cpx = clinopyroxene; opq = opaque accessory phases

**Table II-a.** Petrographic descriptions of Crawfish Inlet and Krestof Island granitoid lithologies (*cont.*)

| Sample | Texture | Minerals | Other | Uncrossed Polars Image | Crossed Polars Image |
|---|---|---|---|---|---|
| CP13-06A | seriate; hypidio-morphic; 0.2-5 mm; avg. grain 1.25 mm | plg, qtz, bt, chl, hbl | many plg grains heavily zoned; large plg grains are euhedral; ferromagnesian phases anhedral and/or altered; some large bt grains (5 mm) | 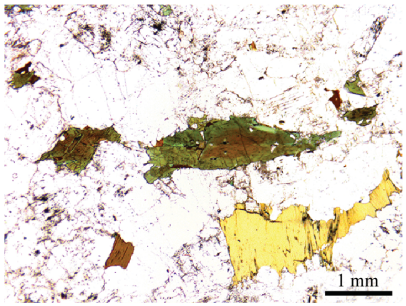  | 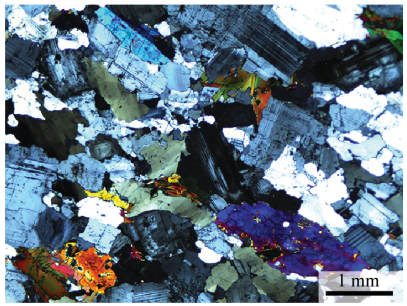  |
| CP13-07A | seriate; 0.25-3.0 mm; avg. grain 1 mm | plg, qtz, bt, hbl, chl, opq | plg exhibit resorbed cores and shreddy textures; plg zonations common; bt locally altered to chl; more bt than other CP samples ***except*** CP13-01 | 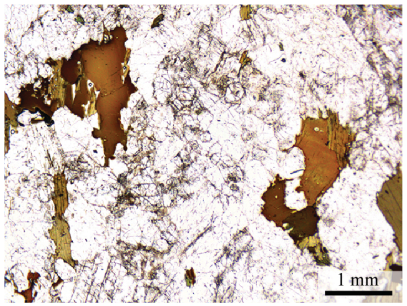  | 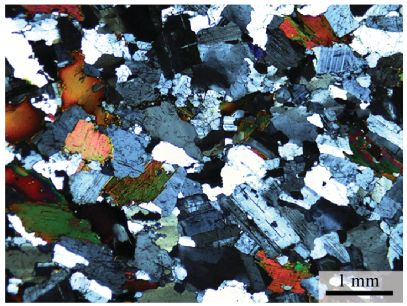  |
| CP13-09A | porphyritic phaneritic; 0.5-4.25 mm; avg. grains 0.75 ***or*** 1.75 mm | plg, qtz, bt, chl (rare) | some plg zoning; bt rarely replaced by chl; two distinct grain size pop. (0.75 and 1.75 mm); ferro-magnesian phases generally larger grains | 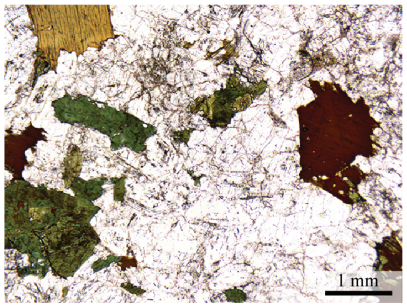  | 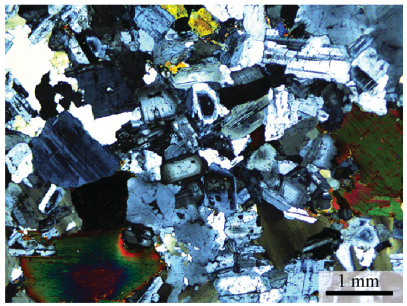  |

Minerals are given in order of decreasing abundance using the following abbreviations: qtz = quartz; plg = plagioclase; bt = biotite; hbl = hornblende; chl = chlorite; cpx = clinopyroxene; opq = opaque accessory phases

**Table II-a.** Petrographic descriptions of Crawfish Inlet and Krestof Island granitoid lithologies (*cont.*)

| Sample | Texture | Minerals | Other | Uncrossed Polars Image | Crossed Polars Image |
|---|---|---|---|---|---|
| CP13-12A | phaneritic; hypidio-morphic; 0.4-2.75 mm; avg. grain 1 mm | plg, qtz, chl, bt | plg commonly exhibits heavily resorbed grains; bt altered to chl; slightly smaller grain size than most CP ***except*** CP13-09A; 'shreddy', poik-ilitic textures | 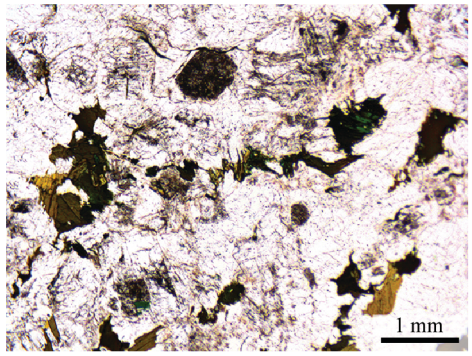  | 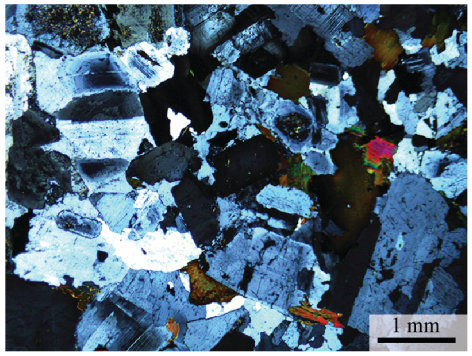  |
| CP13-13 | seriate; hypidiomor-phic; 0.25-3.0 mm; avg. grain 1.5 mm | plg, qtz, bt, hbl | some resorbed plg cores; largely zoned plg are common; one hbl grain intergrown with bt; minimal alteration | 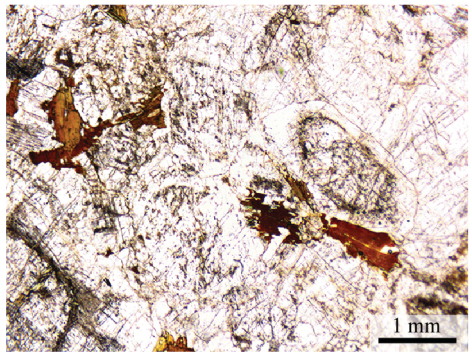  | 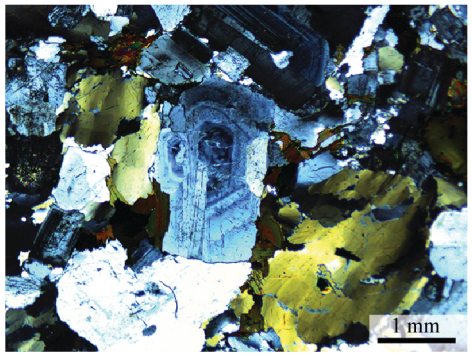  |

Minerals are given in order of decreasing abundance using the following abbreviations: qtz = quartz; plg = plagioclase; bt = biotite; hbl = hornblende; chl = chlorite; cpx = clinopyroxene; opq = opaque accessory phases

**Table II-a.** Petrographic descriptions of Crawfish Inlet and Krestof Island granitoid lithologies (*cont.*)

| Sample | Texture | Minerals | Other | Uncrossed Polars Image | Crossed Polars Image |
|---|---|---|---|---|---|
| KP13-01A | seriate; hypidio-morphic; 0.2-1.4 mm; avg. grain 0.75 mm | plg, qtz, bt, chl, hbl (small xtls), opq | bt locally altered to chl; smaller grain size than CP; opq minerals more common than CP; some poikilitic textures near ferromag-nesian clusters; some alteration | 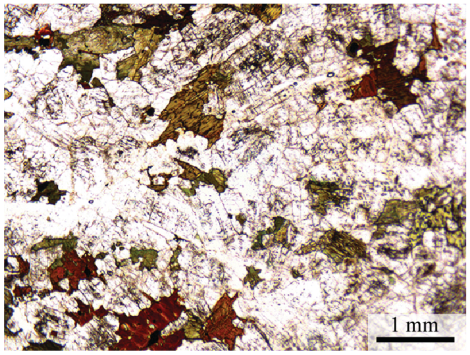  | 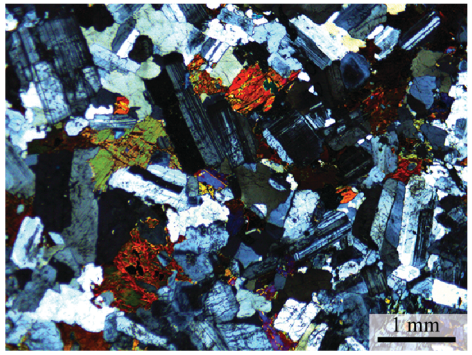  |
| KP13-02A | seriate; 0.25-1.75 mm; avg. grain 0.8 mm | plg, qtz, bt, hbl | few resorbed plg cores; zoned plg grains common; bt oikocrysts with plag and qtz inside; minimal alteration | 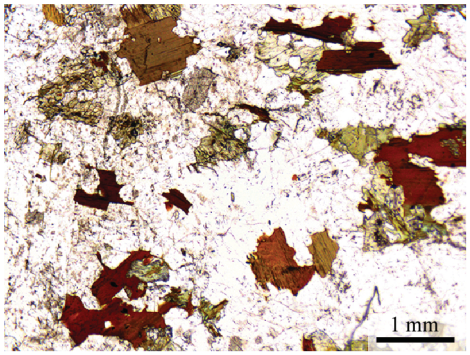  | 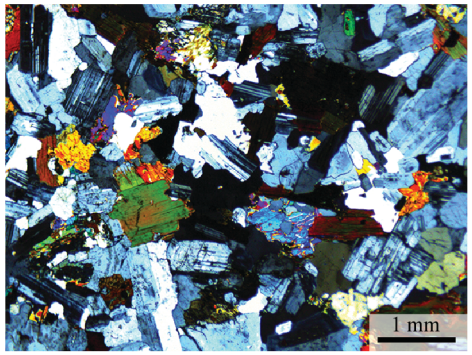  |

Minerals are given in order of decreasing abundance using the following abbreviations: qtz = quartz; plg = plagioclase; bt = biotite; hbl = hornblende; chl = chlorite; cpx = clinopyroxene; opq = opaque accessory phases

**Table II-b.** Petrographic descriptions of Crawfish Inlet and Krestof Island enclave lithologies

| Sample | Texture | Minerals | Other | Uncrossed Polars Image | Crossed Polars Image |
|---|---|---|---|---|---|
| CP13-07D | porphyritic; grain size <0.1 mm - 1 mm; avg. grain size = 0.2 mm | plg, hbl, bt, cpx, opq | quenching textures omnipresent; acicular apatite; poikilitic plag; few grains of cpx; by far most aphanitic enclave sample; few large bt or hbl grains | 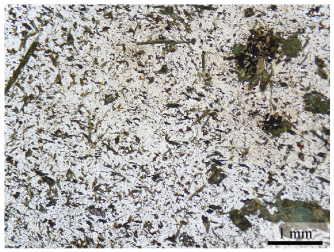  | 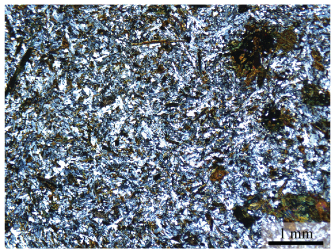  |
| CP13-07B | porphyritic; grain size 0.1 mm - 1.25 mm; avg. grain size = 0.4 mm | plg, bt, hbl, chl, opq | quenching textures present but not as abundant; acicular apatite; more hbl than any other Crawfish sample from this study | 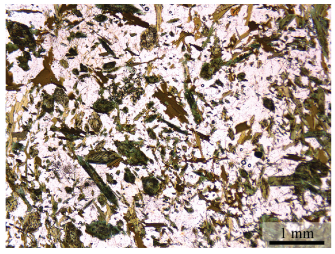  | 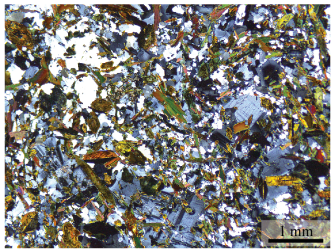  |
| KP13-01C | extremely porphyritic; grain size 0.1 mm - 2.25 mm; avg. grain size = 0.35 mm | plg, hbl, bt, opq | distinct from Crawfish -07B/D enclaves; hbl most abundant ferromagnesian phase; large plag grains in aphanitic matrix; acicular apatite is sparse | 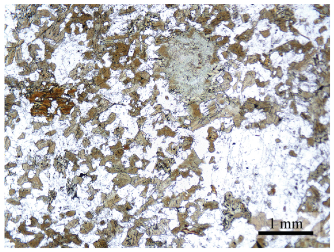  | 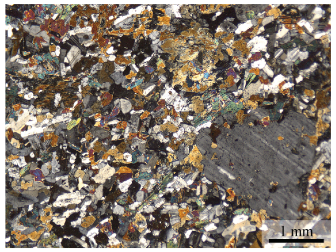  |

Minerals are given in order of decreasing abundance using the following abbreviations: qtz = quartz; plg = plagioclase; bt = biotite; hbl = hornblende; chl = chlorite; cpx = clinopyroxene; opq = opaque accessory phases

**Table II-b.** Petrographic descriptions of Crawfish Inlet and Krestof Island enclave lithologies (*cont.*)

| Sample | Texture | Minerals | Other | Uncrossed Polars Image | Crossed Polars Image |
|---|---|---|---|---|---|
| KP13-02B Contact | | | crenulated contact between enclave KP13-02B and host granitoid KP13-02A. Labeled figure shown in main body (Figure 8) | 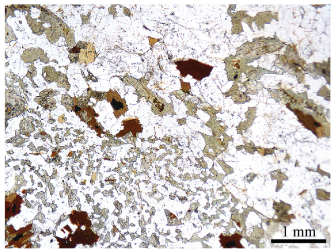  | 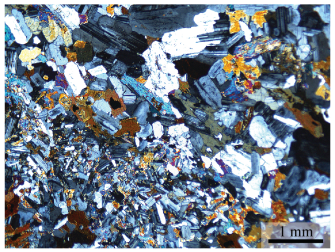  |
| KP13-02B | slightly porphyritic; grain size <0.1 mm - 1.25 mm; avg. grain size = 0.25 | plg, hbl, bt, chl, opq | similar to Krestof enclave -01C but no large plag grains; hbl more abundant than bt; large oxides >0.5 mm present; some acicular apatite observed | 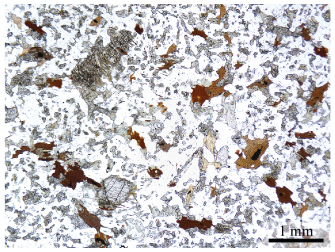  | 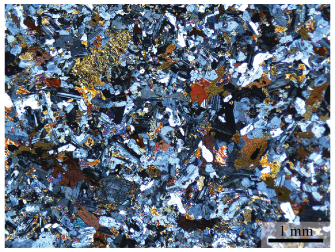  |
| KP13-02C | slightly porphyritic; grain size 0.15 mm - 1.4 mm; avg. grain size = 0.35 mm | plg, hbl, bt, opq | hbl more abundant than bt; some acicular apatite; poikilitic textures more common; crenulated contact with host similar to -02B | 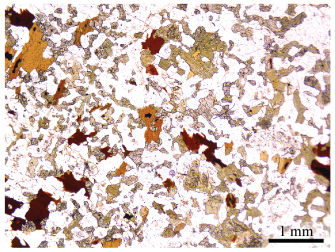  | 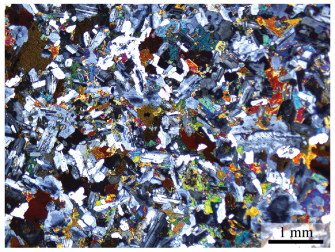  |

Minerals are given in order of decreasing abundance using the following abbreviations: qtz = quartz; plg = plagioclase; bt = biotite; hbl = hornblende; chl = chlorite; cpx = clinopyroxene; opq = opaque accessory phases